Mapping soil moisture using low-frequency radio signals

Feng, Yi

Award date:
2016

Awarding institution:
University of Bath

Chapter 1

Introduction

1.1 Importance of soil moisture

Soil exists at the boundary between the atmosphere and the Earth's subsurface. Soil moisture is the amount of water held within the soil matrix. Volumetric soil moisture is usually expressed as a fraction with respect to the weight and density of the soil. When the soil is said to be fully saturated, the soil moisture content is around 0.41 (or 41%). This, however, depends on the type of soil and its organic composition.

The fractional water content in the upper 10 cm of soil is often referred to as surface layer soil moisture. The top 1 or 2 metres of soil, which contains water available to plants, is known as the root zone. Surface layer and root zone soil moisture are generally called near-surface soil moisture. Many environmental applications benefit from frequent observations of near-surface soil moisture.

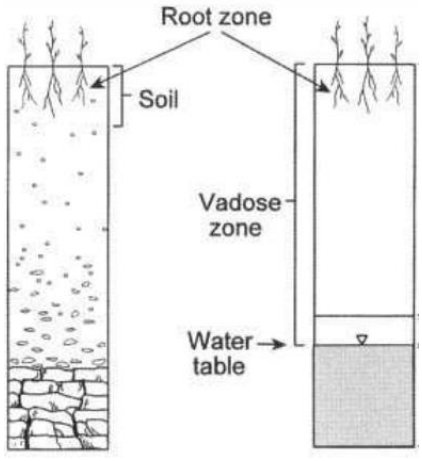

Figure 1.1 – Vertical profiles of the earth's subsurface (Adapted from [1])

Near-surface soil moisture is a highly variable parameter due to precipitation, constant evaporation, and the heterogeneity of the land surface (e.g. [2], [3]). Monitoring the spatial distribution and temporal variation of soil moisture has the following benefits:

- Improved drought prediction and monitoring. Soil moisture is an important parameter in drought forecasting models. Regional droughts could be better predicted and characterised using wide-area soil moisture data measured over a long period of time. (e.g. [4], [5], [6])

- Improved hydrological models for weather prediction. (e.g. [7], [8], [9])

- Improved agricultural management to increase crop yield. (e.g. [10], [11])

- Better understanding of global climate change. The need to understand the environment and climate change led to increases in the number of weather station networks. The continuous monitoring of soil moisture is an essential part of these networks. (e.g. [7])

- Better understanding of evapotranspiration. (e.g. [12, [13])

- Improved flood forecasting. (e.g. [14])

- Water conservation through better irrigation scheduling. Irrigation in agriculture represents over 90% of the world's water usage. Monitoring root zone soil moisture can save water as well as increasing the profitability of farmers. (e.g. [15])

1.2 Scope of the thesis

The importance of near-surface soil moisture, and its role in hydrological processes, is well known. It is widely recognised as one of the fundamental parameters in hydrology and meteorology. The appreciation is reflected by the numerous scientific instruments, remote sensing platforms, and mathematical models that are developed partly or solely for the purpose of estimating soil moisture. Figure 1.2 illustrates the common sources of soil moisture data.

Soil moisture can be directly retrieved from point measurements and remote sensing. The various methods are described in more details in chapter 2. Point measurements are capable of producing accurate results, but the data appears of little use in representing the spatial distribution of soil moisture. Remote sensing yields data on a much more adequate scale of at least tens of kilometres. However, the continuity of measurements is restricted by the revisit period of the satellites, which is typically a few days. The observation depth is only a few centimetres because the measurements are usually made at microwave frequencies.

In addition to direct measurements, soil moisture can be estimated using hydrological models. Model data are often available in a wide range of spatial and temporal resolution. On the other hand, these models require a significant amount of other data as inputs, which could be difficult to obtain ([16]).

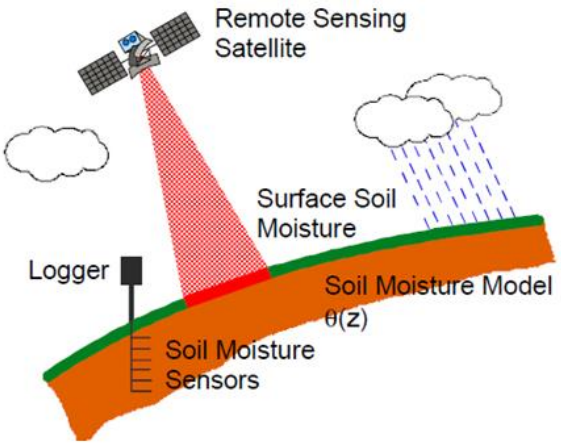

Figure 1.2 – Soil moisture measurement techniques (Adapted from [17])

To improve temporal sampling, a novel remote sensing method is proposed, with the hope of mitigating the drawbacks of microwave remote sensing and hydrological models. This method is expected to produce continuous estimates of wide-area soil moisture with greater observation depth than microwave remote sensing. It is going to be a qualitative validation of the method described in [18], which explored the use of lightning generated radio signals to infer wide-area soil moisture.

1.3 Thesis outline

The thesis is divided into six chapters. This chapter briefly describes the purpose of measuring soil moisture and the limitations of current approaches. Chapter 2 takes a closer look at the various methods used for the *in situ* measurement and remote sensing of soil moisture. Chapter 3 provides a comprehensive overview of the Loran-C navigation system, with particular emphasis on the signal propagation characteristics.

Chapter 4 carries out a preliminary study on what influences the time delay of Loran-C signals. Chapter 5 begins by describing how the delay is related to ground conductivity and soil moisture. The relationships between them are presented through graphs, tables and equations.

In Chapter 5, the theories on Loran-C time delay are implemented into an algorithm, which is used in a validation study to estimate wide-area soil moisture for an inhomogeneous propagation path. A second study then follows, which investigates how sea surface salinity across an all-seawater path can be estimated using a variation of the previous approach. Finally, chapter 6 presents the conclusions and plans for future work.

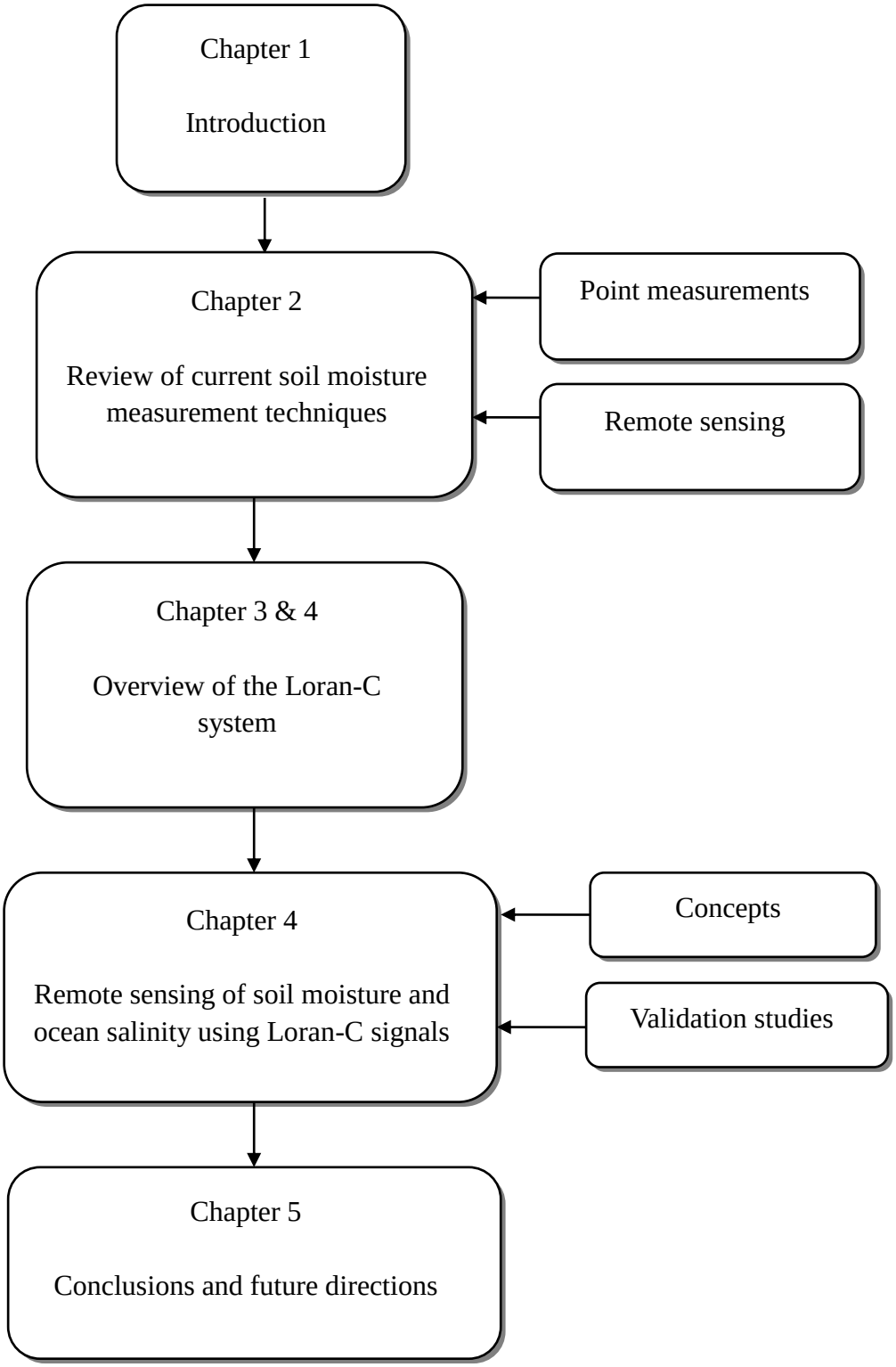

Figure 1.3 – Outline structure of the thesis

Chapter 2

Common methods for measuring soil moisture

2.1 *In situ* measurement of soil moisture

In situ methods have been widely used for measuring near-surface soil moisture. Accurate results could be obtained because the instruments are usually in direct contact with the soil. However, this means only small-scale point measurements are possible. This section briefly describes five of the most typical *in situ* methods, namely the gravimetric method, the neutron method, the gamma ray method, the electrical conductivity method, and Time Domain Reflectometry.

2.1.1 Gravimetric method

The gravimetric method is the standard method of measuring the moisture content of soil samples taken from the field [19]. The idea is oven drying a moist soil sample at 105 ^{o}C and comparing the weight of the water obtained from the moist soil with the weight of the remaining dry soil. The soil sample is usually heated in the oven for 24 hours. The volumetric soil moisture θ is calculated using the following equation:

$$\theta = \frac{W_{water}}{W_{dry}} \quad \frac{\rho_{bulk}}{\rho_{water}} \qquad (2.1)$$

where W_{water} is the weight of water obtained by oven drying, W_{dry} is the weight of the remaining dry soil, ρ_{bulk} is the bulk density of soil, and ρ_{water} is the density of water.

The gravimetric method is straightforward and inexpensive. However, it is a destructive and potentially time consuming method. For organic soils, oven drying can lead to additional loss due to decomposition and oxidation, making it difficult to determine the actual soil moisture profile. This method may also be unsuitable for soils with large amount of clays or rocks.

2.1.2 Neutron method

The neutron method is more widely referred to as the neutron probe method. This indirect method of measuring soil moisture makes use of high energy neutrons, which are emitted into the soil by a radioactive source. Neutrons loss energy and are therefore slowed down as a result of elastic collisions with the nuclei of hydrogen atoms present in water molecules [20]. Hydrogen atoms can effectively slow down fast moving neutrons because of their low atomic weight. The number of slow neutrons counted by the detector per unit time is related to soil moisture.

Compared to the standard method of oven drying and weighing, the neutron method is non-destructive and can determine soil moisture with depth [19]. On the other hand, the equipment used is very expensive and requires extensive calibrations. This can be difficult during a field study. In addition, the radioactive source is a potential health risk.

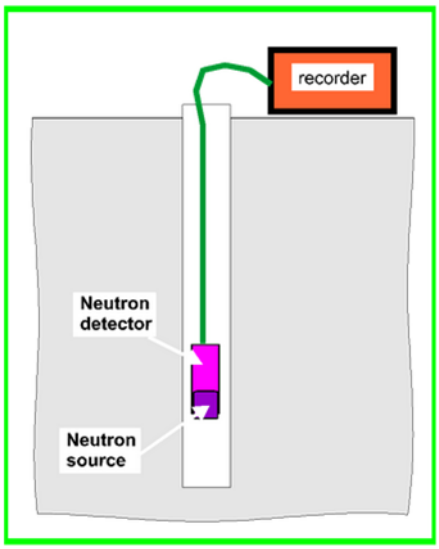

Figure 2.1 – Simplified schematic of a neutron probe (Image from [21])

2.1.3 Gamma ray method

The gamma ray method is another radioactive method for measuring soil moisture, in which the absorption and scattering of gamma rays are related to the density of soil in their path [22]. This method is typically used to produce soil moisture estimates for the 1-2 cm layer.

As with the neutron method, the gamma rays are emitted by a radioactive source. This is potentially harmful to the operator and the surrounding environment. Therefore experiments need to be performed by qualified personnel. Also, due to the cumbersome nature of the equipment, this method is more often used in a laboratory than in the field.

2.1.4 Electrical conductivity method

The electrical conductivity of soil is directly related to its moisture content and the conductivity of the soil water mixture. The most direct way of measuring soil conductivity is to use conductivity probes, which are inexpensive and easy to install and operate. Four-electrode probes are generally preferred to two-electrode probes as they can eliminate the problem of contact resistance.

In some methods, the electrodes are embedded in porous materials such as gypsum blocks. These are called resistance blocks. The blocks absorb moisture from the surrounding soil, and the electrical conductivity measured by the electrodes increases with increasing moisture in the blocks [23]. The soil water potential in a resistance block needs to be in equilibrium with that in the soil. Resistance blocks can overestimate soil moisture and often need to be calibrated in the field [24].

Figure 2.2 – Measuring soil moisture using soil conductivity probe (Image from [25])

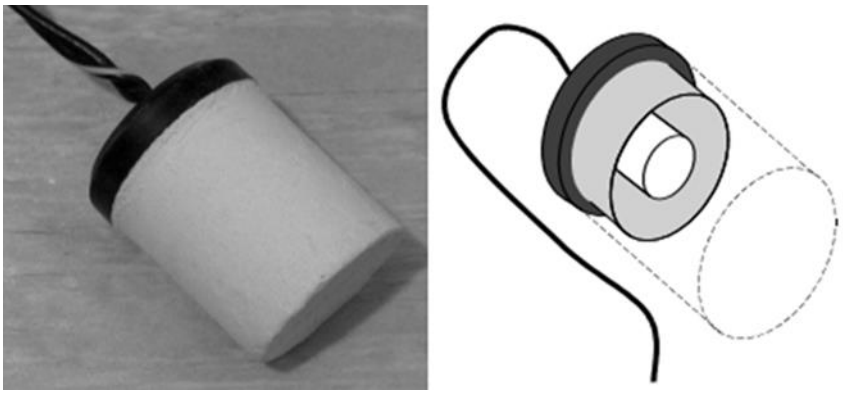

Figure 2.3 – Picture of a gypsum block and simplified schematic showing the placement of the embedded electrodes (Image from [26])

2.1.5 Time Domain Reflectometry

The dielectric constant of a material indicates how polarisable it is in response to an electric field. More often, the relative dielectric constant is mentioned as it is a measure of the material's dielectric property relative to that of free space.

In Time Domain Reflectometry, or TDR, the two-way travel time of an electromagnetic wave propagating along a wave guide is measured. The wave guide is embedded in soil. The velocity of the electromagnetic wave, which is correlated to soil moisture, is determined by the dielectric constant of the soil in contact with the wave guide. The higher the moisture content, the lower the velocity.

Figure 2.4 – TDR soil moisture meter (Image from [27])

TDR is a non-destructive method and requires no soil specific calibrations [28]. The measurements are relatively insensitive to soil temperature and salinity [29]. TDR probes are available in different types. The common insertion probes can be inserted horizontally or vertically into the soil, giving measurements of average soil moisture at the plane or over the depth of insertion. In addition, surface probes are used to measure the moisture content near the soil surface.

2.2 Microwave remote sensing of soil moisture

The *in situ* methods discussed earlier are only capable of producing point measurements of soil moisture. According to [30], soil moisture is very variable in time and space. It is complicated to measure over large areas and long time-spans with appropriate spatial and temporal resolution. Microwave remote sensing of soil moisture is a promising technique for that purpose as it can provide soil moisture information on large scales in a timely fashion.

In microwave remote sensing, electromagnetic radiation in the microwave region of the radio spectrum is measured by an active or passive sensor. Active microwave remote sensing requires an active illumination system, otherwise known as radar, which transmits electromagnetic radiation towards the target and measures the backscatter of energy in the direction of the sensor's receiver [31].

Passive microwave remote sensing uses a radiometer to measure electromagnetic radiation that is naturally emitted from the earth's surface. The radiometer acts as a receiver because the transmission comes from the target itself. Passive microwave sensors generally have low spatial resolution because the fields of view need to be kept large in order to record a signal. A comparison of active and passive microwave remote sensing is made in Table 2.1.

Characteristic	Active microwave	Passive microwave
Spatial resolution	High	Low
Revisit time	Poor – Moderate	Good
Swath width	Narrow – Moderate	Wide
Data rate	Very high	Low
Signal to Noise	Fair – Good	Good – Very good
Roughness effect	Serious	Slight
Vegetation effect	Moderate	Moderate – Serious
Topographic effect	Serious	Slight

Table 2.1 – Comparison of active and passive microwave remote sensing (Adapted from [7])

Band	Frequency (GHz)	Wavelength (cm)
K_a	40-26.5	0.75-1.1
K	26.5-18	1.1-1.67
K_u	18-12.5	1.67-2.4
X	12.5-8	2.4-3.75
C	8-4	3.75-7.5
S	4-2	7.5-15
L	2-1	15-30
P	1-0.3	30-100

Table 2.2 – Microwave band designations (Adapted from [32])

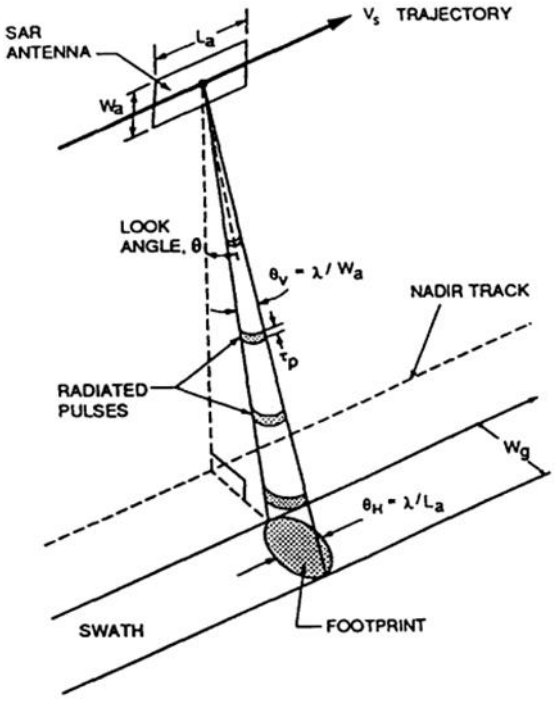

Figure 2.4 – Active microwave remote sensing using synthetic aperture radar (SAR) (Image from [33])

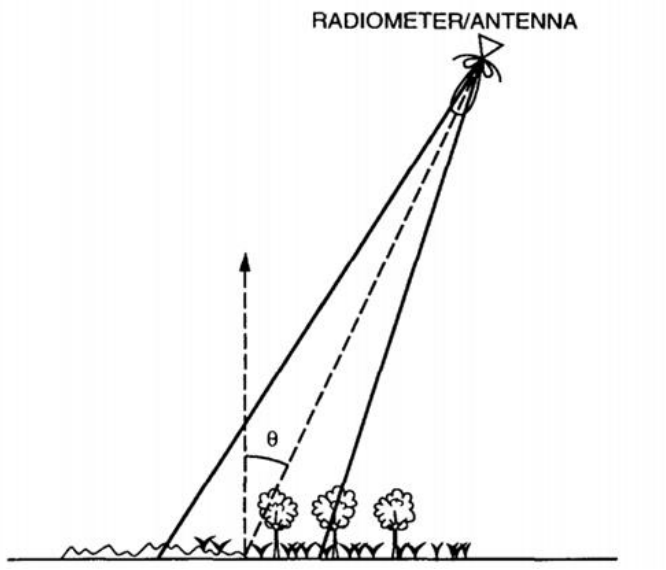

Figure 2.5 – A microwave radiometer viewing a heterogeneous earth surface (Image from [34])

The spatial resolution of passive microwave remote sensing makes it an ideal validation source for the studies presented in this thesis. The following takes a brief look at two typical satellite-based passive microwave systems used for deriving wide-area soil moisture.

The Soil Moisture and Ocean Salinity satellite (SMOS) was developed by the European Space Agency (ESA) as part of its Living Planet Program. It was launched on 2 November 2009 and then entered routine operations in May 2010. The objectives of the mission are [35]:

1. To provide global volumetric soil moisture estimates with an accuracy of 0.04 m^3m^{-3} at a spatial resolution of 35-50 km and a temporal sampling of 1-3 days.

2. To provide global ocean salinity estimates with an accuracy of 0.1 practical salinity scale units for a 10–30 day average for an open ocean area of 200×200 km^2.

The payload of SMOS consists of a passive microwave radiometer operating at 1.413 GHz within the protected L- band [35]. As described in [36], the payload is equipped with 69 individual L-band antennas regularly spaced along Y-shaped arms. This new concept allows the observation of all pixels in the 1000 km wide field of view at a range of incidence angles.

Estimating soil moisture using L-band passive microwave measurements has the following benefits [37]:

1. The sensitivity to soil moisture in approximately the 0–5 cm surface layer (approximately 0–1 cm surface layer for C-band).

2. The lower sensitivity to surface roughness than at higher frequencies.

3. The lower influence of vegetation (with biomass up to 5 kg/m^2) and the atmosphere than at higher frequencies.

Since the commissioning of SMOS, scientists have put great efforts into the validation of its system performance. As mentioned in [38], several studies have shown that point measurements of soil moisture can be representative of larger areas. However, systematic differences between remote-sensing-derived and *in situ* observations are usually detected even though the temporal dynamics are very similar.

Validation results from [39] indicated that the SMOS soil moisture estimates are approaching the level of performance anticipated. However, it was discovered by [40] and [41] that SMOS observations tend to reveal a dry bias.

Being placed in a sun-synchronous orbit, SMOS passes over a location on earth at 6 A.M. and 6 P.M. local solar time (LST). It was found that there is a significant difference between evening and morning soil moisture. Although many of these differences are within the allowable error of 0.04 $m^3\ m^{-3}$, there are several occasions when it is larger [38].

The uncertainties associated with SMOS soil moisture are summarized in [42]. It was concluded that a lot still has to be learnt about soil moisture retrieval from brightness temperatures measured at L-band at such a large scale. Possible error sources in the retrieval mechanism include model parameters (such as roughness), static input (such as soil texture and land cover), and time-variant input (such as surface temperature fields).'

On board NASA's Aqua satellite is another passive microwave radiometer called Advanced Microwave Scanning Radiometer – Earth Observing System (AMSR-E). Unlike its European counterpart, AMSR-E measures brightness temperature at six different frequencies – 6.9, 10.6, 18.7, 23.8, 36.5 and 89.0 GHz [43]. The crossing times of AMSR-E are 1:30 A.M. and 1:30 P.M. LST. Its spatial resolution at 6.9 GHz is 60 km [40].

In [40], the C-band channel of AMSR-E (6.9 GHz) was used for validating the SMOS mission. It was discussed that frequencies in this range (C-band) are more sensitive to errors resulting from the effects of vegetation and surface roughness, and do not retrieve signals from other than the very top cm or two of the soil. Frequencies of 1–2 GHz (L-band) are ideal for soil moisture measurements.

Frequency band	**Frequency (GHz)**
L	1.4-1.427
X	10.6-10.7
K	18.6-18.8
	23.6-24

Table 2.3 – Microwave frequencies protected for remote sensing

NASA's Soil Moisture Active Passive (SMAP) mission, launched on 31 January 2015, is the latest Earth observation satellite to provide global measurements of land surface soil moisture. The satellite is placed in a sun-synchronous orbit, and has a revisit period of 3 days or better. It combines a L-band radar and a L-band radiometer into a single observation system. The combined soil moisture maps are expected to approach the accuracy of radiometer-only retrievals, but with a spatial resolution much higher than the radiometer resolution. The table below shows the range of soil moisture products offered by the SMAP mission:

Product name	**Description**	**Spatial resolution**
L2_SM_P	Soil moisture (radiometer, half orbit)	36 km
L2_SM_A/P	Soil moisture (radar/radiometer, half orbit)	9 km
L3_SM_P	Soil moisture (radiometer, daily composite)	36 km
L3_SM_A/P	Soil moisture (radar/radiometer, daily composite)	9 km
L4_SM	Soil moisture (surface and root zone)	9 km

Table 2.4 – SMAP soil moisture data products (Adapted from Entekhabi et al., 2010)

Chapter 3

Loran-C

3.1 Background to Loran-C

The history of Loran, or 'LOng RAnge Navigation', dates back to the first half of the 20th century. Its earliest version, Loran-A, was developed by the American military midway through the Second World War. The system, which became operational in 1943, was used primarily for guiding the U.S. Air Force over the Pacific Ocean.

Loran-A operated on one of several frequencies between 1,850 and 1,950 kHz. The daytime ground wave coverage over seawater was around 700 nautical miles (NM). This is usually reduced by 200 NM at night. The sky wave range, on the other hand, was significantly longer during the night (~1400 NM) because of weaker ionospheric absorption. The positioning accuracy was about 1 NM for ground wave reception and 6 NM for sky wave reception. By the end of the war, more than 70 Loran-A transmitters were installed, which provided coverage for vast areas of the Pacific and Atlantic oceans as well as selected land regions.

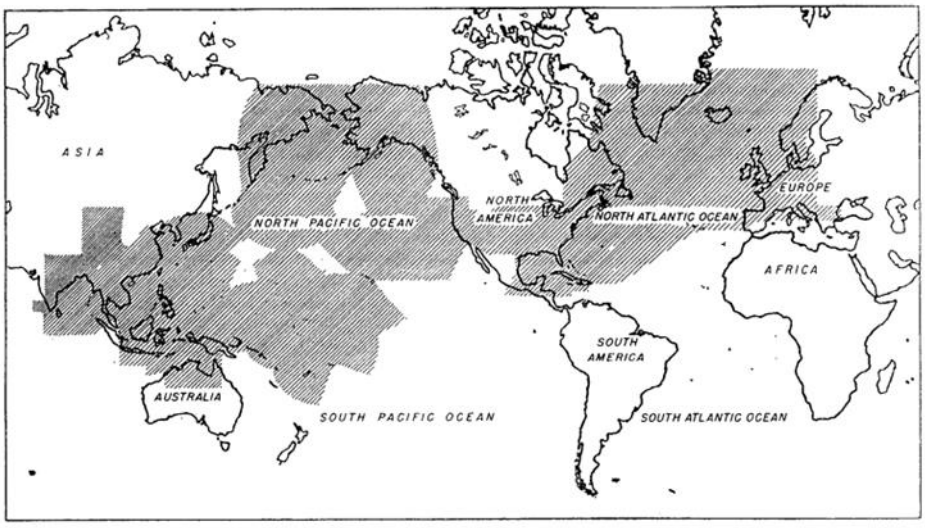

Figure 3.1 – Global coverage of Loran-A at night as of August 1945

(Illustration from [44])

In 1958, Loran-C was introduced as the successor of earlier variants in the Loran family (‘C’ denotes that it is a commercial version). Loran-C was designed to be a low-frequency hyperbolic system that relies mainly on ground waves for navigation. The carrier frequency is 100 kHz, and 99% of its signals occupied the 90 to 110 kHz frequency band. The original system was expected to achieve a maximum absolute accuracy of better than 0.25 NM (460 m).

Loran-C transmitters operate in chains of up to 6 stations. A transmission chain includes a master station and several secondary stations. Secondary stations transmit groups of 8 individual pulses separated by 1ms each. The master station has an additional 9th pulse, which is at 2 ms after the previous pulse. The transmission time of each secondary station from the transmission of the master station is the Emission Delay (ED).

Figure 3.2 – Loran-C transmitter antenna and transmitter building in Lessay, France (Photograph courtesy of [45])

Loran-C transmission chains are characterised by their Group Repetition Interval, or GRI. The designated GRI of the chain is multiplied by 10 to give the actual GRI in microseconds. For example, the Lessay chain in Europe has a designated GRI of 6731, indicating that the time interval between the transmissions of two successive pulse groups from a station is 67310μs.

Some Loran-C transmitters are ‘dual rated’, which means they are part of two transmission chains. In order to avoid confusion, a physical transmitter is often called a ‘stick’, and a stick may be formed by two dual-rated stations.

Configuration	**Designators**	**Example**
Master station with 2 secondary stations	M, X, Y	East China chain (GRI 8390)
	M, W, X	Calcutta chain (GRI 5943)
Master station with 3 Secondary stations	M, X, Y, Z	Canadian West Coast chain (GRI 5990)
Master station with Secondary stations	M, W, X, Y, Z	Southeast U.S. chain (GRI 7980)
Master station with 5 Secondary stations	M, V, W, X, Y, Z	South Central U.S. chain (GRI 9610)

Table 3.1 – Possible configurations of Loran-C transmission chains

The extent of cover from a Loran-C chain is partly determined by the physical locations of its stations. Typical site patterns include the Triad (master and 2 secondaries), the 'Y' (master and 3 secondaries) and the Star (master and 4 or more secondaries). These are illustrated in Figure 3.3.

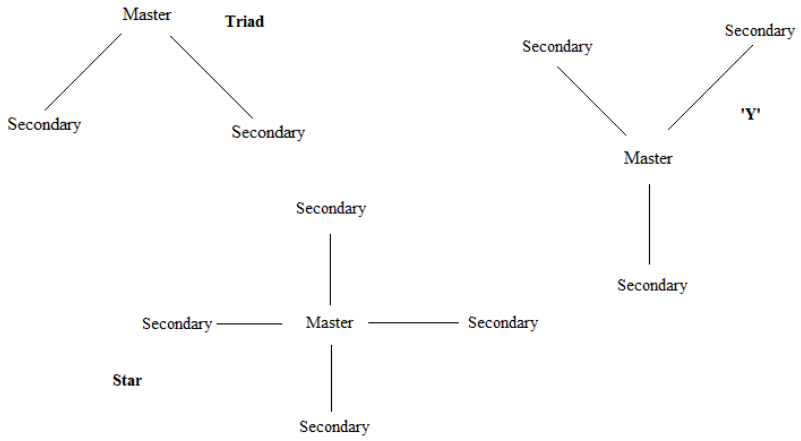

Figure 3.3 – Typical site patterns of Loran-C stations in a transmission chain

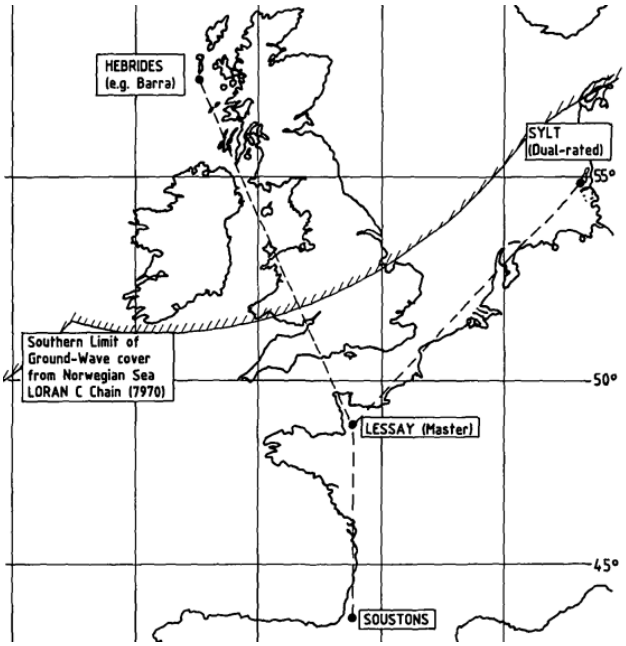

Figure 3.4 – Loran-C stations of the West European experimental chain in a spatial arrangement resembling the letter 'Y' (Illustration from [46])

Loran-C phase code is used to distinguish between master and secondary stations. It uses '+' and '–' to indicate whether a pulse has positive or negative start. The same code pattern is repeated every Pulse Code Interval (PCI), which comprises 2 GRI groups called GRI-A and GRI-B.

	Master station	**Secondary station**
GRI-A	+ + – – + – + – / +	+ + + + + – – +
GRI-B	+ – – + + + + + / –	+ – + – + + – –

Table 3.2 – Loran-C phase code

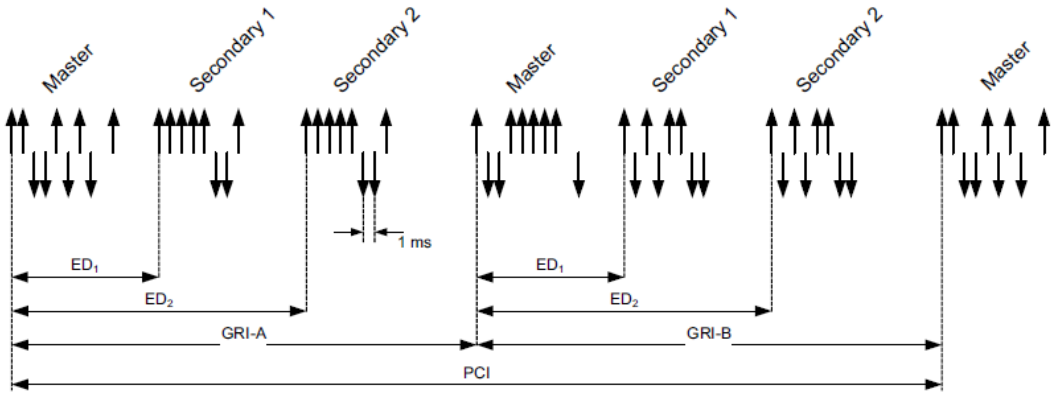

Figure 3.5 – Loran-C transmission sequence (Illustration from [47])

The Loran-C pulse is described mathematically using:

$$v(t) = A\,(\frac{t}{t_p})^2 \exp(2 - 2\frac{t}{t_p}) \cos(\omega t + PC) \quad (3.1)$$

- A is the maximum amplitude;
- t is the time in seconds, and t_p is the time the pulse reaches its peak;
- ω is the angular frequency;
- PC is the phase code of the pulse.

The standard tracking point of a Loran-C pulse with positive phase code is the 3rd upward (negative to positive) zero crossing. The actual time at this point is the Time of Arrival (TOA) of the pulse. For a pulse with negative phase code, the standard tracking point is obviously the 3rd downward zero crossing.

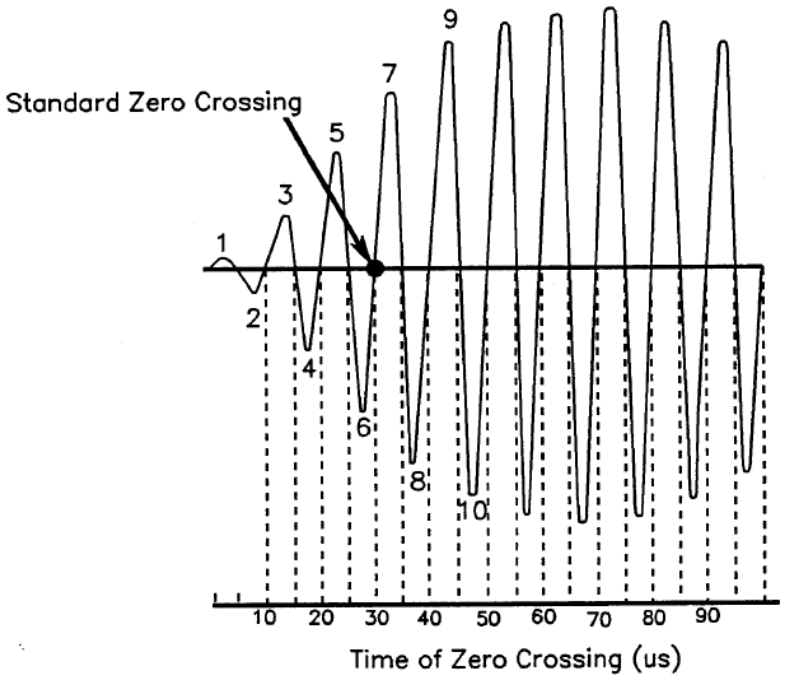

Figure 3.6 – Loran-C pulse showing zero-crossing times and half-cycles (Illustration from [48])

The positioning accuracy of Loran-C is inferior to satellite-based navigation tools like the Global Positioning System (GPS). This, combined with several other factors, has resulted in a noticeable decline in the use of Loran-C. The most recent evidence of this was the complete closure of all transmitting stations in the US in 2010, and the subsequent discontinuation of Loran-C service in Canada.

Loran-C has the ability to provide only 2D navigation, which is another significant drawback compared to the GPS. Although the initial concept of the Loran system was built up based on the purpose of providing guidance for aircraft, Loran-C is unable to deliver any information about the change in height of its receiver. This is one of the reasons why it was not widely incorporated into later generations of aviation technology. At present, operational Loran-C chains can only be found in Europe and East Asia.

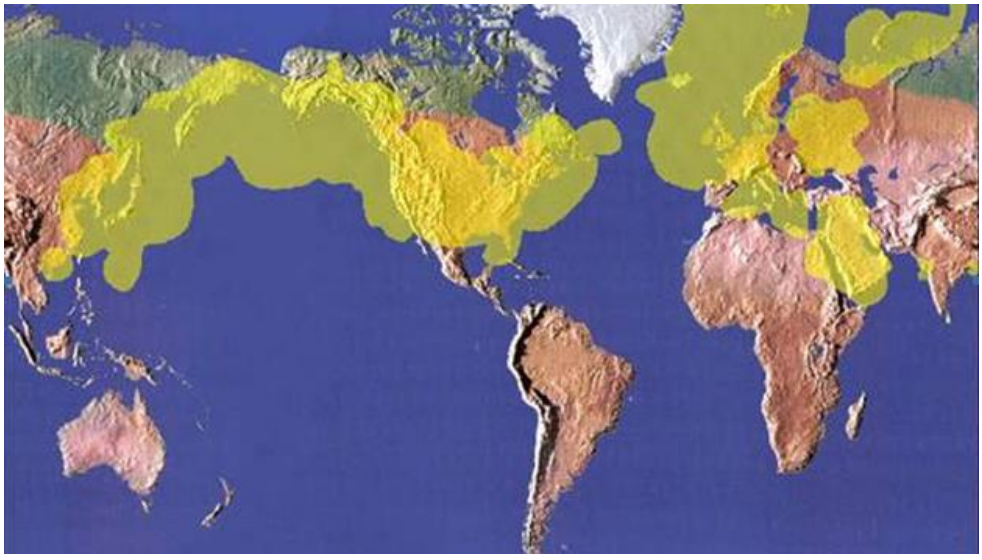

Figure 3.7 – Global coverage of Loran-C before the termination of service in North America in 2010 (Illustration from [49])

Russia has its own version of the Loran-C system – Chayka. Its signals have a unique 'ringing' character at the end of each pulse. Loran-C pulses do not have an interesting waveform like this because their 'tails' are always cut by the transmitter at 250 μs.

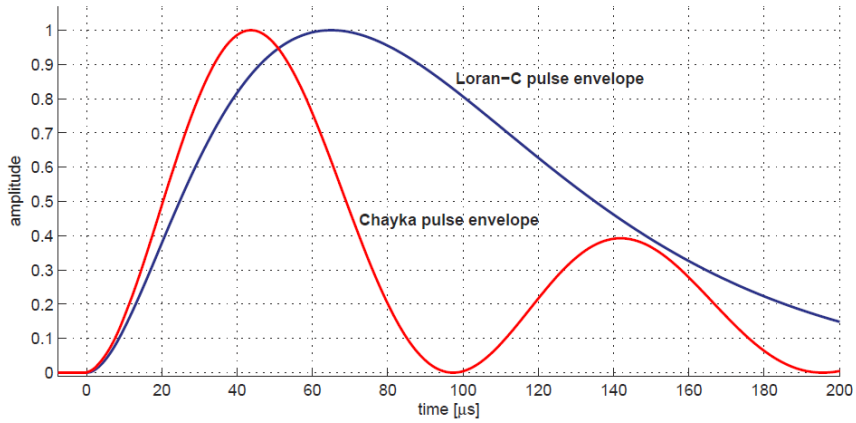

Figure 3.8 – Comparison between the leading part of Loran-C and Chayka pulse envelopes (Illustration from [47])

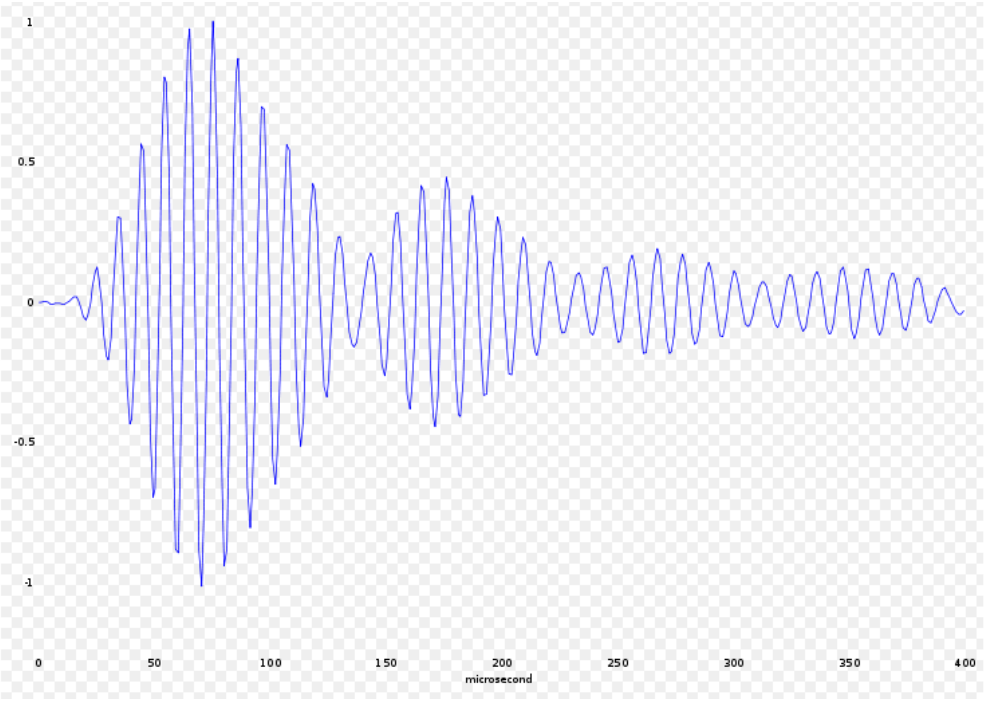

Figure 3.9 – Waveform of a Chayka pulse (Illustration from [50])

3.2 Concepts of wave propagation

Wireless signals are essentially electromagnetic waves that propagate in the absence of artificially created wave-guiding structure. In general, all electromagnetic waves can be broadly categorised by characteristics such as frequency, wavelength and propagation mechanism. These are summarised in the table below, which is known as the radio spectrum.

Band	**Frequency**	**Wavelength**	**Propagation mechanism**	**Applications**
Infra-red	430 THz	0.7 μm	Space wave	Medical and military
Extremely high frequency (EHF)	30 to 300 GHz	1 mm to 1 cm	Space wave	Satellite
Super high frequency (SHF)	3 to 30 GHz	1 to 10 cm	Space wave	Weather and satellite
Ultra high frequency (UHF)	300 MHz to 3 GHz	10 cm to 1 m	Space wave	Mobile phone and TV

Very high frequency (VHF)	30 to 300 MHz	1 to 10 m	Space wave	Aircraft and broadcast
High frequency (HF)	3 to 30 MHz	10 to 100 m	Sky wave	Radar and broadcast
Medium frequency (MF)	300 kHz to 3 MHz	100 m to 1 km	Sky wave	Military and broadcast
Low frequency (LF)	30 to 300 kHz	1 to 10 km	Surface wave	Navigation and broadcast
Very low frequency (VLF)	3 to 30 kHz	10 to 100 km	Surface wave	Military and submarine
Super low frequency (SLF)	300 Hz to 3 kHz	100 to 1,000 km	Surface wave	Military and submarine
Extremely low frequency (ELF)	30 to 300 Hz	1,000 to 10,000 km	Surface wave	Military and submarine

Table 3.3 – The radio spectrum: frequency, wavelength, propagation mechanism and applications

Loran-C signals are transmitted via both ground waves and sky waves. Depending on the frequency, a ground wave may be in the form of surface wave (below 300 kHz) or space wave (above 30 MHz).

At 100 kHz, the wireless link is established through surface waves, which travel across the surface of the earth to reach the receiver. During this process, the wave is often modified by the nature of the terrain along its way. The effective range, being limited to around 1,500 to 2,000 km, is determined by the efficiency of the transmitter as well as the transmission power.

Medium and high-frequency transmissions (300 kHz to 30 MHz) are achieved by sky waves, which are attenuated and refracted by ionized layers in the earth's upper atmosphere (collectively known as the ionosphere). Some layers of the ionosphere can be as high as 700 km above the ground, while some are as near as 70 km.

The ionosphere's absorption is strongly dependent on solar activities. The strength of the received sky wave will be largest at night and then rapidly decreases at sunrise. For Loran-C, the sky wave usually arrives later than the ground wave, which makes the received pulse sky-wave free at the standard tracking point. However, extreme solar activities can sometimes disturb the ionosphere and lead to a much shorter sky wave delay. This is called an 'early sky-wave' condition.

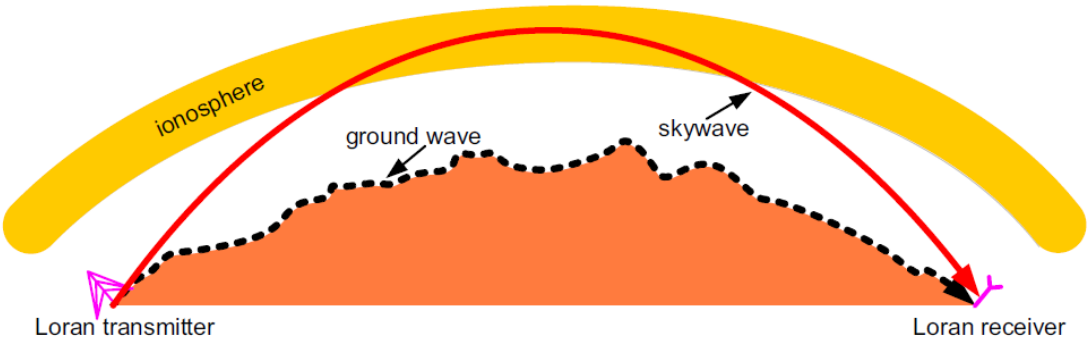

Figure 3.8 – Loran-C wave propagation (Illustration from [47])

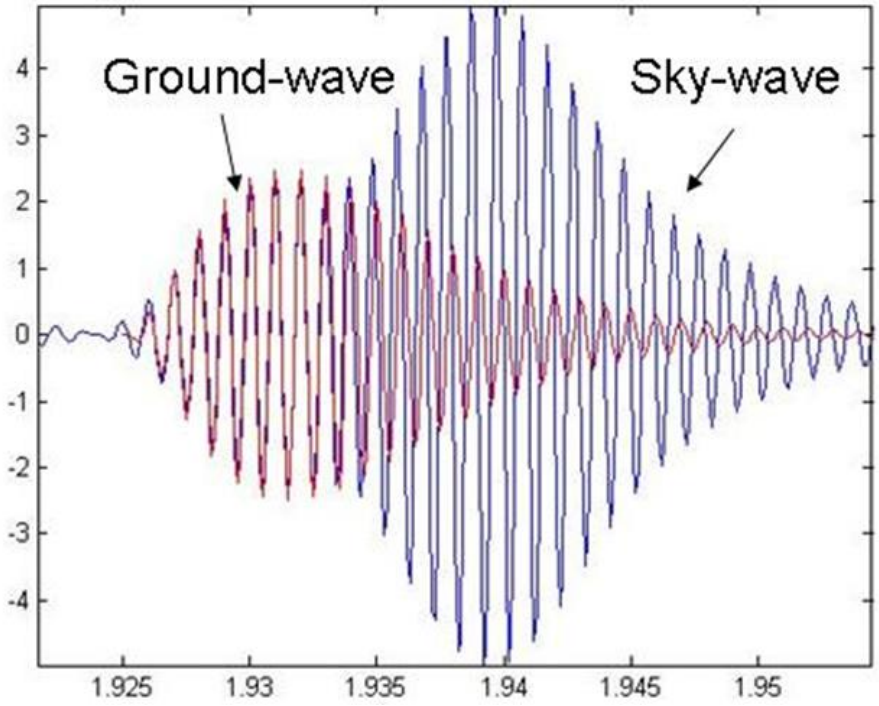

Figure 3.9 – A combined Loran-C pulse received from the Sylt station in Germany

The proposed method of estimating soil moisture uses the ground wave component of Loran-C signals. When ground conductivity is infinite, electromagnetic waves will travel at the speed of light. However, since the wave needs to propagate along the surface of the earth, its velocity is inevitably slowed down because of the physical and electrical properties of the conducting medium.

The propagation of an electromagnetic wave in a conductive medium of conductivity σ leads to the definition of the medium's complex permittivity as:

$$\varepsilon_c = \varepsilon_r - j\frac{\sigma}{\omega\varepsilon_0} \qquad \textbf{(3.2)}$$

where ε_r is the relative permittivity of the medium, and ε_0 is the electric permittivity of free space.

The complex permittivity consists of the real relative permittivity plus an imaginary part involving the conductivity and ε_0:

$$\varepsilon_c = \varepsilon_r + j\varepsilon_I \qquad \textbf{(3.3)}$$

The reduced wave equation is given by:

$$\frac{d^2E_i}{dz^2} + k_o^2\varepsilon_c E_i = 0 \qquad \textbf{(3.4)}$$

where $k_o^2 = \omega^2\mu_0\varepsilon_0$, $\varepsilon_c = \varepsilon_r - j\frac{\sigma}{\omega\varepsilon_0}$ and i = x, y or z.

The complex permittivity produces a complex refractive index:

$$n_c = n - jn_I \qquad \textbf{(3.5)}$$

where n and n_I are real and positive, and $n_c^2 = \varepsilon_c$.

The forward-travelling plane wave solution of equation 1.3 is:

$$E_i(Z) = Ae^{-jk_o n_c z}$$

$$= Ae^{-k_o n_I z} e^{-jk_o n z} \qquad \textbf{(3.6)}$$

The plane wave amplitude changes with z by the exponential factor $e^{-k_o n_I z}$, representing an exponential decay in the amplitude of the wave along the direction of propagation.

The attenuation constant, α (in Neper/m), and the phase propagation constant, β (in rad/m), are defined as:

$$\alpha = k_o n_I \qquad \textbf{(3.7a)}$$

$$\beta = k_o n \qquad \textbf{(3.7b)}$$

For low-loss dielectrics such as land, the conduction current is much smaller than the displacement current. In this case:

$$\alpha = \frac{\sigma}{2}\sqrt{\frac{\mu_0}{\varepsilon_0 \varepsilon_r}} \qquad \textbf{(3.8a)}$$

$$\beta = \omega\sqrt{\mu_0 \varepsilon_0 \varepsilon_r} \qquad \textbf{(3.8b)}$$

Seawater can be considered as a good conductor, in which the conduction current is much greater than the displacement current. In this case:

$$\alpha = \sqrt{\frac{\omega\sigma\mu_0}{2}} \qquad \textbf{(3.9a)}$$

$$\beta = \sqrt{\frac{\omega\mu_0\sigma}{2}} \qquad \textbf{(3.9b)}$$

The skin depth for good conductors, defined as the distance over which the amplitude is attenuated by a factor $\frac{1}{e}$, is expressed as:

$$\delta = \frac{1}{\alpha} \qquad \textbf{(3.10)}$$

3.3 Principles of Loran-C navigation

Loran-C is a hyperbolic navigation system, in which the user's position is determined from the difference in the time of arrival of signals from master-secondary pairs. The time difference (TD) between each station pair is represented by a hyperbolic line of position (LOP). Two LOPs (and hence three stations) are required to fix the position of the receiver.

Suppose that a mariner within the coverage area of three Loran-C stations wants to know the current position of his ship. As illustrated by the example in Figure 1, the master station 'M' is located at the point (-200, 0). The two secondary stations 'X' and 'Y' are located at (200, 0) and (0, 500) respectively. If the Loran-C user records that the measured TD between the arrival of pulses from 'M' and 'X' is 8 ms, and that between 'M' and 'Y' is also 8 ms, then the position of the ship must lie at the intersect of the two hyperbolas (shown in bold in the grid).

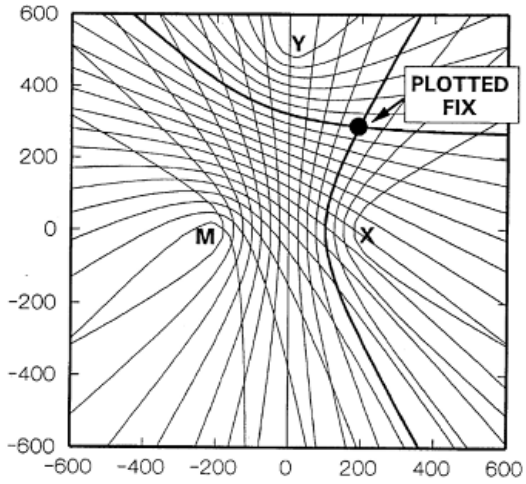

Figure 3.10 – Example of a hyperbolic grid showing the basic principle of position determination in a hyperbolic navigation system (Illustration from [51].

The hyperbolic grid in Figure 3.10 is otherwise known as a hyperbolic lattice. Apart from the LOPs, several other terms are commonly referred to in describing the lattice:

1. A straight line which directly joins a master-secondary pair is termed the baseline. The time it takes for Loran-C pulse to travel along the full length of the baseline is termed baseline travel time.

2. The extension of the baseline beyond the joined master-secondary pair is termed baseline extension.

3. A line that bisects the baseline is termed the centreline. The centreline is also considered as a hyperbolic LOP.

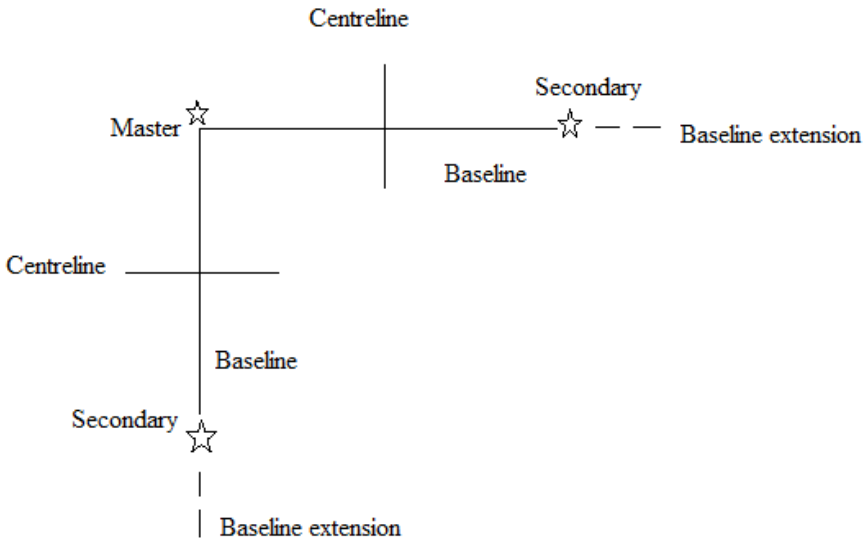

Figure 3.11 – Depiction of baseline, baseline extension and centreline

In some circumstances, two LOPs may intersect at more than one point. This is known as fix ambiguity. The area near baseline extension is where this problem most often occurs. In this situation, another secondary station may be required in order to create an additional LOP to determine which of the two intersects is the correct position.

Measured Loran-C TD data is converted into positioning information (i.e. latitude and longitude) with the help of overprinted charts. LOPs, based on the TD between master-secondary pairs, are printed on these special nautical charts. A Loran-C overprinted chart for a specific coverage area may display TDs for several station pairs. The stations may not belong to the same transmission chain. If the Loran-C receiver does not have the capability to automatically select the most appropriate chain and secondary station for use, then this will need to be done manually by the user.

Loran-C overprinted charts use rate designators and standard colour coding to allow each LOP to be easily identified. The GRI and the secondary station are collectively referred to as the rate, and a distinct colour is assigned to each of the secondary stations in a chain.

On former charts published in the US, the colours blue, magenta, black and green were used for representing secondary stations ‘W’, ‘X’, ‘Y’ and ‘Z’. For example, if the theoretical TD between a master and a secondary ‘X’ is 25750μs (assuming that they belong to the Northeast US chain, GRI 9960), the index for the printed LOP would be ‘9960-X-25750’. In this case, the rate is ‘9960-X’ and the LOP should appear on the chart as a magenta coloured hyperbola.

On standard Loran-C overprinted charts, the spacing between adjacent TDs is usually chosen to be multiples of 5 μs or factors of 100 μs. This means not every possible LOP can be printed on the charts. The user will be required to interpolate between the printed LOPs in order to obtain an accurate position fix.

As an example, imagine that a mariner sees two TDs displayed on the screen of his Loran-C receiver, TD1 = 25744 μs and TD2 = 43952 μs. Suppose that the mariner is in the coverage area of the Northeast US chain (note the stations in this chain, together with other Loran-C stations located in North America, are no longer in use). Referring to his owner's manual, he recognises that '1' denotes the secondary 'X' and '2' denotes the secondary 'Y'. In other words, the two TD readings represent the measured TDs between the master and secondaries 'X' and 'Y'.

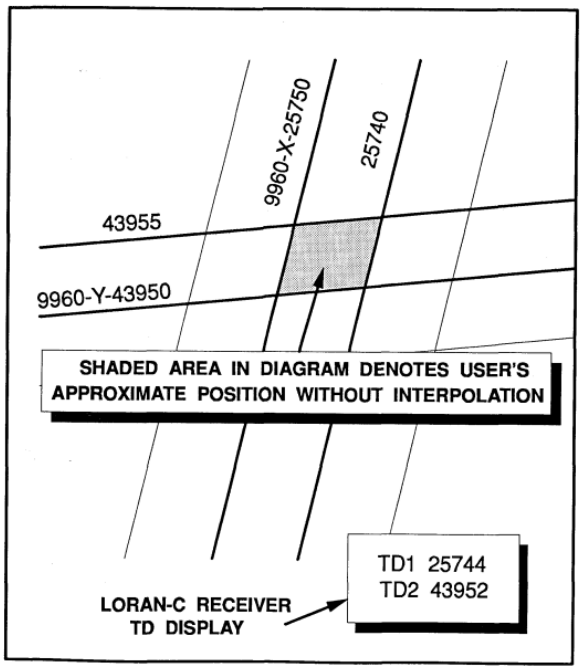

Figure 3.12 – Position determination without interpolation (Illustration from [51]).

The shaded area in Figure 3.12 is the approximate position of the mariner, which was determined without interpolation. In this Figure, the spacing between adjacent TDs for secondary 'X' is 10 μs and that for secondary 'Y' is 5 μs.

It is obvious that TD1 should be 4/10ths of the distance between the LOPs '9960-X-25740' and '9960-X-25750', and TD2 should be 2/5th of the distance between '9960-Y-43950' and '9960-Y-43955'. Figure 3.13 shows how the LOP for TD1 is determined using a Loran-C linear interpolator, which is usually a plastic card with uniform scales marked on it.

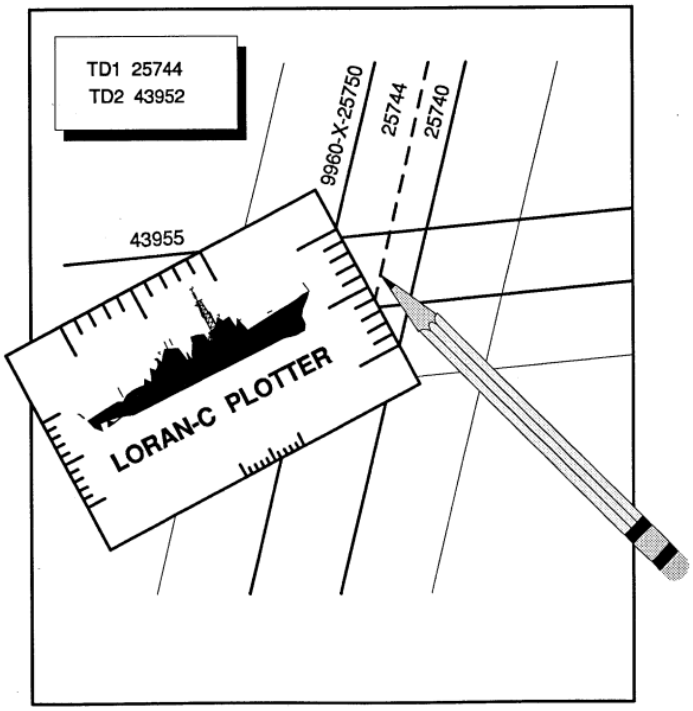

Figure 3.13 – Determining the LOP for TD1 using a linear interpolator (Illustration from [51]).

Nowadays, the conversion from Loran-C TDs to latitude and longitude can be achieved automatically by the receiver. This is a significant contrast to earlier generations of Loran-C receivers, which simply did not have the complex algorithms required for this coordinate conversion.

Some modern receivers have an automatic transmitter selection (ATS) feature, which helps the user to select the stations that are most suitable for the planned voyage. The main function of a Loran-C receiver, as always, is to compute TDs for chosen station pairs by locking onto the correct tracking cycle of the received signals.

Figure 3.14 – Texas Instruments TI9100 Loran-C receiver (Photograph courtesy of National Air and Space Museum, Smithsonian Institution).

Chapter 4

Loran-C time delay

4.1 Time delay of Loran-C signals

For electromagnetic waves travelling through vacuum, the propagation time is simply the total distance divided by the speed of light in free space (299792458 m/s). In Loran-C transmissions, however, the velocity of the signals would be affected by conductivity changes due to constantly varying terrain.

The term 'time delay' refers to the total amount of time it takes for a signal pulse to travel from a transmitter to the receiving end. The factors that contribute to the time delay of Loran-C signals are linked together by the following equation:

$$\text{True propagation time} = \text{PF} + \text{SF} + \text{ASF} \qquad \textbf{(4.1)}$$

The primary factor, or PF, is defined as 'the time of propagation of the signal through the atmosphere [52]'. This is expressed mathematically as:

$$\text{PF (sec)} = \frac{d}{vpf} = \frac{d}{(\frac{c}{\eta})} = \eta\frac{d}{c} \qquad \textbf{(4.2)}$$

- d is the propagation distance.
- vpf is the speed of light in atmosphere, which is 299691162 m/s.
- η is the refractive index in atmosphere. The U.S. Coast Guard used η =1.000338 in its Loran-C signal specification published in 1994 [48].

A slightly different definition of PF also exists, which specifies it as 'the difference in propagation time between a signal traversing through vacuum versus the atmosphere [52]'. The mathematical equation is:

$$\text{PF (sec)} = \frac{d}{vpf} - \frac{d}{c} = \eta\frac{d}{c} - \frac{d}{c} = (\eta\text{-}1)\ \frac{d}{c} \qquad \textbf{(4.3)}$$

The secondary factor, or SF, accounts for 'the difference in propagation time from a signal propagating over an all seawater path rather than through the atmosphere [52]'.

Given the standard assumption that the conductivity of seawater is equal to 5 Siemens per metre (5 S/m), the following equations are provided for the calculation of SF:

For $d \leq 100$ statute mile (160.9 km),

$$\text{SF (}\mu\text{sec)} = -0.1142 + 0.00176d + \frac{0.510483}{d} \qquad \textbf{(4.4)}$$

For $d \geq 100$ statute mile,

$$\text{SF (}\mu\text{sec)} = -0.40758 + 0.00346776d + \frac{24.0305}{d} \qquad \textbf{(4.5)}$$

The most unpredictable influence on the total delay comes from the additional secondary factor (ASF). It is defined as 'the extra delay on the time of arrival of the signal due to propagation over inhomogeneous, rough land path rather than an all seawater path [52]'. In other words, the ASF would be zero if the propagation path is entirely seawater.

In practice, nominal ASF, local grid and differential corrections are needed to create a reliable ASF prediction that satisfies the accuracy requirement for harbor entrance approach (HEA).

Nominal ASF is an averaged value of the additional secondary factor for a relatively large area of tens to hundreds of kilometers. This is available from tabulated data published by the Loran-C service provider. On top of this, local ASF grid is used to take into account specific local variations of ASF within the area covered by the nominal ASF. The remaining error margin is corrected through differential corrections performed by monitoring stations situated on roughly the same path as the receiver.

Figure 4.1 – Nominal (low-density) and harbor entrance approach (high-density) ASF grid (Illustration from [52])

4.2 Ground conductivity and Loran-C time delay

The propagation time t of an electromagnetic wave propagating along a transmission line with length L buried in a conductivity medium (of conductivity σ) is given by [53]:

$$t = \left(\frac{L}{c}\right)\sqrt{\varepsilon_r}\sqrt{\frac{\sqrt{1+\left(\frac{\sigma}{\omega\varepsilon_0\varepsilon_r}\right)^2}+1}{2}} \qquad \textbf{(4.6)}$$

- ε_0 is the permittivity of free space ($8.85418782 \times 10^{-12}$ F/m).
- ε_r is the relative permittivity.
- ω is the angular frequency in rad/s, which is equal to $2\pi f$ where f is the frequency in Hz.

Different types of soil can exhibit completely opposite dielectric properties. For example, soil with more clay contents is considered much more conducting due to the relaxation of water molecules on the surface of clay particles. Sandy soil, on the other hand, is treated as virtually non-conductive. In this case, σ is negligible and the following equation applies [53]:

$$t = \left(\frac{L}{c}\right)\sqrt{\varepsilon_r} \qquad \textbf{(4.7)}$$

Modelled data from the U.S. Department of Commerce and the National Bureau of Standards provides the opportunity to investigate how, at different conductivities, the sum of SF and ASF (PF is independent of conductivity) would behave with increasing propagation distance.

The following assumptions were made:

- Height of propagation, $h = 0$.
- Relative permittivity, $\varepsilon_r = 15$.
- Cyclic frequency, f = 100 kHz.
- Plane earth model is used for propagation distances of 0 to 100 statute miles. This model ignores the curvature of the earth.
- Spherical earth model applies to propagation distances of 100 statute miles or above.
- Both models deal only with a homogenous path with conductivity of 0.0005, 0.001, 0.002, 0.005, 0.05 or 5 S/m.

Conductivity (S/m)	0.0005 S/m	0.001 S/m	0.002 S/m	0.005 S/m	0.05 S/m	5 S/m
Distance (miles)	**SF + ASF (μs)**					
0.1	4.4066	4.4108	4.4138	4.4205	4.4196	4.4209
0.2	3.5351	3.5444	3.5537	3.5633	3.5751	3.5802
0.5	1.4287	1.3499	1.2972	1.2522	1.2014	1.1807
1	0.89338	0.77668	0.69438	0.62225	0.53842	0.50384
2	0.78812	0.62924	0.51684	0.41296	0.29406	0.24479
5	0.94579	0.70510	0.52766	0.35307	0.18108	0.10321
10	1.2334	0.90414	0.65748	0.43407	0.16951	0.059424
20	1.7272	1.2250	0.88285	0.56964	0.19652	0.040878
50	2.4964	1.8704	1.3555	0.86959	0.28272	0.036771
100	3.2957 Plane earth	2.5580 Plane earth	1.8814 Plane earth	1.1919 Plane earth	0.39101 Plane earth	0.043383 Plane earth
	3.4758 Spherical earth	2.6987 Spherical earth	2.0331 Spherical earth	1.3603 Spherical earth	0.52711 Spherical earth	0.17549 Spherical earth
200	4.6994	3.8489	3.0444	2.1180	0.92781	0.42051
500	7.3738	6.5787	5.7176	4.2414	2.2330	1.3579
1000	11.826	10.948	9.9936	7.8031	4.5332	3.0811

Table 4.1 – ‘SF + ASF’ versus propagation distance [54]

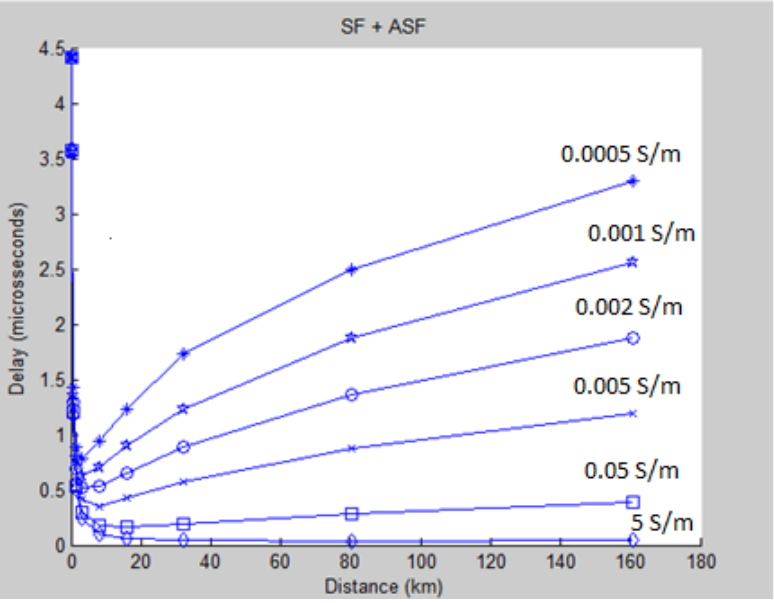

Figure 4.2 – The effect of ground conductivity on 'SF + ASF' for propagation distances of 0 to 160 km (0 to 100 statute miles)

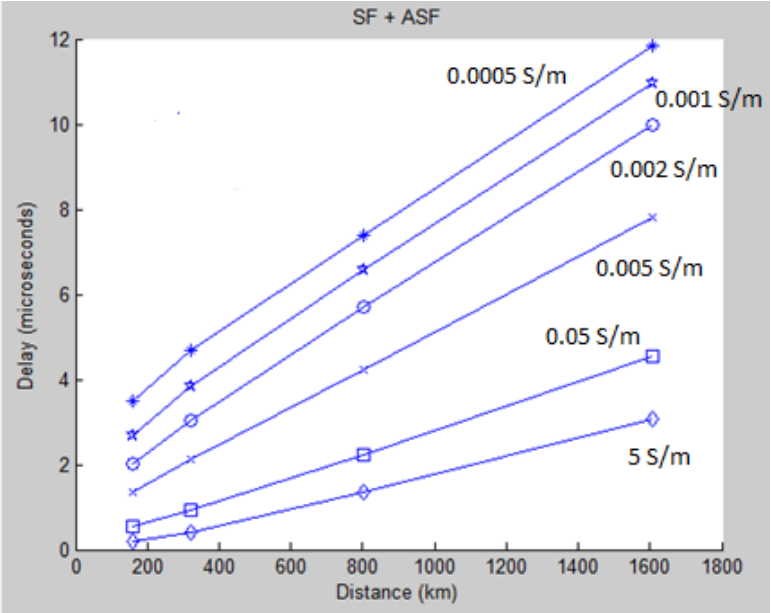

Figure 4.3 – The effect of ground conductivity on 'SF + ASF' for propagation distances of 160 to 1600 km (100 to 1000 statute miles)

The trend observed from the distance versus time delay curves is that at the same propagation distance, ‘SF + ASF’ would be smaller for higher conductivities. The only exception is when the transmitter and receiver are very close together.

As shown in figure 4.2, most curves tend to have a brief region in which the delay drops down sharply from a relatively large value until a point where it starts to gradually rise again with increasing distance from the source. Between 100 and 1600 km, the time delay increases with distance, and the relationship between them is largely linear. Precise information about these relationships can be obtained by creating a linear model:

Conductivity (S/m)	**Gradient**	**Intercept**	**Relationship**
5	0.002024	-0.2069	y = 0.002024x – 0.2069
0.05	0.002776	0.04546	y = 0.002776x + 0.04546
0.005	0.004437	0.6681	y = 0.004437x + 0.6681
0.002	0.005466	1.239	y = 0.005466x + 1.239
0.001	0.005636	1.938	y = 0.005636x + 1.938
0.0005	0.005684	2.728	y = 0.005684x + 2.728

Table 4.2 – Linear model for figure 4.3

The generalized curves are only suitable for a homogeneous path, which is rarely encountered in a practical situation. Millington's Method is a commonly used empirical approach for estimating the ASF of a mixed propagation path – a path that includes various types of terrain and seawater.

The idea is to divide the overall path between transmitter and receiver into a series of homogeneous segments where each segment is represented by a nominal conductivity value. This is illustrated by an example below:

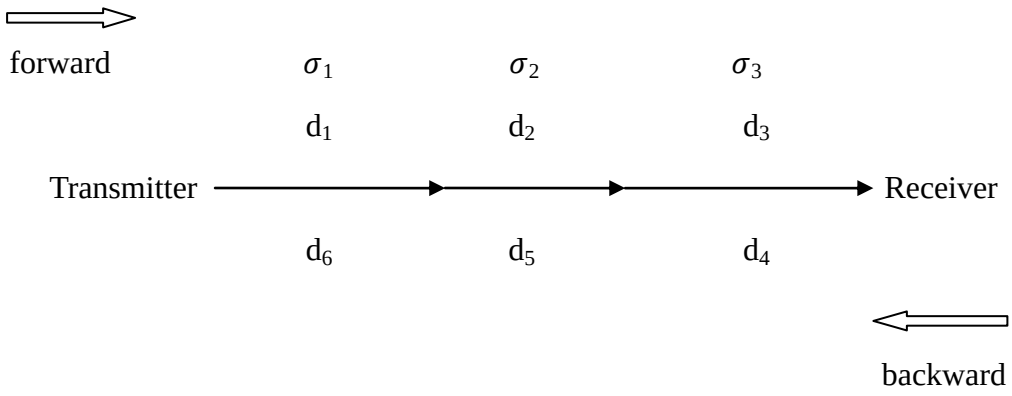

Figure 4.4 – Example of a mixed propagation path which has been divided into three homogeneous paths ($d_1 = d_6$, $d_2 = d_5$ and $d_3 = d_4$)

The sum of SF and ASF for this example is given by the following equations:

$$SF + ASF = \frac{1}{2} \times [(SF + ASF)_{forward} + (SF + ASF)_{backward}] \quad \textbf{(4.8)}$$

where

$$(SF + ASF)_{forward} = (SF + ASF)\sigma_1,d_1 + (SF + ASF)\sigma_2,d_2 + (SF + ASF)\sigma_3,d_3 \quad \textbf{(4.8a)}$$

$$(SF + ASF)_{backward} = (SF + ASF)\sigma_3,d_4 + (SF + ASF)\sigma_2,d_5 + (SF + ASF)\sigma_1,d_6 \quad \textbf{(4.8b)}$$

The incremental times for each segment in the path can be determined from figures 4.2 and 4.3, as well as table 4.2. However, delay curves for a wider range of conductivities are needed to take into account the many types of propagation surface (see table 4.3). The SF, which is calculated using equations 4.4 and 4.5, may be subtracted from the result of equation 4.8 to give the ASF for this path. For a numerical example of a mixed path for ASF calculations by Millington's Method, the reader is referred to reference [51].

Terrain description	**Conductivity (S/m)**
Seawater	5
Rich agricultural land	0.01 – 0.03
Forested land	0.008
Fresh water	0.008
Pastoral land, medium hills and forestation	0.004 – 0.005
Rocky land, dry sandy coastal land	0.002
Mountainous land, cities	0.001
Snow-covered mountains	0.0005

Table 4.3 – Typical conductivity values for seawater, fresh water and various types of terrain (Adapted from [51])

Chapter 5

Remote sensing of soil moisture and ocean salinity using Loran-C signals

5.1 Determining soil moisture from Loran-C delay variation

As described in chapter 4, the theoretical time delay of a Loran-C pulse is computed by adding together atmospheric delay (PF), the seawater delay (SF), and the land path delay (ASF). For navigation purposes, the modeled values of these three factors are stored in virtually all modern Loran-C receivers. However, the ASF variations caused by ground conductivity can only be represented by real-time measurements (Figure 5.1).

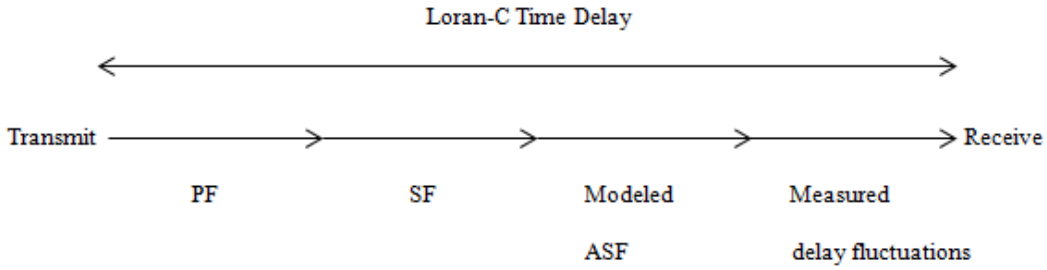

Figure 5.1 – Actual time delay of Loran-C signals

The studies presented in this thesis explore two different methods of measuring the variations in the ASF in addition to the theoretical value. Given a mixed or all-land path, land surface properties should have a significant effect on the measured ASF variations. On the other hand, if the propagation path consists of entirely seawater, then sea surface properties such as temperature and salinity must be the predominant influence. The second scenario is considered in chapter 5.3.

Atmospheric dynamics may also contribute to the measured Loran-C delay variations. The PF is governed by the atmosphere's index of refraction η, which varies between 1.00025 and 1.0004. More often, the refractivity N is considered because it is directly related to certain properties of the atmosphere [55]:

$$N = \frac{77.6p}{T} + \frac{e_s \times 3.73 \times 10^5}{T^2} \qquad (5.1)$$

$$N = (\eta - 1) \times 10^6 \qquad (5.2)$$

- p is the barometric pressure (in millibars).
- T is the absolute temperature (in Kelvin).
- e_s is the partial pressure of water vapor (in millibars).

For the study described in this chapter, the variations in the PF are removed from the overall delay variations. The residual delay is assumed to have a negative correlation with ground conductivity.

In equation 5.1, p and e_s can be calculated from mean sea level pressure and total column water vapor using the following equations:

$$p \text{ (mbar)} = \frac{mean\ sea\ level\ pressure\ (P_a) \times 1000}{101325} \qquad (5.3)$$

$$e_s \text{ (mbar)} = \frac{total\ column\ water\ vapour\ (kgm^{-2}) \times 9.81 \times 1000}{101325} \qquad (5.4)$$

The electrical conductivity of the ground is related to soil moisture by Archie's law [56]:

$$\sigma = W^{\alpha}\beta \qquad (5.5)$$

- σ is the ground conductivity in S/m.
- W is the fractional water content of soil, or soil moisture.
- α is a constant that lies between 1.5 and 2.2.
- β is the conductivity of water in the soil.

The only challenge of directly using equation 5.5 comes from β, because it varies with other properties such as the water's temperature and salinity. It has been suggested that although the relationship between water conductivity and temperature is generally nonlinear, the degree of nonlinearity will be small enough for this relationship to be represented by a linear equation instead. This equation applies within a temperature range of 0 to 30 ℃ [57]:

$$EC_t = EC_{25}\,[1 + a\,(t - 25)] \qquad (5.6)$$

- EC_t is the electrical conductivity of water at temperature t ℃.
- EC_{25} is the electrical conductivity of water at 25 ℃.
- a is a temperature compensation factor, which commonly lies around 0.02 $℃^{-1}$. It was suggested that a representative compensation factor may be used for natural waters with various compositions and salinities.

The following data from the National Physical Laboratory (NPL) shows how the conductivity of seawater varies with temperature and salinity:

Temperature (℃)	**Salinity ($g\ kg^{-1}$)**				
	20	25	30	35	40
	Conductivity (S/m)				
0	1.745	2.137	2.523	2.906	3.285
5	2.015	2.466	2.909	3.346	3.778
10	2.300	2.811	3.313	3.808	4.297
15	2.595	3.170	3.735	4.290	4.837
20	2.901	3.542	4.171	4.788	5.397
25	3.217	3.926	4.621	5.302	5.974

Table 5.1 – Electrical conductivity of seawater at atmospheric pressure [58]

Taking the conductivities at 25 ℃ from table 5.1, and then applying equation **5.6** produces an alternative table shown below:

Temperature (℃)	**Salinity (g kg^{-1})**				
	20	25	30	35	40
	Conductivity (S/m)				
0	1.609	1.963	2.311	2.651	2.987
5	1.930	2.356	2.773	3.181	3.584
10	2.252	2.748	3.235	3.711	4.182
15	2.574	3.141	3.697	4.242	4.779
20	2.895	3.533	4.159	4.772	5.377
25	3.217	3.926	4.621	5.302	5.974

Table 5.2 – Electrical conductivity of seawater at atmospheric pressure (calculated using equation **5.6** where a = 0.02 ℃$^{-1}$)

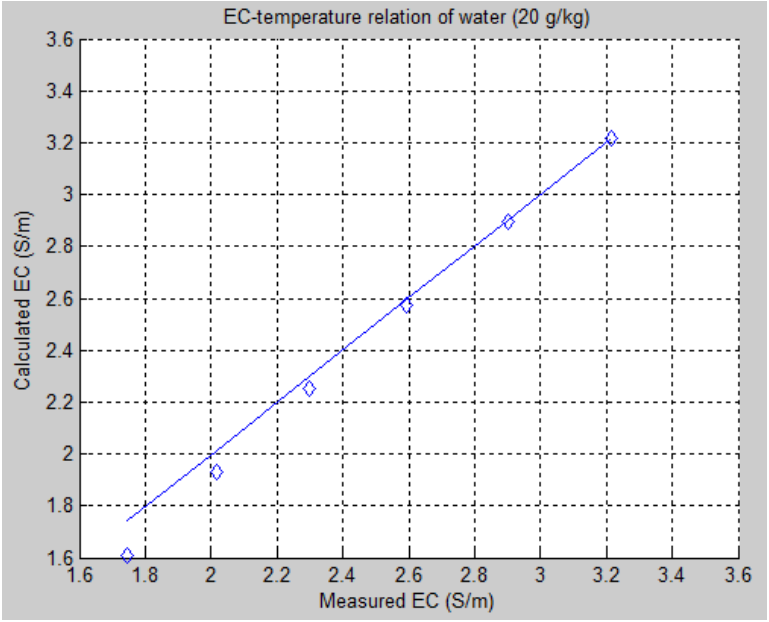

Figure 5.2 – Calculated and measured conductivities of seawater (salinity = 20 g/kg). The straight line indicates exact match.

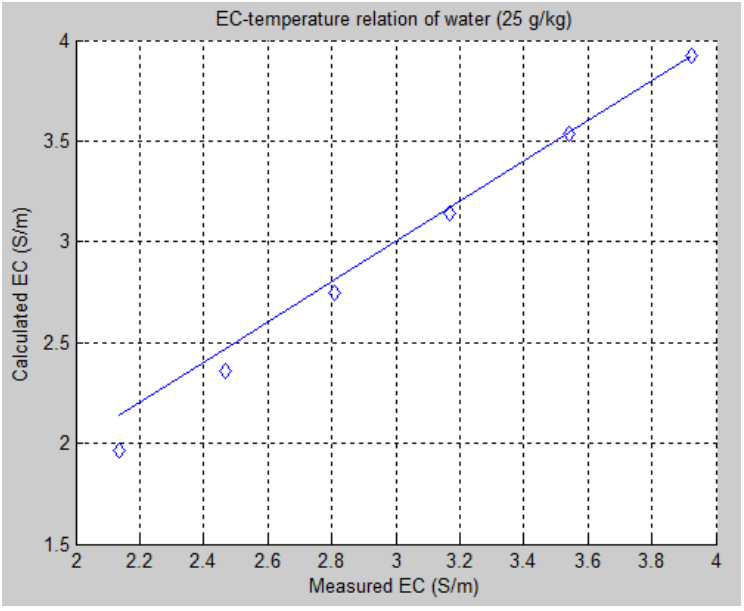

Figure 5.3 – Calculated and measured conductivities of seawater (salinity = 25 g/kg)

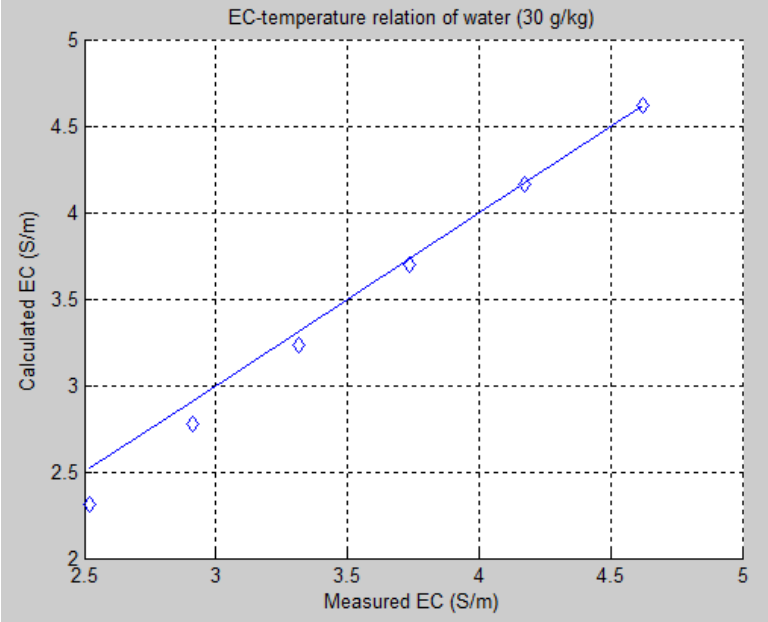

Figure 5.4 – Calculated and measured conductivities of seawater (salinity = 30 g/kg)

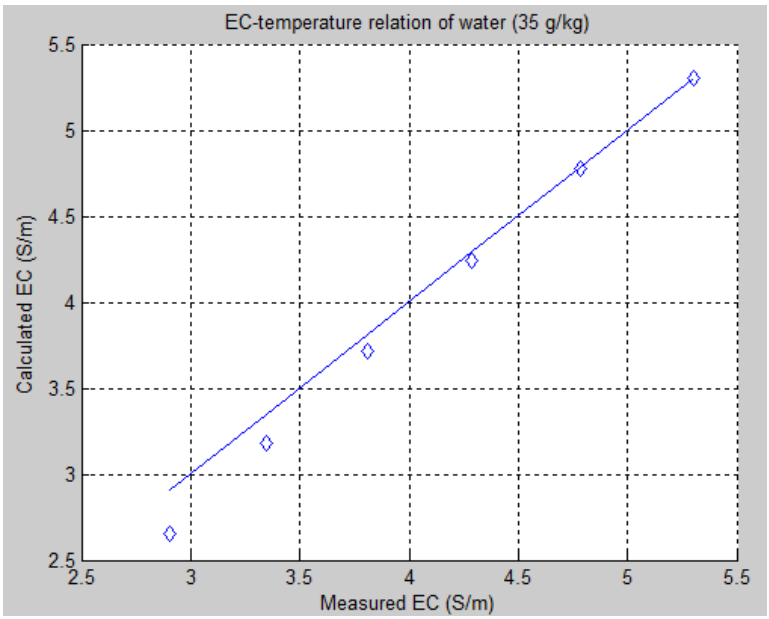

Figure 5.5 – Calculated and measured conductivities of seawater (salinity = 35 g/kg)

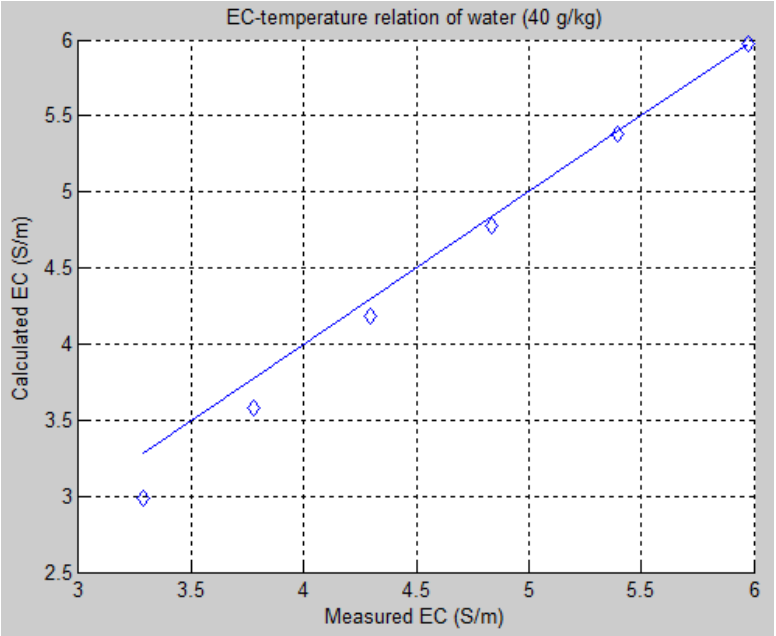

Figure 5.6 – Calculated and measured conductivities of seawater (salinity = 40 g/kg)

Comparison between calculated and measured seawater conductivities shows that equation 5.6 is reasonably accurate with a maximum error margin of less than 0.3 S/m. Therefore, the linear EC-temperature relation would be adequate for the purpose of this research. Further studies may still be necessary since the effect of salinity on the conductivity of water is not yet understood.

5.2 Validation study 1: remote sensing of soil moisture

The method described in this thesis requires real-time measurements of Loran-C time delay variations. In the following study, the measured delay variations of Loran-C signals transmitted from the Lessay station in Northern France and received at Bath between February 1, 2012 and February 21, 2012 was used. The 100 kHz pulses were recorded using a wideband low-frequency receiver deployed at the University of Bath. For technical details about the receiver, the reader is referred to [59].

Figure 5.6 – The wide-band digital low-frequency radio receiver used for recording Loran-C signals (Photograph from [59]).

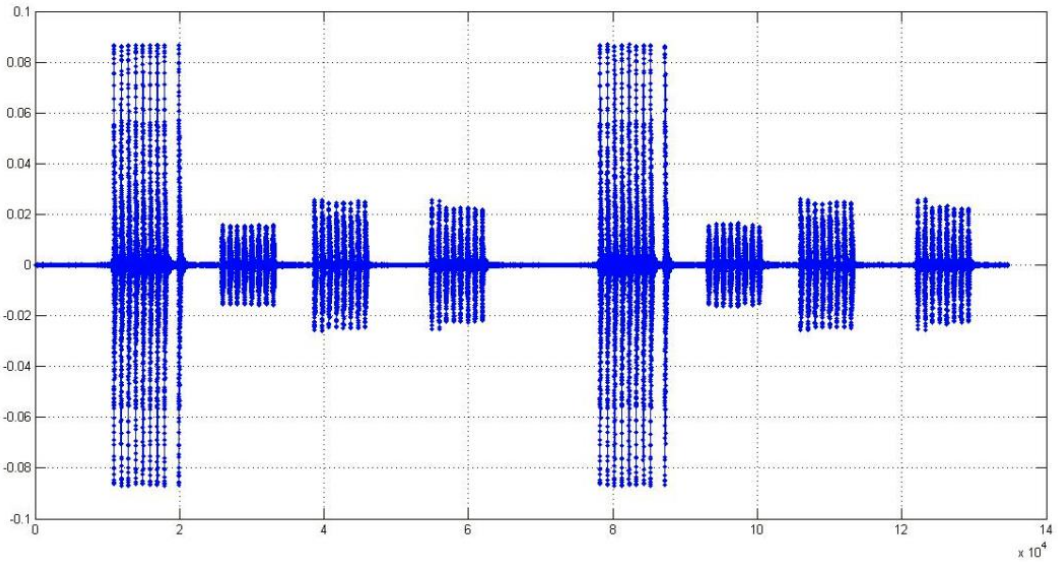

Figure 5.7 – A time-averaged PCI group (2 GRI groups) received in Bath from the Lessay Loran-C chain. The pulse groups are in the order of Lessay (France), Soustons (France), Anthorn (UK) and Sylt (Germany).

.

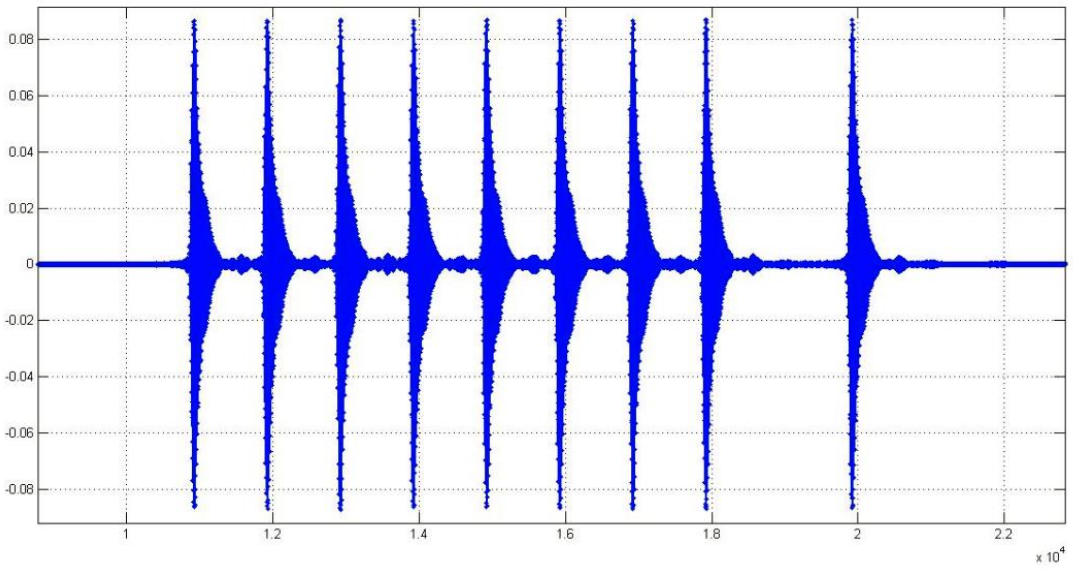

Figure 5.8 – A group of 9 Loran-C pulses received from the Lessay master station.

The received Loran-C waveforms were averaged over 20 seconds, and the variations in time delay was computed by comparing all the pulses with a reference pulse. In Figure 5.9, each data sample in the time series represents the deviation in the delay with respect to the delay of a pulse received on February 18, 2012.

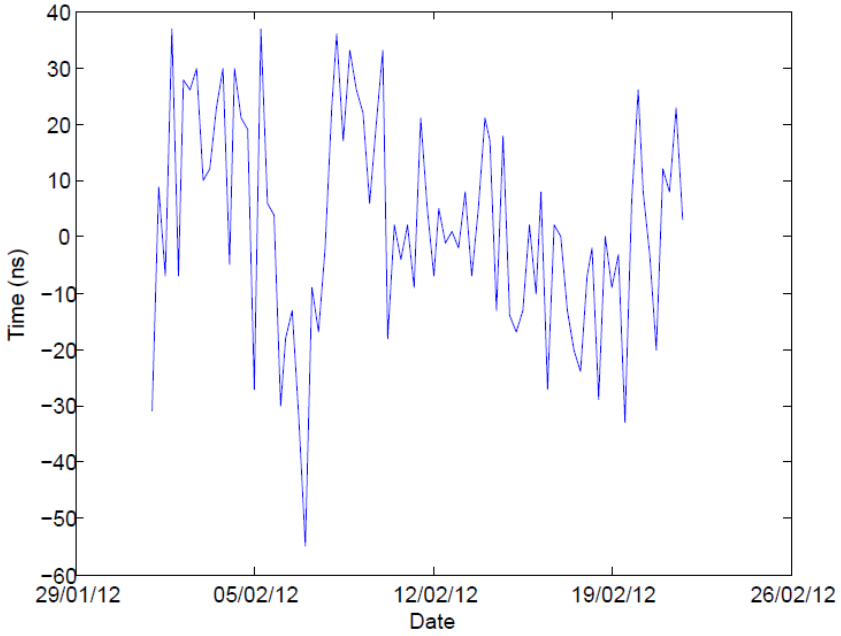

Figure 5.9 – Measured Loran-C delay variations along the propagation path between Lessay and Bath

Measured Loran-C delay variations at around 00:00, 06:00, 12:00, and 18:00 coordinated universal time (UTC) were selected for each day for comparison with the interim reanalysis data from the European Centre for Medium-Range Weather Forecasts (ECMWF). The temporal resolution of this model data is 6 hours.

The modeled soil temperature and soil moisture at 1.5° × 1.5° spatial resolution were retrieved from the interim reanalysis. For the interim reanalysis, the ECMWF adopts a multilayer model where the soil is discretized into four layers. The first three layers: 0 to 7 cm, 7 to 28 cm, and 28 to 100 cm, are considered here. For an overview of the ECMWF's data assimilation system, the reader is referred to [60].

The Loran-C propagation path between Lessay and Bath is approximately 250 km in length. It consists of a seawater section and two land sections. Over the 3-week measurement period, precipitation occurred along both land paths. However, the French section of the Loran-C path is unsuitable for validation studies as the signals have to travel across a very narrow coastal region. Therefore, the location for the retrieval of the ECMWF data is chosen to be between Bath and the south coast of England (~95 km). Since the ECMWF data set is on a 1.5° × 1.5° Gaussian grid, the retrieved soil moisture represents the entire English section of the Loran-C path.

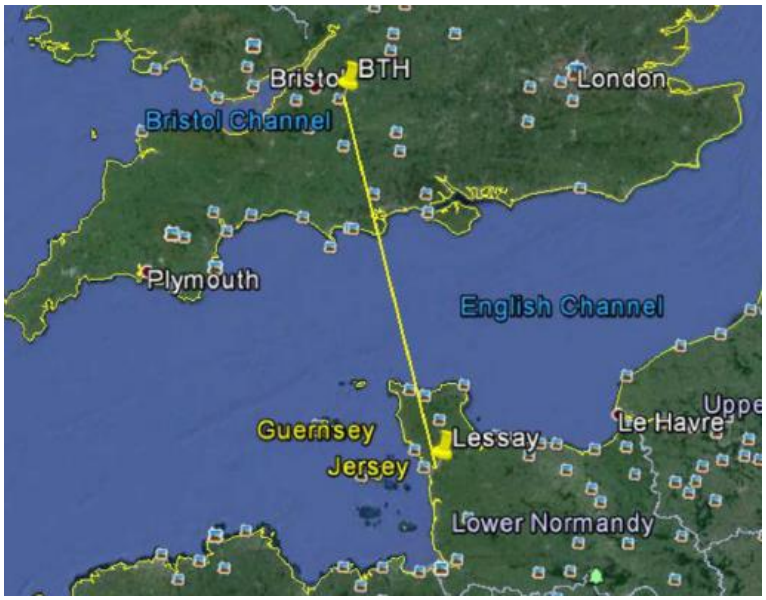

Figure 5.10 – The Loran-C signal propagation path between Lessay and Bath (Image from Google Earth)

The diagram below shows the procedures of estimating soil moisture using the Loran-C method:

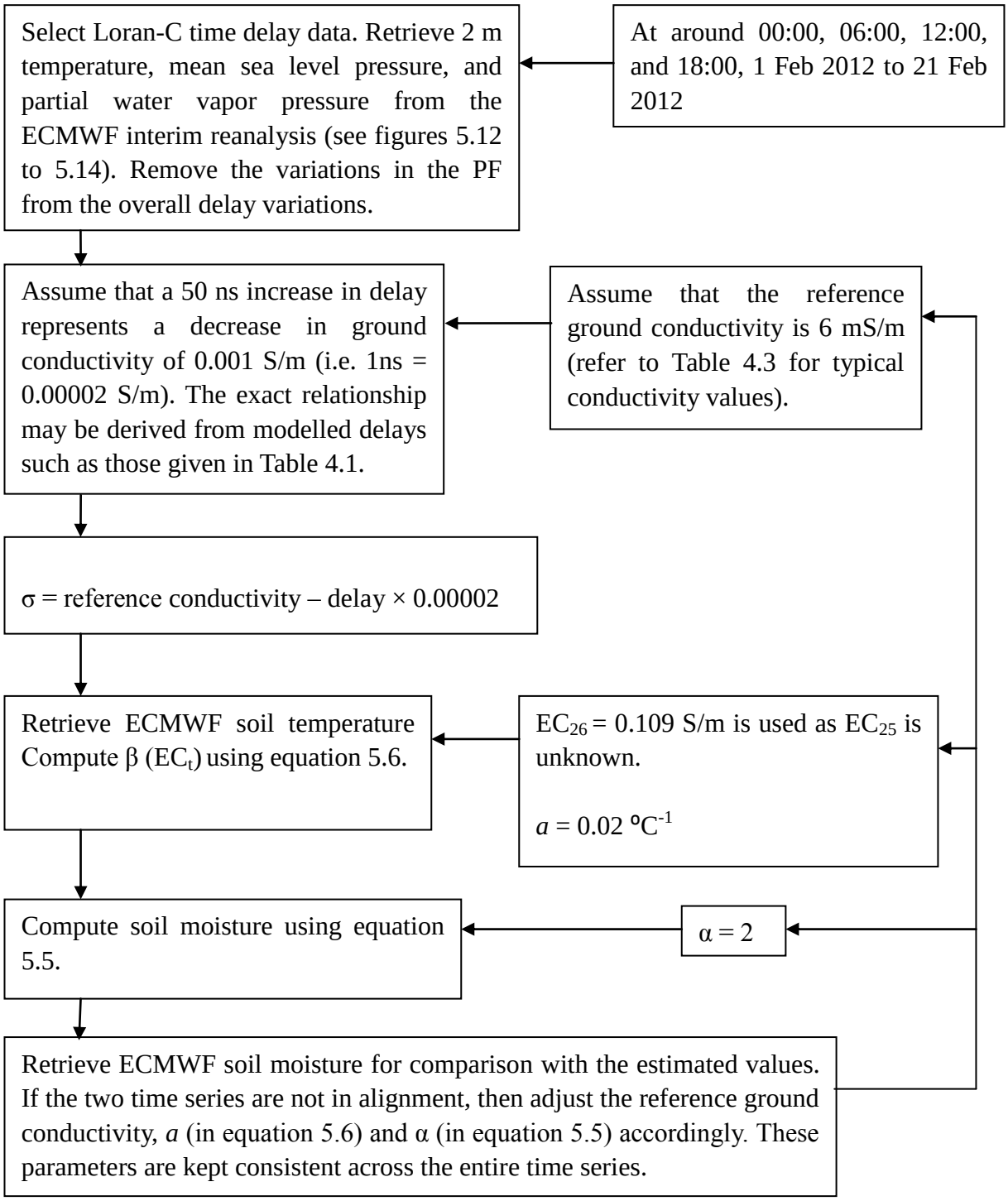

Figure 5.11 – The Loran-C method of estimating soil moisture

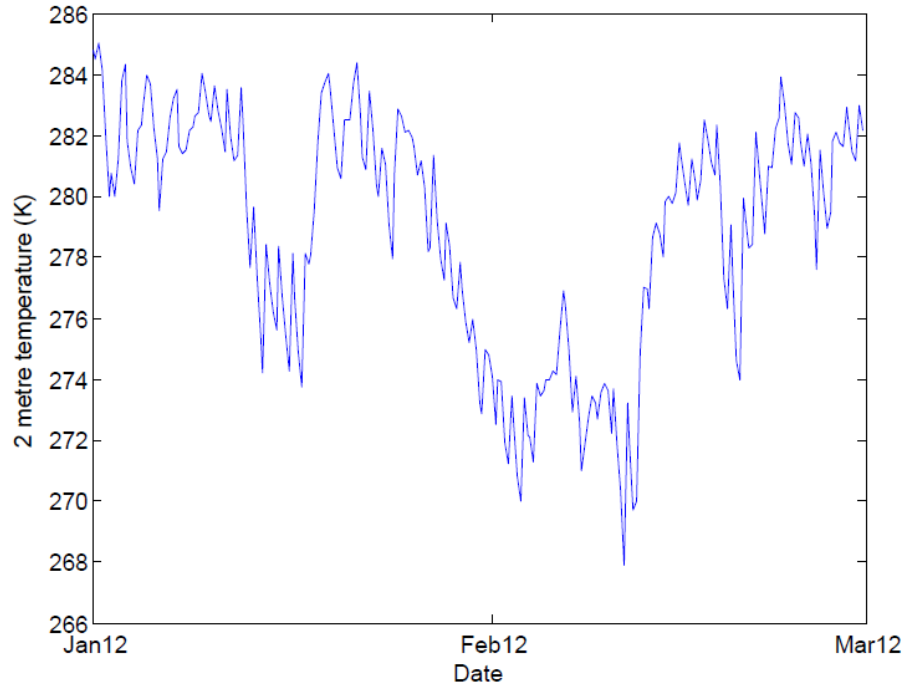

Figure 5.12 – 2 m temperature (Data from the ECMWF)

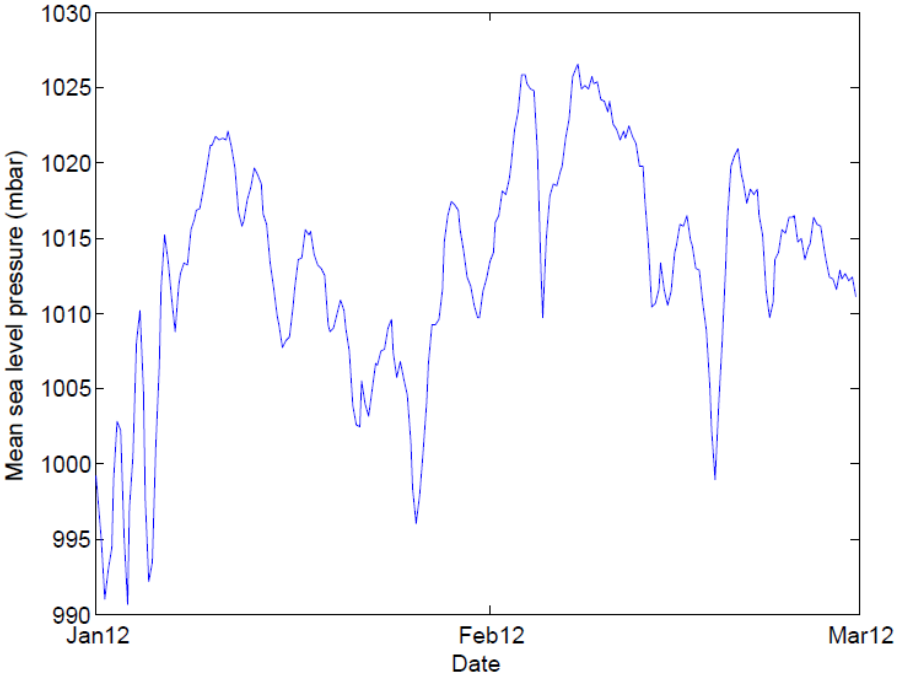

Figure 5.13 – Mean sea level pressure (Data from the ECMWF)

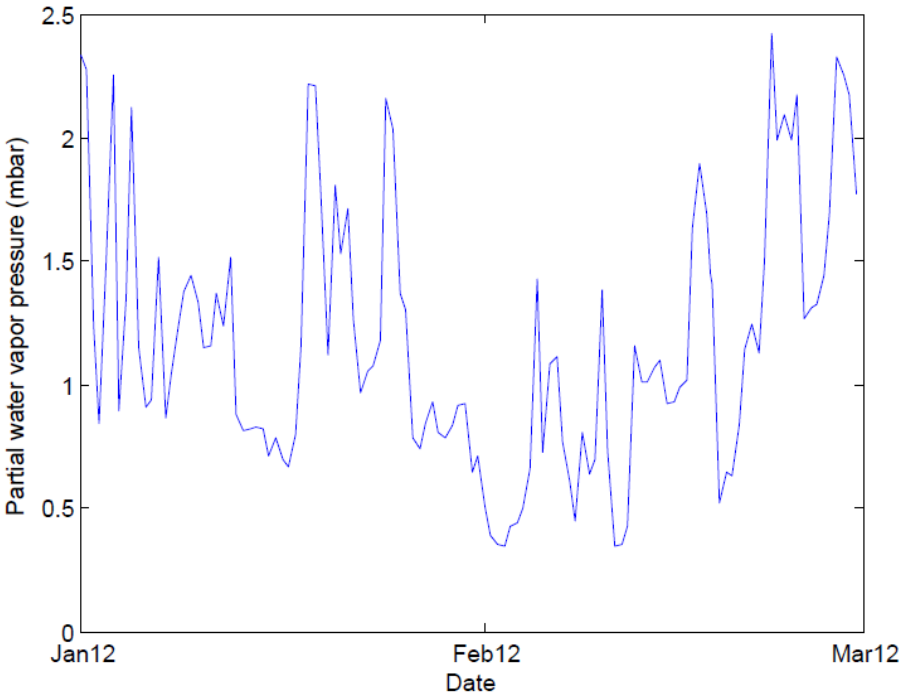

Figure 5.14 – Partial water vapor pressure (Data from the ECMWF)

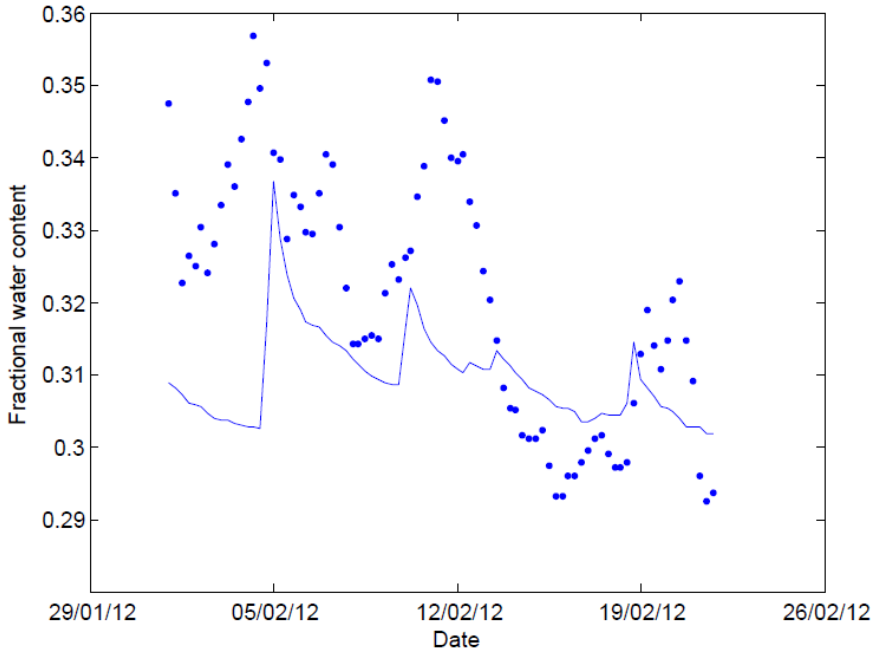

Figure 5.15 – Comparison of the ECMWF soil moisture product (solid line) and the Loran-C estimated soil moisture (dashed line) for the 0-7 cm layer

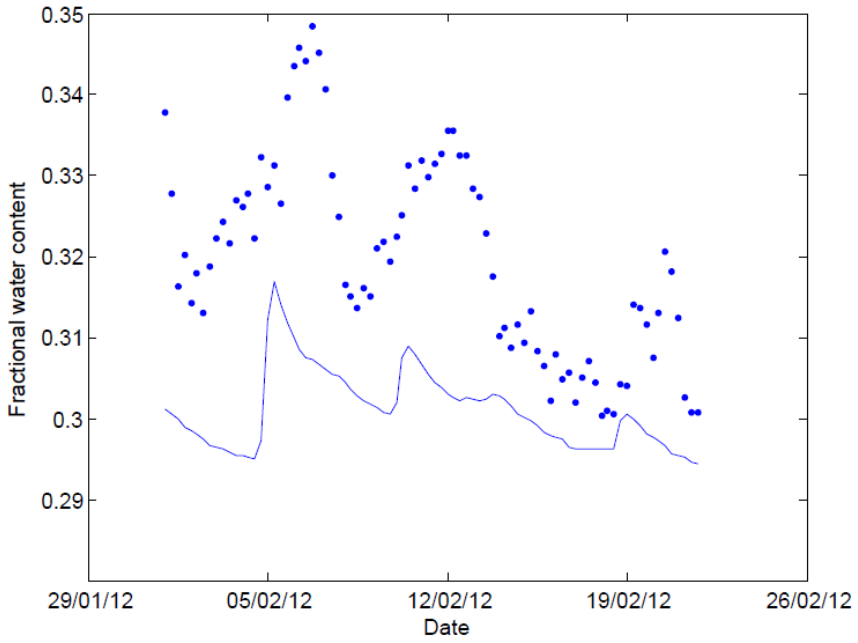

Figure 5.16 – Comparison of the ECMWF soil moisture product (solid line) and the Loran-C estimated soil moisture (dashed line) for the 7-28 cm layer

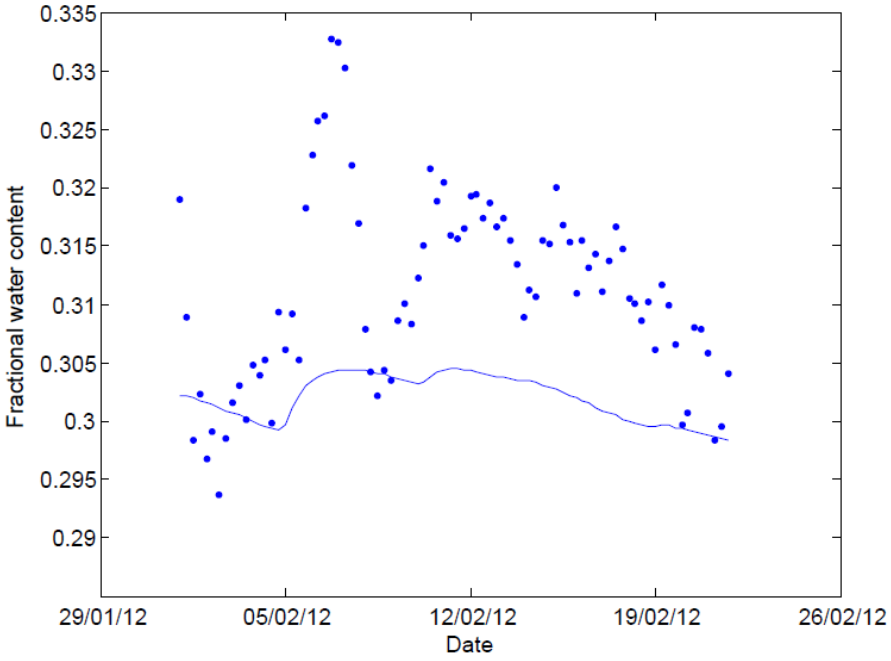

Figure 5.17 – Comparison of the ECMWF soil moisture product (solid line) and the Loran-C estimated soil moisture (dashed line) for the 28-100 cm layer

The time series comparison of the ECMWF soil moisture and the Loran-C estimated soil moisture for the uppermost soil layer (0 to 7 cm) shows good correspondence between the two data sets. For the second layer (7 to 28 cm), however, the estimated soil moisture reveals an apparent wet bias. This is as expected because in figure 5.15, a nominal value of 6 mS/m was chosen as the ground conductivity at the time of the reference delay. The purpose of this was to bring the two sets of values into alignment.

The second layer is less affected by precipitation than the surface layer and is therefore drier overall. This means that the reference conductivity needs to be slightly lowered for this layer (see figure 5.18). The third layer (28 to 100 cm) is insensitive to precipitation, so the Loran-C method was unable to produce an accurate estimation of soil moisture for this layer.

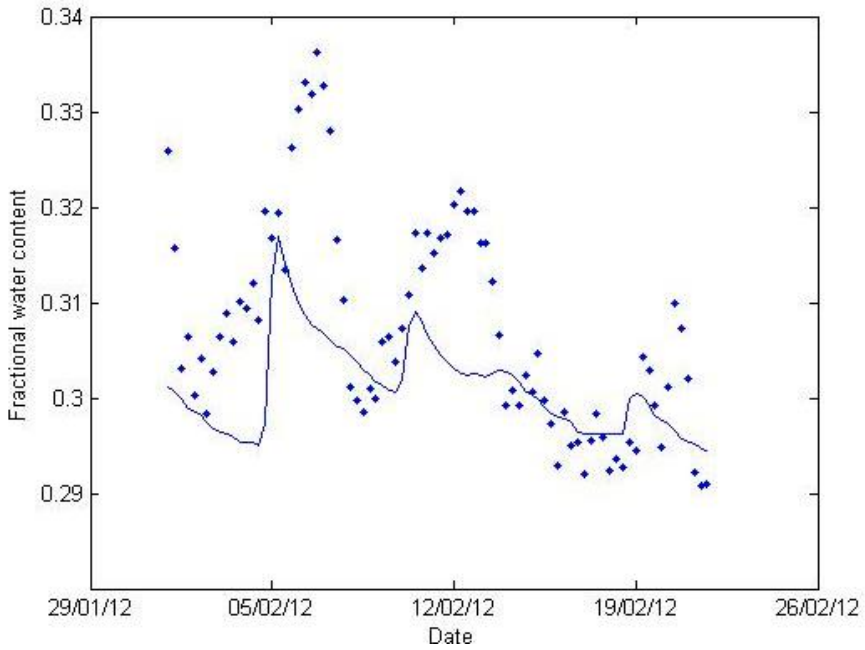

Figure 5.18 – Comparison of the ECMWF soil moisture product (solid line) and the Loran-C estimated soil moisture (dashed line) for the 7-28 cm layer, where the reference conductivity is lowered from 6 mS/m to 5.6 mS/m.

The Loran-C estimated soil moisture in figures 5.15 to 5.18 was computed using the ECMWF soil temperature data at the corresponding depth. A good agreement was obtained after combining the data for the first two layers of soil (see figures 5.19 and 5.20), with linear correlation coefficient $\rho = 0.5808$ and significance level $p = 9\times10^{-9}$.

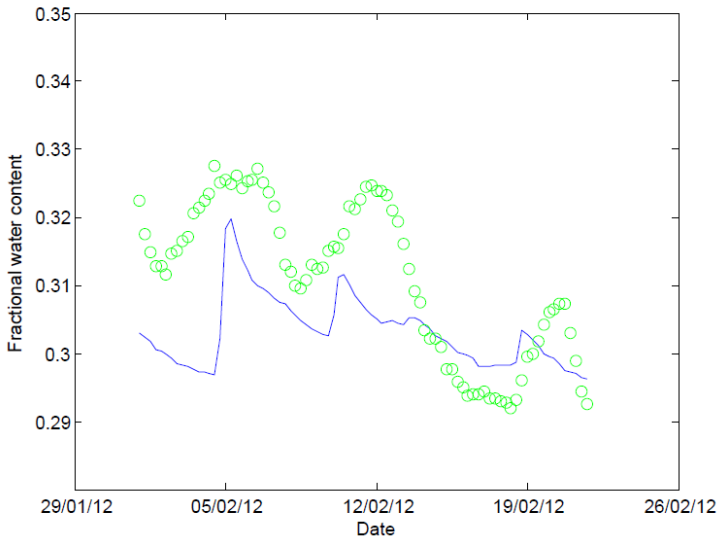

Figure 5.19 – Comparison of the ECMWF soil moisture product (solid line) and the Loran-C estimated soil moisture (dashed line) for the 0-28 cm layer

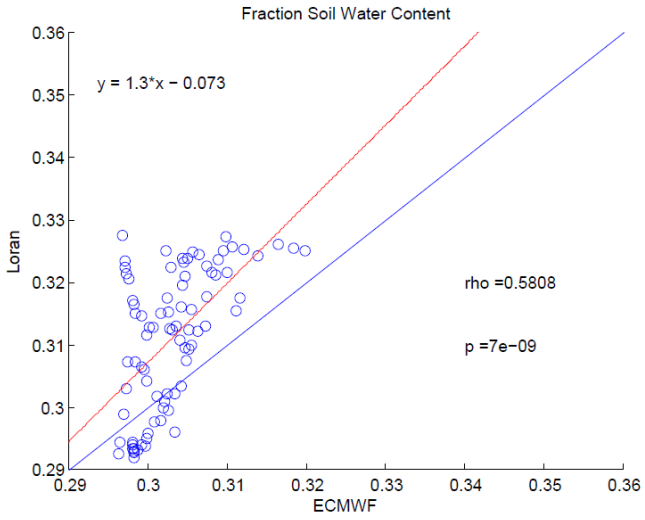

Figure 5.20 – Scatter plot for figure 5.18. The blue line indicates y=x, and the red line is the line of best fit.

Interestingly, combining soil layers 1, 2 and 3 produces a better correlation (see figures 5.21 and 5.22). This could be due to the fact that the 28 to 100 cm layer soil moisture, which varies much slower with time, had smoothed out the distinct transient increases in soil moisture seen in the upper layers. However, the soil moisture appears to have been significantly overestimated because the reference conductivity chosen for the 0-7 cm layer (6 mS/m) was used in this analysis.

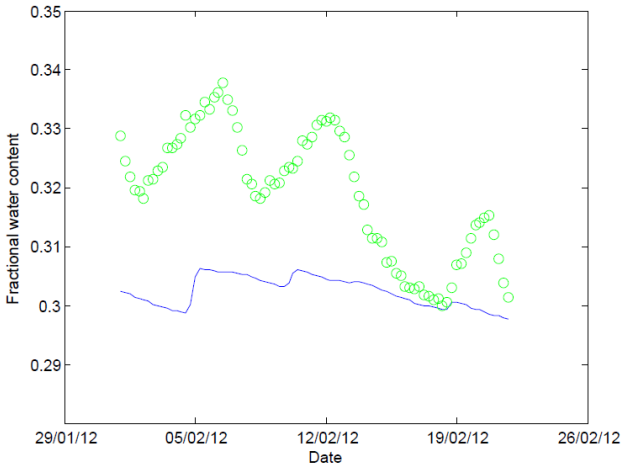

Figure 5.21 – Comparison of the ECMWF soil moisture product (solid line) and the Loran-C estimated soil moisture (dashed line) for the 0-100 cm layer

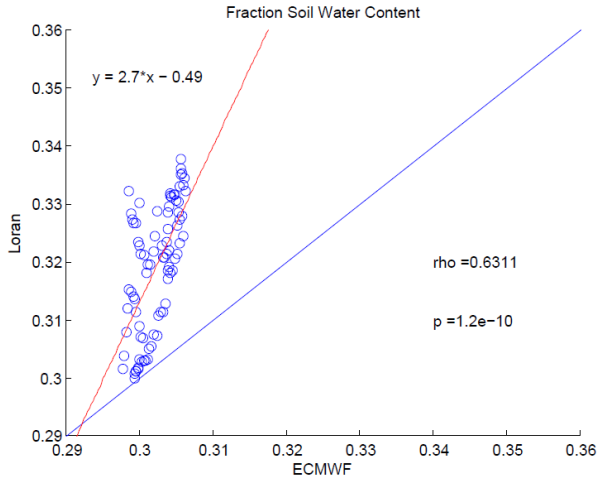

Figure 5.22 – Scatter plot for figure 5.21. The blue line indicates y=x, and the red line is the line of best fit.

Overall, the Loran-C method has slightly overestimated the soil moisture in southern England. The most obvious reason is that precipitation events in northern France may have also contributed to the measured variations in Loran-C time delay. Additionally, the seawater section of the Loran-C path is approximately 105 km long. Any variations in sea surface conductivity would also influence the Loran-C delay. This is validated through a separate study in chapter 5.3.

5.3 Validation study 2: remote sensing of sea surface salinity

Sea surface Salinity is an essential parameter in the study of global ocean circulation and the water cycle. Current sources of salinity data include the European Space Agency's Soil Moisture and Ocean Salinity (SMOS) satellite [61], NASA's Aquarius satellite [62], the UK Met Office's Forecasting Ocean Assimilation Model (FOAM) [63], and *in situ* Argo floats [64].

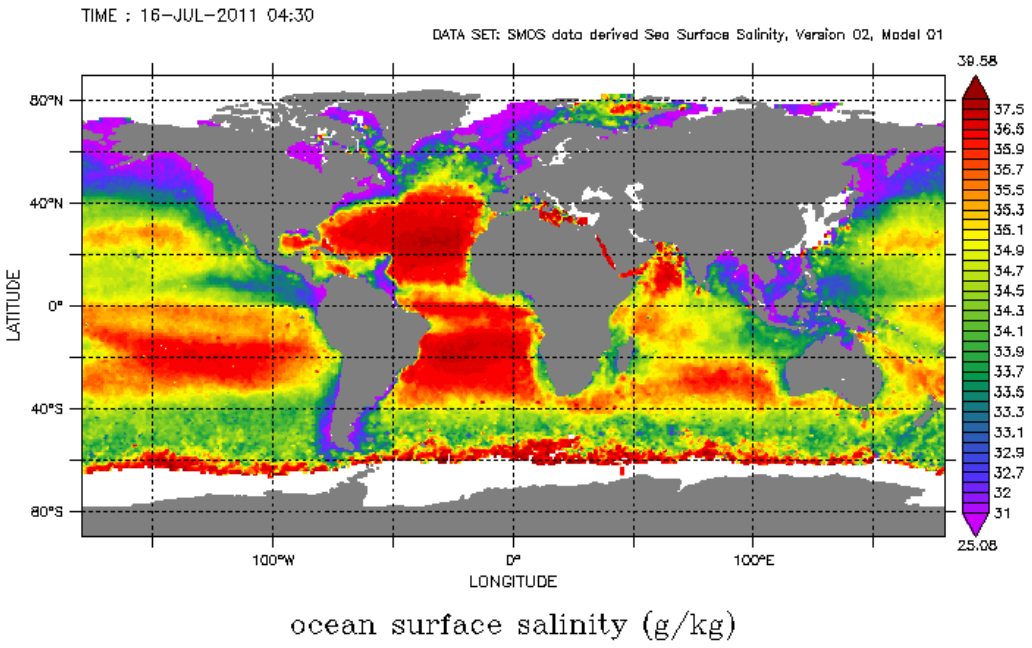

Figure 5.20 – Sea surface salinity from SMOS (Image from [65]).

At present, it is proving difficult to obtain continuous salinity data from either *in situ* or satellite measurements. For example, there are more than 3,000 Argo floats drifting in the World's oceans, each providing seawater temperature and salinity profiles with a temporal resolution of around 10 days. Both Argo and FOAM are capable of producing estimates of sea surface salinity down to 5 m.

In contrast, SMOS (launched in 2009) and Aquarius (launched 2011), which use passive L-band radiometers to determine brightness temperature of the sea surface, can only estimate the salt content in the top few centimetres. For this reason, satellite measurements are particularly sensitive to surface effects such as high wind speeds. Existing remote sensing methods are known to have problems in mid to high latitudes (due to RFI) and in cold waters.

This study attempts to explore a different approach to the current methods, by measuring the time delay variations of Loran-C signals transmitted over a path that consists entirely of seawater. For an all-seawater path, sea surface salinity must have a predominant effect on the measured delay variations.

The time delay variations of Loran-C signals transmitted between the German Sylt station and Harwich in the south east of England were computed using an integrated Loran-C/GPS receiver deployed in at Trinity House in Harwich. The resulting data, which covers a 17-month period between February 2010 and July 2011, has a temporal resolution of 30 seconds.

Figure 5.21 – The Loran-C signal propagation path between Sylt and Harwich (Image from Google Earth)

Atmospheric data fields (surface pressure, 2 m temperature) were retrieved from the ECMWF's Interim Reanalysis at 1° × 1° spatial resolution (Gaussian grid) and 24-hour temporal resolution (see figures 5.22 and 5.23). These were used to compute the PF, whose variations were removed from the overall delay variations. The partial pressure of water vapor (see equation 5.1) was ignored in this study as it has negligible effect on the refractivity *N*.

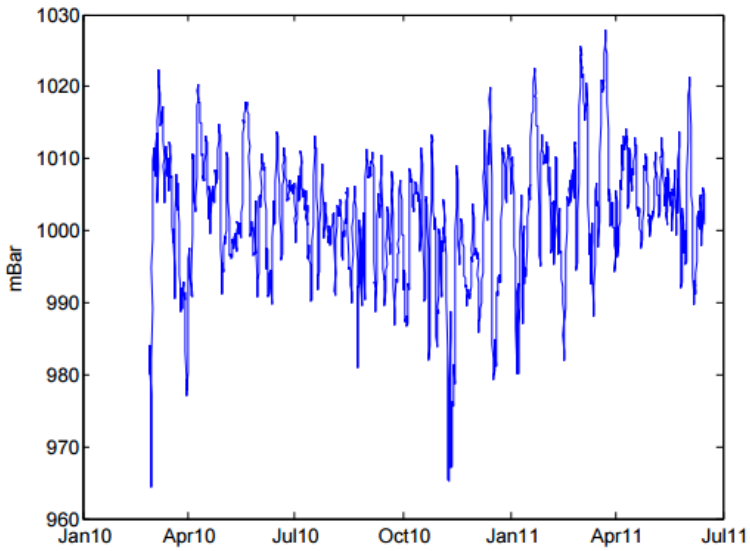

Figure 5.22 – Surface pressure (Data from the ECMWF)

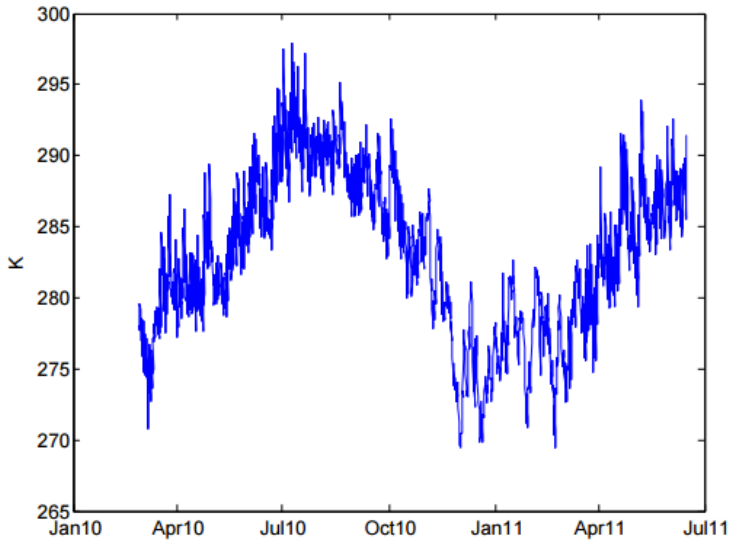

Figure 5.23 – 2 m temperature (Data from the ECMWF)

Sea surface temperature (SST) was also retrieved from the ECMWF at the same spatial and temporal resolution (see figure 5.24). The SST delay shown in figure 5.25 is based on the assumption that across the 560 km path, a 1 K increase in SST represents a 5.6 ns decrease in delay (i.e. 1 ns per 100 km per K). This was inferred from the modelled delays given in [52].

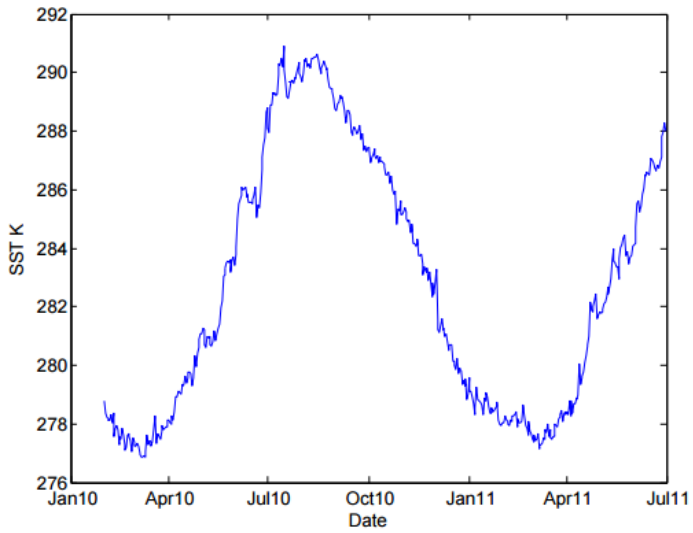

Figure 5.24 – Sea surface temperature (Data from the ECMWF)

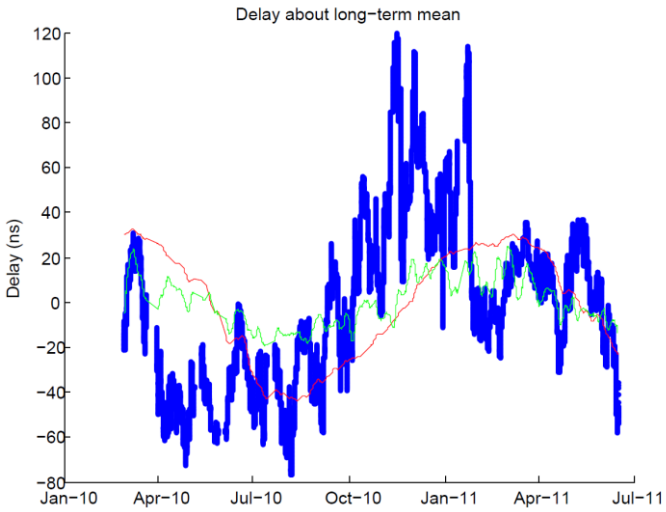

Figure 5.25 – Variations in the Loran-C delay (blue), the modelled atmospheric delay (green), and the modelled SST delay (red).

The modelled variations in the SST delay were also removed from the measured delay variations. The residual delay was compared to daily FOAM data (1° × 1° Latitude/Longitude grid) and monthly SMOS data (1° × 1° Cartesian grid) for the same period. In both cases, the validation data was retrieved at roughly the centre of the path. Aquarius was not used for validation because it is not within the time frame of the measurements. A 24-hour moving average filter was applied to the residual Loran-C delay in order to remove any daily variations which are unlikely to be due to salinity changes.

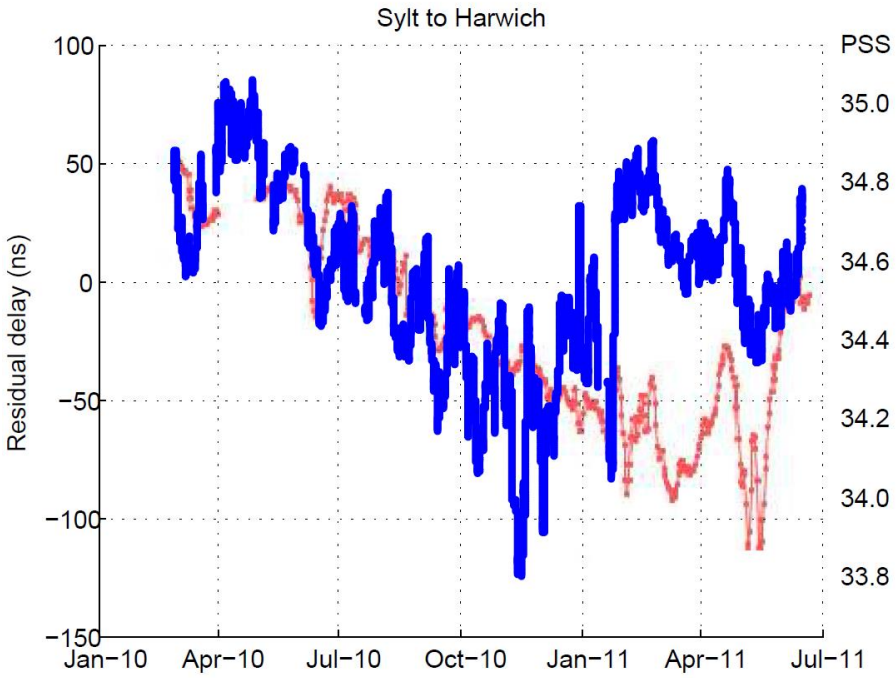

Figure 5.26 – Comparison of the inverted residual Loran-C delay (blue) and the daily FOAM salinity data (red).

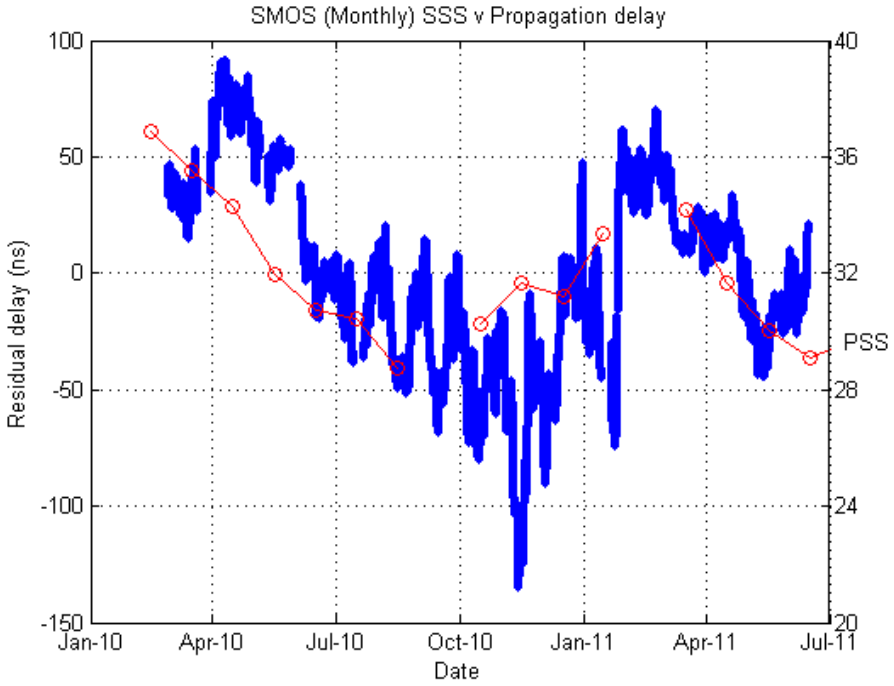

.

Figure 5.27 – Comparison of the inverted residual Loran-C delay (blue) and the monthly SMOS salinity data (red).

In figures 5.26 and 5.27, the residual Loran-C delay was inverted to reflect the variations in the conductivity of seawater. The FOAM data in figure 4.16 corresponds to the top 5 m layer of the ocean. SMOS, on the other hand, is only capable of producing salinity estimates for the top few cm of the sea surface. Since the Loran-C surface wave is not going to penetrate more than 1 m into seawater, the residual delay appears to be in better agreement with the monthly SMOS observations.

Figure 5.28 shows a scatter plot where the residual Loran-C delay data is interpolated onto the time for the SMOS data. The linear correlation coefficient ($\rho = 0.8488$) and significance level ($p = 6.3\times10^{-5}$) suggest that changes in the residual delay are largely echoed by the variations of sea surface salinity.

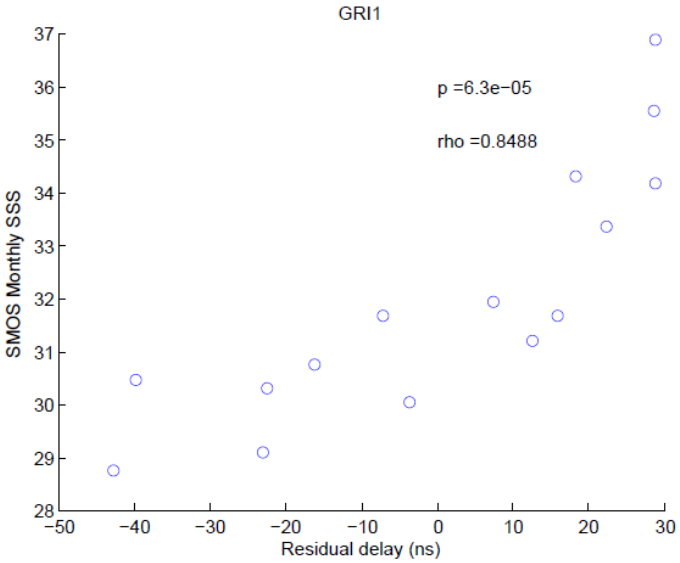

Figure 5.28 – Time-averaged scatter plot for figure 5.27

The sylt station is a dual-rated Loran-C station. It acts as the master station of the Sylt chain as well as a secondary station of the Lessay chain. The delay variations presented in the previous figures were computed using Lessay chain signals. As shown in figures 5.28 and 5.29, similar results were obtained using Loran-C signals received from the Sylt chain.

Name	**Type**	**ED (µs)**	**Power (kW)**
Lessay	M	0	250
Soustons	X	13000	250
Anthorn	Y	27300	250
Sylt	Z	42100	250

Table 5.3 – Stations of the Lessay Loran-C chain (GRI 6731)

Name	Type	ED (µs)	Power (kW)
Sylt	M	0	250
Lessay	X	14100	250
Vaerlandet	Y	29500	250

Table 5.4 – Stations of the Sylt Loran-C chain (GRI 7499)

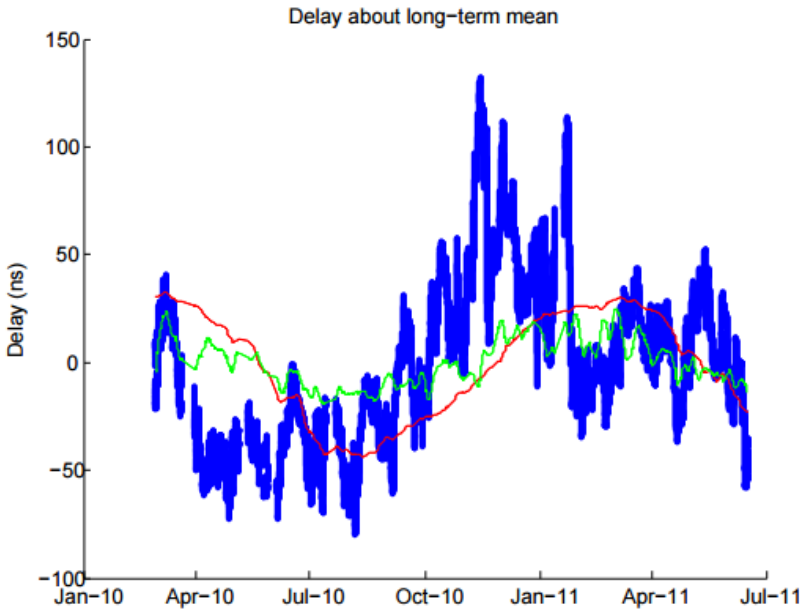

Figure 5.28 - Variations in the time delay of Loran-C signals transmitted by $Sylt_{GRI\_7499}$ (blue), the modelled atmospheric delay (green), and the modelled SST delay (red).

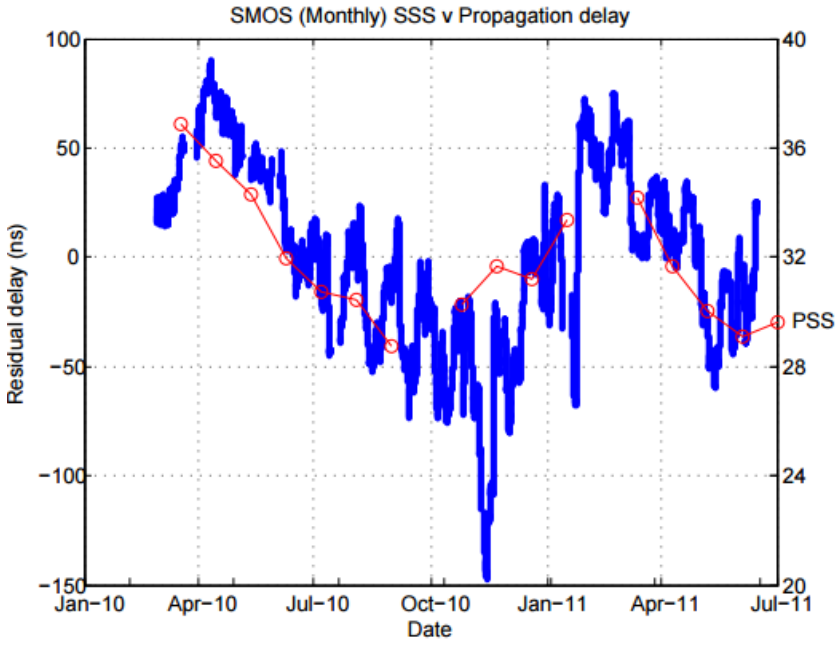

Figure 5.29 – Comparison of the inverted residual Loran-C delay for $Sylt_{GRI\_7499}$ (blue) and the monthly SMOS salinity data (red).

Chapter 6

Conclusions and future work

6.1 Conclusions

This thesis has presented a novel method for the continuous monitoring of wide-area soil moisture. The ability to remotely sense the temporal variation of soil moisture on an adequate spatial scale is essential for geophysical and environmental studies. Soil moisture can be determined from *in situ* measurements, remote sensing, and hydrological models. *In situ*, or point measurements are unable to reveal the spatial distribution of soil moisture, unless a network of instruments is deployed. This is not only prohibitively expensive but also impractical.

Remote sensing is the preferred method of collecting soil moisture data over wide areas on a routine basis. The data, however, is not exactly continuous because of infrequent satellite revisit time. Additionally, the microwave retrieval depth of a few centimetres is not ideal for most applications. Compared to satellite remote sensing, hydrological models can produce data with much improved temporal resolution and observation depth. The main drawback is that these models require a lot of external data, and the model parameters are difficult to determine.

The objective of this research was to explore a method which could overcome the above limitations. It has been proved that the new method was able to produce estimates of wide-area soil moisture with better continuity and observation depth than microwave remote sensing. Also, a simplified algorithm makes it less dependent on external data than any of the current soil moisture retrieval algorithms or models.

The Loran-C method described in this thesis makes an interesting use of low-frequency navigation signals. Loran-C is a hyperbolic navigation system where the position of the user is determined from the time delay of 100 kHz signals transmitted by a network of terrestrial stations. Each Loran-C chain, often consisting of 3 to 4 stations, emits groups of pulses in a pre-defined sequence.

At the frequency used by Loran-C, transmissions occur in the form of ground waves and sky waves. The ground wave follows the curvature of the earth and arrives earlier than the sky wave due to shorter path length. The unique shape of the received pulse makes it easy to identify the ground wave component and determine its arrival time. The variation in the time delay of Loran-C ground waves gives an indication of conductivity changes along their path. The latter is influenced by atmospheric and land surface dynamics.

This thesis described two validation studies. In the first study, an analysis was carried out using the time delay of Loran-C signals recorded over a 3-week period in Bath, from the Lessay station in Northern France. Model data from the ECMWF were used for calculation, calibration, and inter-comparison. Relatively good correspondence between the Loran-C estimated soil moisture and the ECMWF product was found for a soil depth of 0 to 28 cm.

The first validation study discovered that there are properly timed variations in ground conductivity associated with precipitation events. These variations show a time evolution which best matches soil moisture changes with a depth of up to 28 cm in the land surface model. This represents an improvement over satellite measurements in terms of not only the temporal resolution but also the observation depth.

The soil moisture estimated using the Loran-C method requires an assumption of soil conductivity at a reference time and location. This means an external source of soil moisture data is needed in order to initialise the Loran-C soil moisture retrievals. Spaceborne measurements would be the most suitable option as model data are often not available instantaneously. Validation results suggest that the chosen reference conductivity need to be lowered for the layer between 7 and 28 cm because of drier soil conditions.

This thesis also introduced a potential method for the remote sensing of sea surface salinity based on the time delay variations of Loran-C signals measured over 17 months across an all-seawater path between the Sylt station in Germany and Harwich in the UK. Results of the second validation study show that these variations may be explained partly by changes in sea surface temperature and atmospheric conditions. Subtracting these two components, the residual delay revealed a temporal variation similar to that of the sea surface salinity obtained by the SMOS satellite.

In conclusion, the Loran-C remote sensing method could eventually become a standard technique of measuring soil moisture and ocean salinity. The prospect of this depends on further validation results and extended research projects. Some of the possible future research areas are discussed in the following section.

6.2 Direction for future work

The emphasis of thesis has been on exploring a suitable method for improving the temporal sampling of wide-area soil moisture. The Loran-C time delay data used in the first study came from a receiver unit deployed in Bath (BTH). Three other units have been deployed in France – Lannemezan (LMZ), Orleans (ORL) and Rustrel (RST). All of them are capable of receiving Loran-C signals sent by transmitters which belong to the Lessay chain.

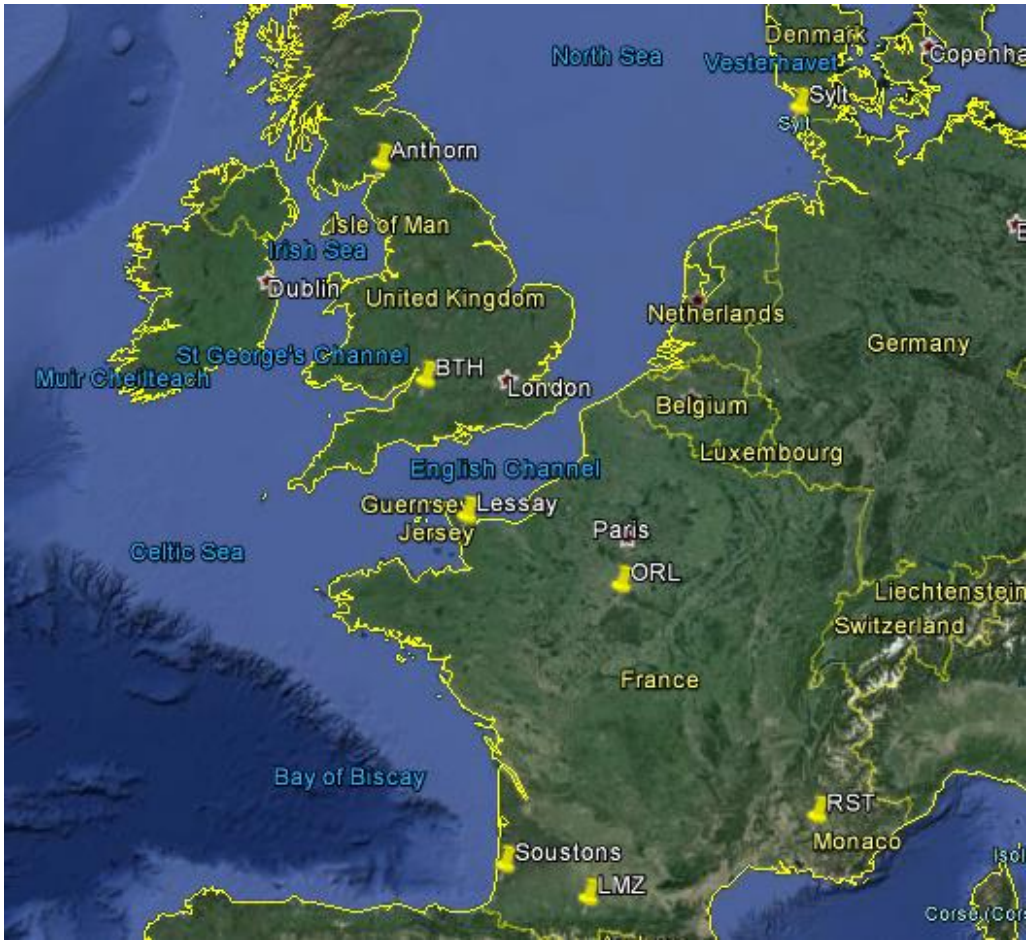

Figure 6.1 – Locations of the four receivers deployed in Bath and France

Since there are four Loran-C stations in the Lessay chain, the receivers being deployed can set up a total of 16 propagation routes. The next step is to select some of these paths, and then conduct a similar analysis to that already described in this thesis to further examine the current approach. The most suitable path should be relatively short and consist entirely (or mostly) of land. Results from these studies will determine whether the current method is able to deliver consistent level of accuracy. This time more validation sources should be considered, especially the latest Soil Moisture Active and Passive (SMAP) mission.

The Loran-C method requires signals to be converted to a numerical format, where the Time of Arrival (TOA) and delay deviation are clearly listed. The data file is then manipulated in combination with external data for calculation, calibration and validation. In the first study, the delay variation was computed from recorded waveforms using MATLAB. It would be interesting to find out if the programs could be slightly modified to measure the delay variation between pairs of receivers.

In fact, the commercial receiver used in the second validation study may be suitable for this purpose because it is specifically designed for Loran-C ASF measurements, which means the data processing is achieved automatically by receiver. The twin-receiver approach is particularly significant for mixed paths such as that between Lessay and Bath (see figure 6.2). Deploying extra receivers at points B and C would allow each of the three homogenous sections to be studied separately.

Figure 6.2 – Locations for the deployment of extra receivers (B and C) along the path between Lessay and Bath

A field campaign may be carried out given the further validation studies produce promising results and that the twin-receiver set-up is feasible. This would involve a network of receivers being deployed across a catchment. Time delay measurements could be made at differing weather conditions, and the duration of the campaign is governed by the capacity of the receiver running unattended.

During the field campaign, the receivers may be deployed in different configurations. For example, they could either be laid out, at uniform spacing, on a line towards a Loran-C transmitter, or in a hexagon where most pairs of receivers lie on a line to one of several transmitters. The hexagonal deployment, in particular, could be used to examine if the Loran-C method is capable of providing 2D maps of soil moisture. The twin-receiver set-up is also essential for future ocean salinity studies, which would hopefully utilise not only the costal transmitters near the receivers, but also the ones which are located further inland.

An uncertainty in the Loran-C method is that it has to rely upon real-time atmospheric and land surface measurements for instantaneous sampling of soil moisture. In a field campaign, the collection of these data will need to be carried out simultaneously with the time delay measurements.

Another issue is that Loran-C signals are transmitted far more frequently than that is necessary for the purpose of conductivity retrieval. This explains why the recorded pulses were averaged and then filtered in the studies described in this thesis. A potential alternative to Loran-C is the low-frequency time signals such as the DCF77, which have a carrier frequency of 77.5 kHz. They enjoy the advantage over Loran-C that their Time-of-Transmission (TOT) could be interpreted from the shape of each individual pulse. This means that rather than having to record them continuously, it would be possible to use the pulses at selected times for analysis. However, only further studies can prove whether the time delay of these signals may be computed in a similar way to Loran-C signals.

Figure 6.3 – Antennas of DCF77 in Mainflingen, Germany (Image from [66])

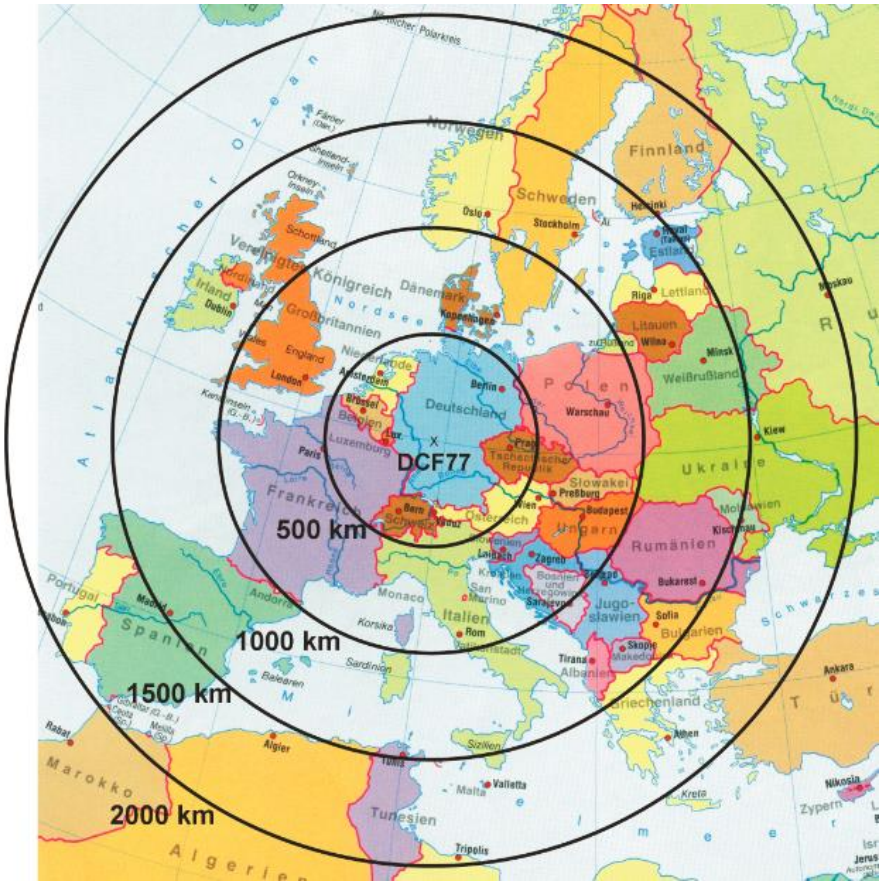

Figure 6.4 – Reception area of DCF77 time signals (Image from [67])

References

[1] Warrick, A. W., 2003. *Soil Water Dynamics*. Oxford: Oxford University Press.

[2] Engman, E. T., 1991. Application of Microwave Remote Sensing of Soil Moisture for Water Resources and Agriculture. *Remote Sensing of Environment*, 35, pp. 213-226.

[3] Wood, E. F., Lin, D. S., Mancini, M., Thongs, D. J., Troch, P. A., Jackson, T. J., Famiglietti, J. S., and Engman, E. T., 1993. Intercomparisons Between Passive and Active Microwave Remote Sensing and Hydrological Modeling for Soil Moisture. *Advances in Space Research*, 13(5), pp. 167-176.

[4] Jackson, T. J., Schmugge, T. J., Nicks, A. D., Coleman, G. A., and Engman, E. T., 1981. Soil Moisture Updating and Microwave Remote Sensing for Hydrological Simulation. *Hydrological Sciences Bulletin*, 26(3), pp. 305-319.

[5] Jackson, T. J., Hawley, M. E., and O'Neill, P. E., 1987. Preplanting Soil Moisture Using Passive Microwave Sensors. *Water Resources Bulletin*, **23**(1), pp. 11-19.

[6] Engman, E. T., 1990. Progress in Microwave Remote Sensing of Soil Moisture. *Canadian Journal of Remote Sensing*, 16(3), pp. 6-14.

[7] Engman, E. T., 1992. Soil Moisture Needs in Earth Sciences. *Proceedings of the International Geoscience and Remote Sensing Symposium (IGARSS), pp.* 477-479.

[8] Betts, A. K., Ball, J. H., Baljaars, A. C. M., Miller, M. J., and Viterbo, P., 1994. Coupling Between Land-Surface, Boundary-Layer Parameterizations and Rainfall on Local and Regional Scales: Lessons from the Wet Summer of 1993. *Fifth Conference on Global Change Studies: American Meteorological Society,* Nashville, 174 -181.

[9] Su, Z., Troch, P. A., de Troch, F. P., Nochtergale, L., and Cosyn, B., 1995. Preliminary Results of Soil Moisture Retrieval From ESAR (EMAC 94) and ERS-1/SAR, Part II: Soil Moisture Retrieval. *Proceedings of the second workshop on hydrological and microwave scattering modelling for spatial and temporal soil moisture mapping from ERS-1 and JERS-1 SAR data and macroscale hydrologic modelling,* Institute National de la Recherche Agronomique, Unité de Science du Sol et de Bioclimatologie, France, pp. 7-19.

[10] Topp, G. C., Davis, J. L., and Annan, A. P., 1980. Electromagnetic Determination of Soil Water Content: Measurements in Coaxial Transmission Lines. *Water Resources Research,* 16(3), pp. 574-582.

[11] Saha, S. K., 1995. Assesment of Regional Soil Moisture Conditions by Coupling Satellite Sensor Data with a Soil-Plant System Heat and Moisture Balance Model. *International Journal of Remote Sensing*, 16(5), pp. 973-980.

[12] Entekhabi, D., Nakamura, H., and Njoku, E. G., 1994. Solving the Inverse Problem for Soil Moisture and Temperature Profiles by Sequential Assimilation of Multifrequency Remotely Sensed Observations. *IEEE Transactions on Geoscience and Remote Sensing,* 32(2), pp. 438-448.

[13] Giacomelli, A., Bacchiega, U., Troch, P. A., and Mancini, M., 1995. Evaluation of Surface Soil Moisture Distribution by Means of SAR Remote Sensing Techniques and Conceptual Hydrological Modelling. *Journal of Hydrology*, 166, pp. 445-459.

[14] Entekhabi, D., Nakamura, H., and Njoku, E. G., 1993. Retrieval of Soil Moisture by Combined Remote Sensing and Modeling. *ESA/NASA International Workshop on Passive Microwave Remote Sensing Research Related to Land-Atmosphere Interactions*, St. Lary, France, pp. 485-498.

[15] Jackson, T. J., 1982. Survey of Applications of Passive Microwave Remote Sensing for Soil Moisture in the USSR. *EOS Transactions of the American Geophysical Union*, 63(19), pp. 497-499.

[16] Ottlé, C., and Vidal-Madjar, D., 1994. Assimilation of Soil Moisture Inferred from Infrared Remote Sensing in a Hydrological Model Over the HAPEX-MOBILHY Region. *Journal of Hydrology,* 158, pp. 241-264.

[17] Soil Moisture Estimation using Remote Sensing [online]. Available: http://users.monash.edu.au/~jpwalker/papers/hydro02.pdf.

[18] Scheftic, W., Cummins, K.L., Krider, E.P., Sternberg, B.K., Goodrich, D., Moran, S. and Scott, R., 2008. Wide-area soil moisture estimation using the propagation of lightning generated low-frequency electromagnetic signals. *Proceedings of the 20th International Lightning Detection Conference*, Tucson, Arizona, USA, pp. 1–8.

[19] Schmugge, T. J., Jackson, T. J., and McKim, H. L., 1980. Survey of Methods for Soil Moisture Determination. *Water Resouroces Research*, 16(6), pp. 961-979.

[20] Chanasyk, D. S., and Naeth, M. A., 1996. Field measurement of soil moisture using neutron probes. *Canadian Journal of Soil Science*, 76(3), pp. 317–323.

[21] Measurement of Soil Water [online]. Available: http://soils.ag.uidaho.edu/soil205-90/Lecture%205.

[22] Zazueta, F. S., and Xin, J., 1994. Soil moisture sensors. Bull. 292, Florida Cooperative Extension Service, Institute of Food and Agricultural Sciences, University of Florida.

[23] Dobriyal, P., Qureshi, A., Badola, R., and Hussain, S. A., 2012. A review of the methods available for estimating soil moisture and its implications for water resource management, *Journal of Hydrology*, 458-459: 110-117.

[24] Amer, S. A., Keefer, T. O., Weltz, M. A., Goodrich, D. C., and Bach, L. B., 1994. Soil moisture sensors for continuous monitoring. *Water Resources*, 30, pp. 69–83.

[25] [online]. Available: http://www.mesasystemsco.com/category.php?cat=3.

[26] Dela, B.F., 2011. Danish Building and Urban Research. *Measurement of soil moisture using gypsum blocks*.

[27] [online].
Available: https://www.enviromonitors.co.uk/shop/tdr100-soilmoisture.

[28] Topp, G. C., and Davis, J. L., 1985. Measurement of soil water content using time-domain reflectometry (TDR): a field evaluation. *Soil Science Society of America Journal*, 49, pp. 19-24.

[29] Roth, C. H., Malicki, M. A., and Plagge., R., 1992. Empirical evaluation of the relationship between soil dielectric constant and volumetric water content as the basis for calibrating soil moisture measurements by TDR. *Journal of Soil Science*, 43, pp. 1–13.

[30] Schlenz, F., Fallmann, J., Marzahn, P., Loew, A., and Mauser, M., 2012. Characterization of rape field microwave emission and implications to surface soil moisture retrievals. *Remote Sensing*, 4, pp. 247–270.

[31] Jackson, T. J., and Le Vine, D. E., 1996. Mapping surface soil moisture using an aircraft-based passive microwave instrument: algorithm and example, *Journal of hydrology*, 184, pp. 85-99.

[32] Lillesand, T. M., and Kiefer, R. W., 1994. *Remote Sensing and Image Interpretation 3rd edition*, John Wiley and Sons, New York.

[33] Ulaby, F. T., Dubois, P. C., and van Zyl, J., 1996. Radar mapping of surface soil moisture, *Journal of Hydrology*, 184, pp. 57-84.

[34] Njoku, E. G., and Entekhabi, D., 1996. Passive microwave remote sensing of soil moisture, *Journal of hydrology*, 184, pp. 101-129.

[35] Mecklenburg, S., Drusch, M., Kerr, Y. H., Font, J., Martin-Neira, M., Delwart, S., Buenadicha, G., Reul, N., Daganzo-Eusebio, E., Oliva, R., and Crapolicchio, R., 2012. ESA's Soil moisture and Ocean Salinity Mission: Mission Performance and Operations. *IEEE Transactions on Geoscience and Remote Sensing*, 50(5), pp. 1354-1366.

[36] Merlin, O., Ruediger, C., Al Bitar, A., Walker, J. P., and Kerr, Y. H., 2012. Disaggregation of SMOS Soil Moisture in Southeastern Australia. *IEEE Transactions on Geosicence and Remote Sensing*, 50(5), pp. 1556-1571.

[37] Gherboudj, I., Magagi, R., Goita, K., Berg, A. A., Toth, B., and Walker, A., 2012. Validation of SMOS Data Over Agricultural and Boreal Forest Areas in Canada. *IEEE Transactions on Geoscience and Remote Sensing*, 50(5), pp. 1623-1635.

[38] Lacava, T., Matgen, P., Brocca, L., Bittelli, M., Pergola, N., Moramarco, T., and Tramutoli, V., 2012. A First Assessment of the SMOS Soil Moisture Product With In Situ and Modeled Data in Italy and Luxembourg. *IEEE Transactions on Geoscience and Remote Sensing*, 50(5), pp. 1612-1622.

[39] Jackson, T. J., Bindlish, R., Cosh, M. H., Zhao, T., Starks, P. J., Bosch, D. D., Seyfried, M., Moran, M. S., Goodrich, D. C., Kerr, Y. H., and Leroux, D., 2012. Validation of Soil Moisture and Ocean Salinity (SMOS) Soil Moisture Over Watershed Networks in the U.S. *IEEE Transactions on Geoscience and Remote Sensing*, 50(5), pp. 1530-1543.

[40] Collow, T. W., Robock, A., Basara, J. B., and Illston, B. G., 2012. Evaluation of SMOS retrievals of soil moisture over the central United States with currently available in situ observations. *Journal of Geophysical Research: Atmospheres*, 117, D09113.

[41] Al Bitar, A., Leroux, D., Kerr, Y. H., Merlin, O., Richaume, P., Sahoo, A., and Wood, E. F., 2012. Evaluation of SMOS Soil Moisture Products Over Continental US Using the SCAN/SNOTEL Network. *IEEE Transactions on Geoscience and Remote Sensing*. 50(5), pp. 1572-1586.

[42] dall'Amico, J. T., Schlenz, F., Loew, A., and Mauser, W., 2012. First Results of SMOS Soil Moisture Validation in the Upper Danube Catchment. *IEEE Transactions on Geoscience and Remote Sensing*, 50(5), pp. 1507-1516.

[43] Draper, C. S., Walker, J. P., Steinle, P. J., de Jeu, R. A. M., and Holmes, T. R. H., 2009. An evaluation of AMSR-E derived soil moisture over Australia. *Remote Sensing of Environment*, 113(4), pp. 703-710.

[44] *Milestones: Loran, 1940 - 1946* [online].
Available: http://ethw.org/Milestones:Loran,_1940_-_1946

[45] *LORAN C STATION: LESSAY* [online].
Available: http://www.loran-europe.eu/viewpage.php?page_id=15

[46] U.S. Coast Guard, 1962. *The Loran-C system of navigation*.

[47] Pelgrum, W., 2006. *New Potential of Low-Frequency Radionavigation in the 21st Century*, Delft.

[48] U.S. Department of Transportation, U.S. Coast Guard, 1994. *Specification of the Transmitted Loran-C Signal*.

[49] General Lighthouse Authorities of the United Kingdom and Ireland., 2006. *The Case for eLoran* [online].
Available:
http://www.professordavidlast.co.uk/cms_items/f20091128134302.pdf.

[50] *File:Chayka pulse.svg* [online].
Available: http://en.wikipedia.org/wiki/File:Chayka_pulse.svg.

[51] U.S. Department of Homeland Security, U.S. Coast Guard, 1992. *Loran-C User Handbook.*

[52] Lo, S., Leathem, M., Offermans, G., Gunther, G. T., Hamilton, B. A., Peterson, B., Johnson, G., and Enge, P., 2009. Defining Primary, Secondary, Additional Secondary Factors for RTCM Minimum Performance Specifications (MPS). *38th Annual Convention and Technical Symposium of the International Loran Association*, Portland, Maine, USA.

[53] Sun, Z. J., Young, G. D., McFarlane, R. A., and Chambers, B.M., 2000. The effect of soil electrical conductivity on moisture determination using time-domain reflectometry in sandy soil. *Canadian Journal of Soil Science*, 80(1), pp. 13-22.

[54] Johler, J. R., Kellar, W. J., and Walters, L. C., 1956. National Bureau of Standards Circular 573, pp. 1-38. *Phase of the low radiofrequency ground wave*.

[55] Skolnik, M. I., 2008. *Radar Handbook*. 3rd ed. London: McGraw-Hill Professional.

[56] Scheftic, W., Cummins, K.L., Krider, E.P., Sternberg, B.K., Goodrich, D., Moran, S. and Scott, R., 2007. Wide-Area Soil Moisture Estimation Using the Propagation of Low-Frequency Electromagnetic Signals. *The Fourth Symposium on Southwest Hydrometeorology*, Tucson, Arizona, USA.

[57] Hayashi, M., 2004. Temperature-electrical conductivity relation of water for environmental monitoring and geophysical data inversion. *Environmental Monitoring and Assessment*, 96, pp. 119-128.

[58] National Physical Laboratory. *2.7.9 Physical properties of sea water* [online].
Available: http://www.kayelaby.npl.co.uk/general_physics/2_7/2_7_9.html.

[59] Füllekrug, M., 2009. Wideband digital low-frequency radio receiver. *Measurement Science and Technology*, 21(1), pp. 015901-1–015901-9.

[60] Dee, D.P., Uppala, S.M., Simmons, A.J., Berrisford, P., Poli, P., Kobayashi, S., Andrae, U., Balmaseda, M.A.,Balsamo, G., Bauer, P., Bechtold, P., Beljaars, A.C.M., van de Berg, L., Bidlot, J., Bormann, N., Delsol, C., Dragani, R.,Fuentes, M., Geer, A.J., Haimberger, L., Healy, S.B., Hersbach, H., Holm, E.V., Isaksen, L., Kallberg, P., Kohler, M., Matricardi, M., McNally, A.P., Monge-Sanz, B.M., Morcrette, J-J., Park, B-K., Peubey, C., de Rosnay, P., Tavolato, C., Thepaut., J-N.and Vitart, F., 2011. The ERA-Interim reanalysis: Configuration and performance of the data assimilation system *Quarterly Journal of the Royal Meteorological Society.*, 137(656), pp. 553–597.

[61] Reul, N., Fournier, S., Boutin, J., Hernandez, O., Maes, C., Chapron, B., Alory, G., Quilfen, Y., Tenerelli, J., Morisset, S., Kerr, Y., Mecklenburg, S. and Steven, D., 2013. Sea Surface Salinity Observations from Space with the SMOS Satellite: A New Means to Monitor the Marine Branch of the Water Cycle. *Surveys in Geophysics*, DOI: 10.1007/s10712-013-9244-0, pp. 1-42.

[62] Lagerloef, G., deCharon, A., Lindstrom, E., 2013. Ocean Salinity and the Aquarius/SAC-D Mission: A New Frontier in Ocean Remote Sensing. *Marine Technology Society Journal.* 47(5), pp. 26-30.

[63] Bell, M.J., Forbes, R.M. and Hines, A., 2000. Assessment of the FOAM global data assimilation system for real-time operational ocean forecasting. *Journal of Marine Systems*, 25(1), pp. 1-22.

[64] Banks, C.J., Gommenginger, C.P., Srokosz, M.A. and Snaith, H.M., 2012. Validating SMOS Ocean Surface Salinity in the Atlantic with Argo and Operational Ocean Model Data. *IEEE Transactions on Geoscience and Remote Sensing*, 50(5), pp. 1688-1702.

[65] *Sea surface salinity (SSS) from SMOS* [online].
Available: http://icdc.zmaw.de/1/daten/ocean/smos-sss.html.

[66] [online].
Available: https://en.wikipedia.org/wiki/DCF77#/media/File:Dcf77.jpg.

[67] [online].
Available: https://en.wikipedia.org/wiki/DCF77#/media/File:Dcf_weite.jpg.

Appendices

Appendix 1: Experimental data

The table below shows the Loran-C delay variation measured at the University of Bath, Bath, UK, using a wide-band digital low-frequency radio receiver. The signals were received from the Lessay master station in Northern France.

Time	Delay variation (ns)
01-Feb-2012 00:00:18	-3.1000000000000000e+001
01-Feb-2012 06:00:18	9.0000000000000000e+000
01-Feb-2012 12:00:18	-7.0000000000000000e+000
01-Feb-2012 18:00:18	3.7000000000000000e+001
02-Feb-2012 00:00:18	-7.0000000000000000e+000
02-Feb-2012 06:00:18	2.8000000000000000e+001
02-Feb-2012 12:00:18	2.6000000000000000e+001
02-Feb-2012 18:00:18	3.0000000000000000e+001
03-Feb-2012 00:00:18	1.0000000000000000e+001
03-Feb-2012 06:00:18	1.2000000000000000e+001
03-Feb-2012 12:00:18	2.3000000000000000e+001
03-Feb-2012 18:00:18	3.0000000000000000e+001
04-Feb-2012 00:00:18	-5.0000000000000000e+000
04-Feb-2012 06:00:18	3.0000000000000000e+001
04-Feb-2012 12:00:18	2.1000000000000000e+001
04-Feb-2012 18:00:18	1.9000000000000000e+001
05-Feb-2012 00:00:18	-2.7000000000000000e+001

05-Feb-2012 06:00:18	3.7000000000000000e+001
05-Feb-2012 12:00:18	6.0000000000000000e+000
05-Feb-2012 18:00:18	4.0000000000000000e+000
06-Feb-2012 00:00:18	-3.0000000000000000e+001
06-Feb-2012 06:00:18	-1.8000000000000000e+001
06-Feb-2012 12:00:18	-1.3000000000000000e+001
06-Feb-2012 18:00:18	-3.2000000000000000e+001
07-Feb-2012 00:00:18	-5.5000000000000000e+001
07-Feb-2012 06:00:18	-9.0000000000000000e+000
07-Feb-2012 12:00:18	-1.7000000000000000e+001
07-Feb-2012 18:00:18	-2.0000000000000000e+000
08-Feb-2012 00:00:18	2.3000000000000000e+001
08-Feb-2012 06:00:18	3.6000000000000000e+001
08-Feb-2012 12:00:18	1.7000000000000000e+001
08-Feb-2012 18:00:18	3.3000000000000000e+001
09-Feb-2012 00:00:18	2.6000000000000000e+001
09-Feb-2012 06:00:18	2.2000000000000000e+001
09-Feb-2012 12:00:18	6.0000000000000000e+000
09-Feb-2012 18:00:18	2.0000000000000000e+001
10-Feb-2012 00:00:18	3.3000000000000000e+001
10-Feb-2012 06:00:18	-1.8000000000000000e+001
10-Feb-2012 12:00:18	2.0000000000000000e+000

10-Feb-2012 18:00:18	-4.0000000000000000e+000
11-Feb-2012 00:00:18	2.0000000000000000e+000
11-Feb-2012 06:00:18	-9.0000000000000000e+000
11-Feb-2012 12:00:18	2.1000000000000000e+001
11-Feb-2012 18:00:18	5.0000000000000000e+000
12-Feb-2012 00:01:45	-7.0000000000000000e+000
12-Feb-2012 06:00:18	5.0000000000000000e+000
12-Feb-2012 12:01:45	-1.0000000000000000e+000
12-Feb-2012 18:00:18	1.0000000000000000e+000
13-Feb-2012 00:00:18	-2.0000000000000000e+000
13-Feb-2012 06:01:45	8.0000000000000000e+000
13-Feb-2012 12:00:18	-7.0000000000000000e+000
13-Feb-2012 18:00:18	5.0000000000000000e+000
14-Feb-2012 00:00:18	2.1000000000000000e+001
14-Feb-2012 06:00:18	1.7000000000000000e+001
14-Feb-2012 12:00:18	-1.3000000000000000e+001
14-Feb-2012 18:00:18	1.8000000000000000e+001
15-Feb-2012 00:00:18	-1.4000000000000000e+001
15-Feb-2012 06:00:18	-1.7000000000000000e+001
15-Feb-2012 12:00:18	-1.3000000000000000e+001
15-Feb-2012 18:00:18	2.0000000000000000e+000
16-Feb-2012 00:00:18	-1.0000000000000000e+001

16-Feb-2012 06:00:18	8.0000000000000000e+000
16-Feb-2012 12:00:18	-2.7000000000000000e+001
16-Feb-2012 18:00:18	2.0000000000000000e+000
17-Feb-2012 00:00:18	0.0000000000000000e+000
17-Feb-2012 06:00:18	-1.3000000000000000e+001
17-Feb-2012 12:00:18	-2.0000000000000000e+001
17-Feb-2012 18:00:18	-2.4000000000000000e+001
18-Feb-2012 00:00:18	-7.0000000000000000e+000
18-Feb-2012 06:00:18	-2.0000000000000000e+000
18-Feb-2012 12:00:18	-2.9000000000000000e+001
18-Feb-2012 18:00:18	0.0000000000000000e+000
19-Feb-2012 00:00:18	-9.0000000000000000e+000
19-Feb-2012 06:00:18	-3.0000000000000000e+000
19-Feb-2012 12:00:18	-3.3000000000000000e+001
19-Feb-2012 18:00:18	6.0000000000000000e+000
20-Feb-2012 00:00:18	2.6000000000000000e+001
20-Feb-2012 06:00:18	8.0000000000000000e+000
20-Feb-2012 12:00:18	-3.0000000000000000e+000
20-Feb-2012 18:00:18	-2.0000000000000000e+001
21-Feb-2012 00:00:18	1.2000000000000000e+001
21-Feb-2012 06:00:18	8.0000000000000000e+000
21-Feb-2012 12:00:18	2.3000000000000000e+001

21-Feb-2012 18:00:18	3.0000000000000000e+000

Table A.1 – Measured Loran-C delay variation between Lessay and Bath

Appendix 2: Data from the ECMWF interim reanalysis

The following tables include the ECMWF model data retrieved for the first validation study. The data used for the second study are not included because of the long measurement period.

Appendix 2.1: 2 metre temperature

Time	Temperature (K)
2012-02-01 00:00:00	272.6252747
2012-02-01 06:00:00	272.1989441
2012-02-01 12:00:00	274.3609619
2012-02-01 18:00:00	273.2030945
2012-02-02 00:00:00	270.8467407
2012-02-02 06:00:00	270.0264587
2012-02-02 12:00:00	273.7871094
2012-02-02 18:00:00	271.4982605
2012-02-03 00:00:00	268.6233826
2012-02-03 06:00:00	267.4779053
2012-02-03 12:00:00	273.2163086
2012-02-03 18:00:00	270.9111023
2012-02-04 00:00:00	267.9628296
2012-02-04 06:00:00	266.0128174
2012-02-04 12:00:00	273.638092
2012-02-04 18:00:00	275.0054932
2012-02-05 00:00:00	276.677002
2012-02-05 06:00:00	275.4811096
2012-02-05 12:00:00	277.5301819
2012-02-05 18:00:00	276.1815796
2012-02-06 00:00:00	274.8841553
2012-02-06 06:00:00	274.8592529
2012-02-06 12:00:00	277.8457031
2012-02-06 18:00:00	277.2156067
2012-02-07 00:00:00	275.5328979
2012-02-07 06:00:00	274.4353333
2012-02-07 12:00:00	275.7688599
2012-02-07 18:00:00	274.5841064
2012-02-08 00:00:00	270.3127136
2012-02-08 06:00:00	270.622345
2012-02-08 12:00:00	273.0119019

2012-02-08 18:00:00	273.1330872
2012-02-09 00:00:00	272.4376221
2012-02-09 06:00:00	270.9342957
2012-02-09 12:00:00	273.7132874
2012-02-09 18:00:00	274.7502441
2012-02-10 00:00:00	273.7838745
2012-02-10 06:00:00	274.2372437
2012-02-10 12:00:00	275.0087891
2012-02-10 18:00:00	272.9471436
2012-02-11 00:00:00	269.5392761
2012-02-11 06:00:00	267.0950317
2012-02-11 12:00:00	273.6845398
2012-02-11 18:00:00	271.076416
2012-02-12 00:00:00	267.9747314
2012-02-12 06:00:00	270.9268494
2012-02-12 12:00:00	277.0733337
2012-02-12 18:00:00	277.7149353
2012-02-13 00:00:00	276.5943298
2012-02-13 06:00:00	276.1469421
2012-02-13 12:00:00	279.6577454
2012-02-13 18:00:00	279.5626526
2012-02-14 00:00:00	278.4065552
2012-02-14 06:00:00	277.1266479
2012-02-14 12:00:00	280.7052612
2012-02-14 18:00:00	280.5767822
2012-02-15 00:00:00	280.4923401
2012-02-15 06:00:00	280.0862427
2012-02-15 12:00:00	282.9854736
2012-02-15 18:00:00	281.855957
2012-02-16 00:00:00	280.4201965
2012-02-16 06:00:00	279.5127563
2012-02-16 12:00:00	282.4550781
2012-02-16 18:00:00	281.0357056
2012-02-17 00:00:00	280.3157959
2012-02-17 06:00:00	281.2679443
2012-02-17 12:00:00	283.4187317
2012-02-17 18:00:00	282.6676025
2012-02-18 00:00:00	281.046875
2012-02-18 06:00:00	280.865509
2012-02-18 12:00:00	282.7173157
2012-02-18 18:00:00	278.3053589
2012-02-19 00:00:00	275.2331238
2012-02-19 06:00:00	274.5307007

2012-02-19 12:00:00	279.4133301
2012-02-19 18:00:00	277.1149902
2012-02-20 00:00:00	272.2314758
2012-02-20 06:00:00	271.3492126
2012-02-20 12:00:00	280.3040771
2012-02-20 18:00:00	279.4975281
2012-02-21 00:00:00	278.9250488
2012-02-21 06:00:00	279.4365234
2012-02-21 12:00:00	282.9424133
2012-02-21 18:00:00	281.5970764

Table A.2 – 2 metre temperature (data from the ECMWF)

Appendix 2.2: Mean sea level pressure

Time	Pressure (Pa)
2012-02-01 00:00:00	101917.3672
2012-02-01 06:00:00	102022.4219
2012-02-01 12:00:00	102239.7813
2012-02-01 18:00:00	102360.8828
2012-02-02 00:00:00	102505.0547
2012-02-02 06:00:00	102455.2891
2012-02-02 12:00:00	102517.2422
2012-02-02 18:00:00	102601.4141
2012-02-03 00:00:00	102799.0313
2012-02-03 06:00:00	102876.7266
2012-02-03 12:00:00	103044.8125
2012-02-03 18:00:00	103023.1406
2012-02-04 00:00:00	103013.4766
2012-02-04 06:00:00	102875.0469
2012-02-04 12:00:00	102700.4141
2012-02-04 18:00:00	102068.9688
2012-02-05 00:00:00	101213.4688
2012-02-05 06:00:00	101475.0234
2012-02-05 12:00:00	101928.625
2012-02-05 18:00:00	102076.7266
2012-02-06 00:00:00	102175.6484
2012-02-06 06:00:00	102203.7813
2012-02-06 12:00:00	102320.8438
2012-02-06 18:00:00	102352.5078
2012-02-07 00:00:00	102592.8203
2012-02-07 06:00:00	102710.5781
2012-02-07 12:00:00	103028.4766
2012-02-07 18:00:00	103093.5781
2012-02-08 00:00:00	103263.5859
2012-02-08 06:00:00	103114.5313
2012-02-08 12:00:00	103085.8984
2012-02-08 18:00:00	103011.9766
2012-02-09 00:00:00	103056.2344
2012-02-09 06:00:00	102979.9609
2012-02-09 12:00:00	102937.4766
2012-02-09 18:00:00	102748.7734
2012-02-10 00:00:00	102688.7656

2012-02-10 06:00:00	102583.8281
2012-02-10 12:00:00	102679.5156
2012-02-10 18:00:00	102616.8594
2012-02-11 00:00:00	102648.3984
2012-02-11 06:00:00	102568.5781
2012-02-11 12:00:00	102649.1328
2012-02-11 18:00:00	102624.6406
2012-02-12 00:00:00	102692.4531
2012-02-12 06:00:00	102584.3594
2012-02-12 12:00:00	102577.2109
2012-02-12 18:00:00	102423.9453
2012-02-13 00:00:00	102465.2813
2012-02-13 06:00:00	102226.2891
2012-02-13 12:00:00	101913.25
2012-02-13 18:00:00	101559.3594
2012-02-14 00:00:00	101700.9688
2012-02-14 06:00:00	101790.6953
2012-02-14 12:00:00	101863.0078
2012-02-14 18:00:00	101610.0156
2012-02-15 00:00:00	101591.0313
2012-02-15 06:00:00	101678.9375
2012-02-15 12:00:00	101916.1484
2012-02-15 18:00:00	101936.2188
2012-02-16 00:00:00	102086.8203
2012-02-16 06:00:00	101972.7734
2012-02-16 12:00:00	102009.5938
2012-02-16 18:00:00	101832.5938
2012-02-17 00:00:00	101769.3594
2012-02-17 06:00:00	101573.7578
2012-02-17 12:00:00	101547.5
2012-02-17 18:00:00	101314.0156
2012-02-18 00:00:00	101066.4531
2012-02-18 06:00:00	100565.9844
2012-02-18 12:00:00	100204.3359
2012-02-18 18:00:00	100194.2422
2012-02-19 00:00:00	100829.6406
2012-02-19 06:00:00	101213.7656
2012-02-19 12:00:00	101707.6406
2012-02-19 18:00:00	101998.9453
2012-02-20 00:00:00	102337.9531
2012-02-20 06:00:00	102316.3438
2012-02-20 12:00:00	102294.3438
2012-02-20 18:00:00	102069.9297

2012-02-21 00:00:00	102041.4141
2012-02-21 06:00:00	101888.4844
2012-02-21 12:00:00	101984.3203
2012-02-21 18:00:00	101935.0625

Table A.3 – Mean sea level pressure (data from the ECMWF)

Appendix 2.3: Total column water vapour

Time	Water vapour (kgm^{-2})
2012-02-01 00:00:00	4.386452675
2012-02-01 06:00:00	3.693221569
2012-02-01 12:00:00	3.813461065
2012-02-01 18:00:00	3.915596485
2012-02-02 00:00:00	3.907165289
2012-02-02 06:00:00	3.83915782
2012-02-02 12:00:00	3.913367033
2012-02-02 18:00:00	3.986830235
2012-02-03 00:00:00	4.170555592
2012-02-03 06:00:00	4.9171381
2012-02-03 12:00:00	4.859291553
2012-02-03 18:00:00	4.608161449
2012-02-04 00:00:00	4.507627487
2012-02-04 06:00:00	5.923774719
2012-02-04 12:00:00	9.717940331
2012-02-04 18:00:00	14.58702564
2012-02-05 00:00:00	13.767169
2012-02-05 06:00:00	6.42601347
2012-02-05 12:00:00	8.240325928
2012-02-05 18:00:00	11.2105217
2012-02-06 00:00:00	12.89841366
2012-02-06 06:00:00	13.58665943
2012-02-06 12:00:00	12.99729824
2012-02-06 18:00:00	11.5212183
2012-02-07 00:00:00	8.085753441
2012-02-07 06:00:00	7.50532341
2012-02-07 12:00:00	7.355676651
2012-02-07 18:00:00	6.260039806
2012-02-08 00:00:00	3.642304897
2012-02-08 06:00:00	5.644704342
2012-02-08 12:00:00	6.38824749
2012-02-08 18:00:00	6.984108925
2012-02-09 00:00:00	6.32817173
2012-02-09 06:00:00	5.264849186
2012-02-09 12:00:00	7.523567677
2012-02-09 18:00:00	15.29961491
2012-02-10 00:00:00	16.6605854

2012-02-10 06:00:00	14.41982651
2012-02-10 12:00:00	11.95671844
2012-02-10 18:00:00	8.230678558
2012-02-11 00:00:00	4.515190601
2012-02-11 06:00:00	3.664562702
2012-02-11 12:00:00	3.548267841
2012-02-11 18:00:00	4.007186413
2012-02-12 00:00:00	5.28373909
2012-02-12 06:00:00	9.953033447
2012-02-12 12:00:00	12.98752975
2012-02-12 18:00:00	12.37717056
2012-02-13 00:00:00	10.52185535
2012-02-13 06:00:00	11.29748821
2012-02-13 12:00:00	10.32898045
2012-02-13 18:00:00	10.90217113
2012-02-14 00:00:00	11.8764677
2012-02-14 06:00:00	11.02993584
2012-02-14 12:00:00	11.61993885
2012-02-14 18:00:00	10.78968143
2012-02-15 00:00:00	9.608246803
2012-02-15 06:00:00	8.520976067
2012-02-15 12:00:00	9.581495285
2012-02-15 18:00:00	10.3304615
2012-02-16 00:00:00	9.216101646
2012-02-16 06:00:00	8.959547997
2012-02-16 12:00:00	11.05693913
2012-02-16 18:00:00	15.97101784
2012-02-17 00:00:00	17.65800095
2012-02-17 06:00:00	19.60630608
2012-02-17 12:00:00	18.51200485
2012-02-17 18:00:00	18.72526741
2012-02-18 00:00:00	16.52532387
2012-02-18 06:00:00	13.99415779
2012-02-18 12:00:00	15.87093067
2012-02-18 18:00:00	6.083303928
2012-02-19 00:00:00	5.495224953
2012-02-19 06:00:00	6.296785831
2012-02-19 12:00:00	6.941553116
2012-02-19 18:00:00	6.490981579
2012-02-20 00:00:00	6.683453083
2012-02-20 06:00:00	7.505367756
2012-02-20 12:00:00	10.09964085
2012-02-20 18:00:00	12.32210255

2012-02-21 00:00:00	12.71198845
2012-02-21 06:00:00	13.92651558
2012-02-21 12:00:00	14.83804607
2012-02-21 18:00:00	15.01062202

Table A.4 – Total column water vapour (data from the ECMWF)

Appendix 2.4: Soil temperature level 1

Time	Temperature (K)
2012-02-01 00:00:00	274.5381775
2012-02-01 06:00:00	274.1607666
2012-02-01 12:00:00	275.2344055
2012-02-01 18:00:00	274.7623596
2012-02-02 00:00:00	274.1671448
2012-02-02 06:00:00	272.9131775
2012-02-02 12:00:00	273.2249756
2012-02-02 18:00:00	274.0359802
2012-02-03 00:00:00	273.2891541
2012-02-03 06:00:00	272.0882263
2012-02-03 12:00:00	272.0806274
2012-02-03 18:00:00	272.928772
2012-02-04 00:00:00	271.315979
2012-02-04 06:00:00	269.5004883
2012-02-04 12:00:00	269.7747192
2012-02-04 18:00:00	271.4406433
2012-02-05 00:00:00	271.9547119
2012-02-05 06:00:00	272.893158
2012-02-05 12:00:00	273.0348511
2012-02-05 18:00:00	274.5167236
2012-02-06 00:00:00	276.2349548
2012-02-06 06:00:00	275.7157288
2012-02-06 12:00:00	277.5260315
2012-02-06 18:00:00	276.3363953
2012-02-07 00:00:00	276.1096497
2012-02-07 06:00:00	274.7104797
2012-02-07 12:00:00	275.8479004
2012-02-07 18:00:00	276.2774963
2012-02-08 00:00:00	276.371521
2012-02-08 06:00:00	274.9947205
2012-02-08 12:00:00	274.5185547
2012-02-08 18:00:00	274.8900757
2012-02-09 00:00:00	275.7933655
2012-02-09 06:00:00	274.3379211
2012-02-09 12:00:00	274.2675171
2012-02-09 18:00:00	274.5719604
2012-02-10 00:00:00	274.4048462
2012-02-10 06:00:00	274.7140503

2012-02-10 12:00:00	275.4982605
2012-02-10 18:00:00	274.147522
2012-02-11 00:00:00	271.7564392
2012-02-11 06:00:00	271.1166077
2012-02-11 12:00:00	272.1119995
2012-02-11 18:00:00	273.7185364
2012-02-12 00:00:00	273.33255
2012-02-12 06:00:00	273.4373474
2012-02-12 12:00:00	273.3077087
2012-02-12 18:00:00	275.1893921
2012-02-13 00:00:00	275.5002441
2012-02-13 06:00:00	275.0504456
2012-02-13 12:00:00	277.5031128
2012-02-13 18:00:00	277.5601196
2012-02-14 00:00:00	277.4707031
2012-02-14 06:00:00	276.6844482
2012-02-14 12:00:00	279.1938782
2012-02-14 18:00:00	279.4679871
2012-02-15 00:00:00	279.9129639
2012-02-15 06:00:00	279.4285278
2012-02-15 12:00:00	282.0150146
2012-02-15 18:00:00	281.3782349
2012-02-16 00:00:00	281.7718811
2012-02-16 06:00:00	279.7333374
2012-02-16 12:00:00	282.7130737
2012-02-16 18:00:00	280.7432251
2012-02-17 00:00:00	279.775177
2012-02-17 06:00:00	280.0619507
2012-02-17 12:00:00	281.6151733
2012-02-17 18:00:00	281.7280884
2012-02-18 00:00:00	280.8233337
2012-02-18 06:00:00	280.5800171
2012-02-18 12:00:00	281.9483032
2012-02-18 18:00:00	279.7880554
2012-02-19 00:00:00	277.0903015
2012-02-19 06:00:00	275.8531799
2012-02-19 12:00:00	279.5700989
2012-02-19 18:00:00	278.8565369
2012-02-20 00:00:00	275.6221619
2012-02-20 06:00:00	273.8280334
2012-02-20 12:00:00	276.2424927
2012-02-20 18:00:00	277.9974365
2012-02-21 00:00:00	277.6591797

2012-02-21 06:00:00	278.1235657
2012-02-21 12:00:00	281.3414307
2012-02-21 18:00:00	280.6348267

Table A.5 – 0-7 cm soil temperature (data from the ECMWF)

Appendix 2.5: Soil temperature level 2

Time	Temperature (K)
2012-02-01 00:00:00	276.0227356
2012-02-01 06:00:00	275.7770691
2012-02-01 12:00:00	275.5696106
2012-02-01 18:00:00	275.9952698
2012-02-02 00:00:00	275.5960693
2012-02-02 06:00:00	275.3330383
2012-02-02 12:00:00	275.1018677
2012-02-02 18:00:00	274.9880066
2012-02-03 00:00:00	274.8087769
2012-02-03 06:00:00	274.6411438
2012-02-03 12:00:00	274.4667969
2012-02-03 18:00:00	274.3179626
2012-02-04 00:00:00	274.2119446
2012-02-04 06:00:00	274.0508118
2012-02-04 12:00:00	273.9503174
2012-02-04 18:00:00	273.8475037
2012-02-05 00:00:00	273.8071594
2012-02-05 06:00:00	273.7969055
2012-02-05 12:00:00	273.7987061
2012-02-05 18:00:00	273.8576355
2012-02-06 00:00:00	273.8951416
2012-02-06 06:00:00	273.9920959
2012-02-06 12:00:00	274.0634155
2012-02-06 18:00:00	274.5976868
2012-02-07 00:00:00	274.9939575
2012-02-07 06:00:00	275.3701782
2012-02-07 12:00:00	275.5812378
2012-02-07 18:00:00	275.9773865
2012-02-08 00:00:00	275.4508057
2012-02-08 06:00:00	275.1506653
2012-02-08 12:00:00	274.8242188
2012-02-08 18:00:00	275.1222534
2012-02-09 00:00:00	274.8998108
2012-02-09 06:00:00	274.8782959
2012-02-09 12:00:00	274.7244263
2012-02-09 18:00:00	275.2098694
2012-02-10 00:00:00	275.1349792
2012-02-10 06:00:00	275.1650696

2012-02-10 12:00:00	275.2167358
2012-02-10 18:00:00	275.4707642
2012-02-11 00:00:00	275.1600342
2012-02-11 06:00:00	274.3564453
2012-02-11 12:00:00	274.1477966
2012-02-11 18:00:00	274.1338501
2012-02-12 00:00:00	274.0723572
2012-02-12 06:00:00	274.0665588
2012-02-12 12:00:00	274.0534363
2012-02-12 18:00:00	274.3831482
2012-02-13 00:00:00	274.6231079
2012-02-13 06:00:00	274.8599548
2012-02-13 12:00:00	275.1376038
2012-02-13 18:00:00	275.9622803
2012-02-14 00:00:00	276.4953308
2012-02-14 06:00:00	276.678009
2012-02-14 12:00:00	276.8503418
2012-02-14 18:00:00	277.7379761
2012-02-15 00:00:00	277.9866333
2012-02-15 06:00:00	278.2815552
2012-02-15 12:00:00	278.5355835
2012-02-15 18:00:00	279.3255615
2012-02-16 00:00:00	278.9398804
2012-02-16 06:00:00	278.9942627
2012-02-16 12:00:00	278.9483032
2012-02-16 18:00:00	279.8060608
2012-02-17 00:00:00	279.625946
2012-02-17 06:00:00	279.6071472
2012-02-17 12:00:00	279.870697
2012-02-17 18:00:00	280.4707031
2012-02-18 00:00:00	280.4591064
2012-02-18 06:00:00	280.2200012
2012-02-18 12:00:00	280.2037354
2012-02-18 18:00:00	280.2796021
2012-02-19 00:00:00	279.2373657
2012-02-19 06:00:00	278.1307373
2012-02-19 12:00:00	277.7990112
2012-02-19 18:00:00	278.4414978
2012-02-20 00:00:00	277.2374878
2012-02-20 06:00:00	276.252594
2012-02-20 12:00:00	275.8512268
2012-02-20 18:00:00	276.9671631
2012-02-21 00:00:00	277.3637085

2012-02-21 06:00:00	277.5867004
2012-02-21 12:00:00	278.1470642
2012-02-21 18:00:00	279.1804504

Table A.6 – 7-28 cm soil temperature (data from the ECMWF)

Appendix 2.6: Soil temperature level 3

Time	Temperature (K)
2012-02-01 00:00:00	279.2619019
2012-02-01 06:00:00	279.1589661
2012-02-01 12:00:00	279.0521851
2012-02-01 18:00:00	278.9612122
2012-02-02 00:00:00	278.8701477
2012-02-02 06:00:00	278.7720642
2012-02-02 12:00:00	278.6678772
2012-02-02 18:00:00	278.5558167
2012-02-03 00:00:00	278.4501038
2012-02-03 06:00:00	278.3426514
2012-02-03 12:00:00	278.2321777
2012-02-03 18:00:00	278.1173096
2012-02-04 00:00:00	278.0086975
2012-02-04 06:00:00	277.8994751
2012-02-04 12:00:00	277.7909546
2012-02-04 18:00:00	277.6723633
2012-02-05 00:00:00	277.5682983
2012-02-05 06:00:00	277.4700012
2012-02-05 12:00:00	277.3761597
2012-02-05 18:00:00	277.2926331
2012-02-06 00:00:00	277.212677
2012-02-06 06:00:00	277.1393738
2012-02-06 12:00:00	277.0733948
2012-02-06 18:00:00	277.0219116
2012-02-07 00:00:00	276.9975281
2012-02-07 06:00:00	276.9920349
2012-02-07 12:00:00	276.995636
2012-02-07 18:00:00	277.0185547
2012-02-08 00:00:00	277.0305786
2012-02-08 06:00:00	277.0260315
2012-02-08 12:00:00	277.002594
2012-02-08 18:00:00	276.9892578
2012-02-09 00:00:00	276.9700623
2012-02-09 06:00:00	276.95047
2012-02-09 12:00:00	276.9234924
2012-02-09 18:00:00	276.9065552
2012-02-10 00:00:00	276.8989563
2012-02-10 06:00:00	276.8897095

2012-02-10 12:00:00	276.8812256
2012-02-10 18:00:00	276.8830566
2012-02-11 00:00:00	276.8809509
2012-02-11 06:00:00	276.8491211
2012-02-11 12:00:00	276.7991028
2012-02-11 18:00:00	276.7408752
2012-02-12 00:00:00	276.6913147
2012-02-12 06:00:00	276.6437073
2012-02-12 12:00:00	276.5980225
2012-02-12 18:00:00	276.5556641
2012-02-13 00:00:00	276.5349426
2012-02-13 06:00:00	276.5260315
2012-02-13 12:00:00	276.5263062
2012-02-13 18:00:00	276.559021
2012-02-14 00:00:00	276.6134338
2012-02-14 06:00:00	276.6800537
2012-02-14 12:00:00	276.743927
2012-02-14 18:00:00	276.8291321
2012-02-15 00:00:00	276.9363403
2012-02-15 06:00:00	277.0498657
2012-02-15 12:00:00	277.1629028
2012-02-15 18:00:00	277.2983704
2012-02-16 00:00:00	277.4320679
2012-02-16 06:00:00	277.5538635
2012-02-16 12:00:00	277.65979
2012-02-16 18:00:00	277.7951965
2012-02-17 00:00:00	277.9221191
2012-02-17 06:00:00	278.0369263
2012-02-17 12:00:00	278.1487427
2012-02-17 18:00:00	278.2750854
2012-02-18 00:00:00	278.4064941
2012-02-18 06:00:00	278.5236206
2012-02-18 12:00:00	278.626709
2012-02-18 18:00:00	278.7307434
2012-02-19 00:00:00	278.8039856
2012-02-19 06:00:00	278.8226013
2012-02-19 12:00:00	278.8026733
2012-02-19 18:00:00	278.8057861
2012-02-20 00:00:00	278.7911987
2012-02-20 06:00:00	278.7251892
2012-02-20 12:00:00	278.6281738
2012-02-20 18:00:00	278.5593262
2012-02-21 00:00:00	278.5286255

2012-02-21 06:00:00	278.512085
2012-02-21 12:00:00	278.5097656
2012-02-21 18:00:00	278.5506897

Table A.7 – 28-100 cm soil temperature (data from the ECMWF)

Appendix 2.7: Soil moisture layer 1

Time	Water content
2012-02-01 00:00:00	0.308832705
2012-02-01 06:00:00	0.308262825
2012-02-01 12:00:00	0.307228476
2012-02-01 18:00:00	0.306069881
2012-02-02 00:00:00	0.305864394
2012-02-02 06:00:00	0.30553177
2012-02-02 12:00:00	0.304691076
2012-02-02 18:00:00	0.303867608
2012-02-03 00:00:00	0.303835094
2012-02-03 06:00:00	0.30372116
2012-02-03 12:00:00	0.303315312
2012-02-03 18:00:00	0.302951008
2012-02-04 00:00:00	0.302820832
2012-02-04 06:00:00	0.302719116
2012-02-04 12:00:00	0.302618355
2012-02-04 18:00:00	0.31736955
2012-02-05 00:00:00	0.3367652
2012-02-05 06:00:00	0.328781307
2012-02-05 12:00:00	0.32376951
2012-02-05 18:00:00	0.320498168
2012-02-06 00:00:00	0.318874657
2012-02-06 06:00:00	0.317199498
2012-02-06 12:00:00	0.316850573
2012-02-06 18:00:00	0.316653937
2012-02-07 00:00:00	0.315429002
2012-02-07 06:00:00	0.314480543
2012-02-07 12:00:00	0.314113528
2012-02-07 18:00:00	0.31342271
2012-02-08 00:00:00	0.312256217
2012-02-08 06:00:00	0.31142962
2012-02-08 12:00:00	0.310614586
2012-02-08 18:00:00	0.309880733
2012-02-09 00:00:00	0.309340566
2012-02-09 06:00:00	0.308921486
2012-02-09 12:00:00	0.308750391
2012-02-09 18:00:00	0.308547914
2012-02-10 00:00:00	0.316361904
2012-02-10 06:00:00	0.321993202

2012-02-10 12:00:00	0.319648325
2012-02-10 18:00:00	0.316388577
2012-02-11 00:00:00	0.314550996
2012-02-11 06:00:00	0.313316494
2012-02-11 12:00:00	0.312515408
2012-02-11 18:00:00	0.311576039
2012-02-12 00:00:00	0.310810864
2012-02-12 06:00:00	0.310230225
2012-02-12 12:00:00	0.311635286
2012-02-12 18:00:00	0.311258703
2012-02-13 00:00:00	0.310747355
2012-02-13 06:00:00	0.310773253
2012-02-13 12:00:00	0.313349098
2012-02-13 18:00:00	0.312115818
2012-02-14 00:00:00	0.311234057
2012-02-14 06:00:00	0.31029436
2012-02-14 12:00:00	0.3093521
2012-02-14 18:00:00	0.30808714
2012-02-15 00:00:00	0.307786793
2012-02-15 06:00:00	0.307367325
2012-02-15 12:00:00	0.306453049
2012-02-15 18:00:00	0.305507272
2012-02-16 00:00:00	0.305432111
2012-02-16 06:00:00	0.305400521
2012-02-16 12:00:00	0.304932207
2012-02-16 18:00:00	0.303484082
2012-02-17 00:00:00	0.303619236
2012-02-17 06:00:00	0.30395177
2012-02-17 12:00:00	0.304716468
2012-02-17 18:00:00	0.304454058
2012-02-18 00:00:00	0.304348379
2012-02-18 06:00:00	0.304448187
2012-02-18 12:00:00	0.30615744
2012-02-18 18:00:00	0.31440413
2012-02-19 00:00:00	0.309426695
2012-02-19 06:00:00	0.308075398
2012-02-19 12:00:00	0.306921571
2012-02-19 18:00:00	0.305654377
2012-02-20 00:00:00	0.305353969
2012-02-20 06:00:00	0.304993182
2012-02-20 12:00:00	0.303908944
2012-02-20 18:00:00	0.302889258
2012-02-21 00:00:00	0.302874833

2012-02-21 06:00:00	0.302737236
2012-02-21 12:00:00	0.30198276
2012-02-21 18:00:00	0.301975489

Table A.8 – 0-7 cm soil moisture (data from the ECMWF)

Appendix 2.8: Soil moisture layer 2

Time	Water content
2012-02-01 00:00:00	0.301086217
2012-02-01 06:00:00	0.300591528
2012-02-01 12:00:00	0.29990828
2012-02-01 18:00:00	0.298865616
2012-02-02 00:00:00	0.298467159
2012-02-02 06:00:00	0.298124373
2012-02-02 12:00:00	0.297501326
2012-02-02 18:00:00	0.296690881
2012-02-03 00:00:00	0.296478152
2012-02-03 06:00:00	0.296301872
2012-02-03 12:00:00	0.295878619
2012-02-03 18:00:00	0.295431465
2012-02-04 00:00:00	0.295364499
2012-02-04 06:00:00	0.295267761
2012-02-04 12:00:00	0.295039713
2012-02-04 18:00:00	0.29727456
2012-02-05 00:00:00	0.312302232
2012-02-05 06:00:00	0.316874862
2012-02-05 12:00:00	0.314099461
2012-02-05 18:00:00	0.311767042
2012-02-06 00:00:00	0.309932232
2012-02-06 06:00:00	0.308619559
2012-02-06 12:00:00	0.307621628
2012-02-06 18:00:00	0.307253987
2012-02-07 00:00:00	0.306718946
2012-02-07 06:00:00	0.306017697
2012-02-07 12:00:00	0.305387318
2012-02-07 18:00:00	0.305209041
2012-02-08 00:00:00	0.304436505
2012-02-08 06:00:00	0.303715289
2012-02-08 12:00:00	0.30291146
2012-02-08 18:00:00	0.302296042
2012-02-09 00:00:00	0.301739156
2012-02-09 06:00:00	0.301308393
2012-02-09 12:00:00	0.300818861
2012-02-09 18:00:00	0.300661385
2012-02-10 00:00:00	0.302068293
2012-02-10 06:00:00	0.307590544

2012-02-10 12:00:00	0.308955431
2012-02-10 18:00:00	0.308017254
2012-02-11 00:00:00	0.306630522
2012-02-11 06:00:00	0.305486441
2012-02-11 12:00:00	0.304492831
2012-02-11 18:00:00	0.303757071
2012-02-12 00:00:00	0.303112566
2012-02-12 06:00:00	0.302536905
2012-02-12 12:00:00	0.302289337
2012-02-12 18:00:00	0.302616656
2012-02-13 00:00:00	0.30235973
2012-02-13 06:00:00	0.302206397
2012-02-13 12:00:00	0.302504897
2012-02-13 18:00:00	0.302928269
2012-02-14 00:00:00	0.30276221
2012-02-14 06:00:00	0.302321255
2012-02-14 12:00:00	0.301601082
2012-02-14 18:00:00	0.300661296
2012-02-15 00:00:00	0.300223112
2012-02-15 06:00:00	0.299835503
2012-02-15 12:00:00	0.299113214
2012-02-15 18:00:00	0.298274517
2012-02-16 00:00:00	0.29800415
2012-02-16 06:00:00	0.297802716
2012-02-16 12:00:00	0.297407269
2012-02-16 18:00:00	0.296442986
2012-02-17 00:00:00	0.296250939
2012-02-17 06:00:00	0.296192586
2012-02-17 12:00:00	0.296226054
2012-02-17 18:00:00	0.2961815
2012-02-18 00:00:00	0.296275705
2012-02-18 06:00:00	0.296289444
2012-02-18 12:00:00	0.29628098
2012-02-18 18:00:00	0.299826205
2012-02-19 00:00:00	0.300492406
2012-02-19 06:00:00	0.300036192
2012-02-19 12:00:00	0.2992329
2012-02-19 18:00:00	0.298092633
2012-02-20 00:00:00	0.297693431
2012-02-20 06:00:00	0.297335297
2012-02-20 12:00:00	0.29660511
2012-02-20 18:00:00	0.295756847
2012-02-21 00:00:00	0.2954261

2012-02-21 06:00:00	0.295203149
2012-02-21 12:00:00	0.294706941
2012-02-21 18:00:00	0.294398785

Table A.9 – 7-28cm soil moisture (data from the ECMWF)

Appendix 2.9: Soil moisture layer 3

Time	Water content
2012-02-01 00:00:00	0.302241266
2012-02-01 06:00:00	0.302160263
2012-02-01 12:00:00	0.302045971
2012-02-01 18:00:00	0.301790386
2012-02-02 00:00:00	0.30164054
2012-02-02 06:00:00	0.301471651
2012-02-02 12:00:00	0.30122149
2012-02-02 18:00:00	0.300908446
2012-02-03 00:00:00	0.300703406
2012-02-03 06:00:00	0.300507545
2012-02-03 12:00:00	0.300254524
2012-02-03 18:00:00	0.299951345
2012-02-04 00:00:00	0.299752593
2012-02-04 06:00:00	0.299560249
2012-02-04 12:00:00	0.29937011
2012-02-04 18:00:00	0.299206257
2012-02-05 00:00:00	0.299717605
2012-02-05 06:00:00	0.301087826
2012-02-05 12:00:00	0.302179277
2012-02-05 18:00:00	0.302987993
2012-02-06 00:00:00	0.303472221
2012-02-06 06:00:00	0.303795815
2012-02-06 12:00:00	0.304035962
2012-02-06 18:00:00	0.304209769
2012-02-07 00:00:00	0.30431819
2012-02-07 06:00:00	0.304377347
2012-02-07 12:00:00	0.304377437
2012-02-07 18:00:00	0.304378808
2012-02-08 00:00:00	0.304324269
2012-02-08 06:00:00	0.304261446
2012-02-08 12:00:00	0.304133564
2012-02-08 18:00:00	0.30401963
2012-02-09 00:00:00	0.303818405
2012-02-09 06:00:00	0.303674638
2012-02-09 12:00:00	0.303486377
2012-02-09 18:00:00	0.303323209
2012-02-10 00:00:00	0.303170145
2012-02-10 06:00:00	0.303369582

2012-02-10 12:00:00	0.303813577
2012-02-10 18:00:00	0.304181159
2012-02-11 00:00:00	0.304437399
2012-02-11 06:00:00	0.304530889
2012-02-11 12:00:00	0.304520667
2012-02-11 18:00:00	0.304406285
2012-02-12 00:00:00	0.304309756
2012-02-12 06:00:00	0.304193228
2012-02-12 12:00:00	0.304042757
2012-02-12 18:00:00	0.303922385
2012-02-13 00:00:00	0.303837001
2012-02-13 06:00:00	0.303737938
2012-02-13 12:00:00	0.303629071
2012-02-13 18:00:00	0.303564012
2012-02-14 00:00:00	0.303525597
2012-02-14 06:00:00	0.303451657
2012-02-14 12:00:00	0.303312659
2012-02-14 18:00:00	0.303094923
2012-02-15 00:00:00	0.302926719
2012-02-15 06:00:00	0.302751571
2012-02-15 12:00:00	0.302516371
2012-02-15 18:00:00	0.302228153
2012-02-16 00:00:00	0.302005649
2012-02-16 06:00:00	0.301789522
2012-02-16 12:00:00	0.301553667
2012-02-16 18:00:00	0.30116576
2012-02-17 00:00:00	0.300929278
2012-02-17 06:00:00	0.300707728
2012-02-17 12:00:00	0.30051285
2012-02-17 18:00:00	0.300196677
2012-02-18 00:00:00	0.300021768
2012-02-18 06:00:00	0.299850404
2012-02-18 12:00:00	0.299651653
2012-02-18 18:00:00	0.299573541
2012-02-19 00:00:00	0.299616069
2012-02-19 06:00:00	0.299639225
2012-02-19 12:00:00	0.299658
2012-02-19 18:00:00	0.299413204
2012-02-20 00:00:00	0.299375176
2012-02-20 06:00:00	0.299293578
2012-02-20 12:00:00	0.299095809
2012-02-20 18:00:00	0.298967898
2012-02-21 00:00:00	0.298817098

2012-02-21 06:00:00	0.298672676
2012-02-21 12:00:00	0.298492372
2012-02-21 18:00:00	0.298348904

Table A.10 – 28-100 cm soil moisture (data from the ECMWF)

Appendix 3: Publications and conference presentation

Appendix 3.1: Publications

1. Feng, Y. and Astin, I., 2015. Remote sensing of soil moisture using the propagation of Loran-C navigation signals. *IEEE Geoscience and Remote Sensing Letters*, 12 (1), pp. 195-198.

2. Astin, I. and Feng, Y., 2015. Remote sensing of sea surface salinity using the propagation of low-frequency navigation signals. *Ocean Science*, 11 (5), pp. 695-698.

Appendix 3.2: Conference presentation

Feng, Y. and Astin, I., 2014. Remote sensing of soil moisture using Loran-C signals. *European Geosciences Union General Assembly*, Vienna, Austria. Poster Presentation.